NOTE TO USERS

COMPUTATIONAL APPROACH FOR MODELING BODY AND HEAD MOVEMENTS DURING LOCOMOTION

by

Mikhail Kunin

A dissertation submitted to the Graduate Faculty in Computer Science in partial fulfillment of the requirements for the degree of Doctor of Philosophy, The City University of New York.

2005

INFORMATION TO USERS

The quality of this reproduction is dependent upon the quality of the copy submitted. Broken or indistinct print, colored or poor quality illustrations and photographs, print bleed-through, substandard margins, and improper alignment can adversely affect reproduction.

In the unlikely event that the author did not send a complete manuscript and there are missing pages, these will be noted. Also, if unauthorized copyright material had to be removed, a note will indicate the deletion.

ProQuest Information and Learning Company
300 North Zeeb Road
P.O. Box 1346
Ann Arbor, MI 48106-1346

This manuscript has been read and accepted for the Graduate Faculty in Computer Science in satisfaction of the dissertation requirement for the degree of Doctor of Philosophy.

12/29/04
Date

Theodore Raphan
Chairman of Examining Committee

12/29/04
Date

Theodore Raphan
Executive Officer

Professor Michael Anshel

Professor Bernard Cohen

Professor Victor Pan

Professor John Simpson

Professor Theodore Raphan (Advisor)

Supervisory Committee

The City University of New York

Abstract

COMPUTATIONAL APPROACH FOR MODELING BODY AND HEAD MOVEMENTS DURING LOCOMOTION

by

Mikhail Kunin

Adviser: Professor Theodore Raphan

In this thesis, the nature of the invariant points in space that govern head translation and rotation in three-dimensional space and the anatomical basis for the coordinate frames that represent the head rotation was investigated. An algorithm was developed for approximating the pivots and axes for roll, pitch and yaw rotations of the head based on 4x4 displacement matrices, which represent translation and rotation of a rigid body in three dimensions. Head configurations in space were sampled (Optotrak 3020, Northern Digital, Inc.) and converted to a sequence of displacement matrices, D_0 , D_1 ,..D_N. From a window of matrices around the ith sample, D_{i-n} ,.D_i ,..D_{i+n}, a filter was obtained, giving the axis-angle of the rotation. Incremental displacement matrices around the ith sample were used to obtain vectors in the direction of the rotation axis from the rotational part of the incremental displacement matrix. An average axis was obtained for the window of displacement matrices by varying k. Axes were computed as a function of time by incrementing i from n to N-n. Procedures were developed to accurately calibrate

the OPTOTRAK data relative to landmarks associated with the body and head. Studies of voluntary head movement and those during locomotion showed that the derived estimator was stationary and the axes of rotation of the head formed an approximately orthogonal basis. Determination of the yaw rotation axis compared favorably with the orientation of dens of C2 as determined from MRI studies. The method was also applied to finding head fixation points (HFP) in three dimensions using a Karhunen-Loeve transformation. The eccentricity of the distribution increased with walking velocity and was confined principally to the yaw plane in space. When the head movement was projected into the sagittal plane of the head, gain and phase of head rotation relative to its translation was obtained and could be modeled as a second order system, reflecting the behavior of the vestibulo-collic reflex (VCR). This new approach to filtering of three-dimensional rotation and translation of rigid body data gave insight into the compensatory mechanisms that govern head rotation in three dimensions during straight walking.

ACKNOWLEDGEMENTS

I would like to express my deepest gratitude to my mentor, Professor Theodore Raphan, for his guidance and encouragement throughout the course of this research. I am particularly grateful for the many hours of technical discussions with him and the valuable suggestions he has made to this study, including the choice of this interesting research area, and his meticulous attention to the details in the writing of this thesis.

I would also like to thank all the members of my doctoral examination committee, Professors Mike Anshel (City College), Bernard Cohen (Mt. Sinai School of Medicine), Victor Pan, John I. Simpson (New York University Medical School), for the time and effort each has taken to read and give constructive comments.

I would especially like to thank Dr. Bernard Cohen for his encouragement and suggestions, especially in the early stages of the work, when the ideas for this work were first being formulated.

I would also like to thank Drs. Sergei Yakushin and Mingjia Dai for much helpful discussion. I would also like to express my appreciation to Yevgeny Buharin and Dmitri Ogorodnikov for implementing and helping maintain the VMF program, which was utilized in my work.

I would also like to thank Dr. Ted Brown, Executive Officers of the Computer Science department of the Graduate Center of CUNY and Dr. Aaron Tenenbaum, Chairman of the Department of Computer and Information Science at Brooklyn College of CUNY for their support during the course of this study. The fellowship support from

the Graduate Center and the tuition support from Brooklyn College were instrumental in helping me support myself during the course of this work.

I would especially like to thank my wife, Li Ming, for her irreplaceable help and support throughout the course of this work.

Finally, I would like to acknowledge the financial support of the National Institute of Health under grants DC03284 (National Institute of Deafness and Communicative Disorders, NIDCD), DC05222 (National Institute of Deafness and Communicative Disorders, NIDCD), P30 D2C0504 (National Institute of Deafness and Communicative Disorders, NIDCD), EY 04148 (National Eye Institute), and a NASA Cooperative Agreement NCC 9-58 with the National Space Biomedical Research Institute (NSBRI). I would also like to acknowledge the support from New York State HEAT grant (CUNY) and grants from PSC-CUNY.

TABLE OF CONTENTS

LIST OF TABLES

LIST OF ILLUSTRATIONS

CHAPTER 1 INTRODUCTION

Eye movement or oculomotor control is important for directing gaze so that objects of interest can be clearly seen. This is accomplished in part by making rapid eye movements or saccades from one point to another (Dodge and Cline 1901; Robinson 1964) or by following objects with smooth pursuit (Robinson 1965). Another important component of oculomotor control is to maintain stable gaze and orientation of the head, body and eyes in the presence of changing accelerations during linear and circular walking, running, and jumping (Hirasaki, Moore et al. 1999; Hirasaki, Moore et al. 1999; Moore, Hirasaki et al. 1999; Imai, Moore et al. 2001). These functions are subserved by the angular VCR (aVCR), linear VCR (lVCR), angular VOR (aVOR), and linear VOR (lVOR). The kinematical and dynamic behavior of these systems and their interaction can be modeled by dynamical systems. Recently, the kinematical relationships between the motions of the body, head and eyes have been described as linear translations and rotations of the body, head and eyes relative to a trajectory coordinate frame, which translates in two dimensions relative to a spatial coordinate frame (Imai, Moore et al. 2001). Although the transformations between the body, head and eyes have been described as relationships among the different coordinate frames, the frames have been defined in terms of rigid body structures and not related to anatomical landmarks. One purpose of this thesis is to develop a procedure for establishing well-defined coordinate frames for the body head and eyes, relate these frames to well-defined body and head landmarks, and develop a scheme for relating the relative motion of the coordinate frames in three dimensions. Another purpose of this study is to develop a methodology using homogeneous transformations (Fu, Gonzales et al. 1987) to model the kinematical

changes in body, head, and eye movements during walking while following an arbitrary trajectory in three-dimensional space. These transformations can be represented as 4x4 matrices and form a group structure known as SE(3) (Murray, Li et al. 1994). We define these matrices as displacement matrices. How these matrices can be used to extrapolate, interpolate, and filter body, head and eye movements during locomotor trajectories in space is not known. It is also not clear how the invariants that have been found during locomotion, such as head and gaze fixation points (Hirasaki, Moore et al. 1999; Hirasaki, Moore et al. 1999; Moore, Hirasaki et al. 1999; Imai, Moore et al. 2001) relative to the body are represented in terms of such matrices. The development of such a methodology would establish relatively simple criteria for studying locomotion and is developed in this thesis.

Locomotion on a treadmill or overground activates both the aVOR and lVOR and generates compensatory eye movements in response to head rotation in the vertical plane (Grossman, Leigh et al. 1988; Demer and Virre 1996; Crane and Demer 1997; Moore, Hirasaki et al. 1999). Horizontal nystagmus is generated, which maintains constant gaze in space during head oscillation during straight walking and turning (Grasso, Prevost et al. 1998; Imai, Moore et al. 2001). In addition, there are orienting head and eye movements, which tend to align gaze with the GIA (Imai, Moore et al. 2001). A model-based investigation of the temporal aspects of ocular compensation in three dimensions during locomotion, however, has not been carried out. In this study, we have developed the computational tools that will be necessary to make this possible.

The organization of the thesis is as follows: Chapter 2 summarizes the work that has been carried out that defines the parameters of locomotion and how the vestibular

system might help to coordinate the trunk, head and eye movements during the locomotion process. Chapter 3 defines coordinate frames for the body, head and eyes and how we have related these coordinate frames to body landmarks. Chapter 4 describes the equipment (OPTOTRAK, Northern Digital) used to calibrate and measure trunk and head movements. We also describe the computational procedures that were developed to acquire and analyze the data. Chapter 5 develops the theoretical and algorithmic bases for how the compensatory and orienting components of the lVCR contribute to the kinematics and dynamics of head movements in two dimensions during treadmill and overground locomotion as well as perturbed walking. Chapter 6 introduces the mathematical background and derives formulas for computing the axes and pivot points of moving rigid bodies, as well as their distribution in space. Chapter 7 applies the methods of Chapter 6 to describe the axes of head yaw rotations in different pitch positions. Chapter 8 presents our results regarding the trunk and head movements during treadmill and overground locomotion.

CHAPTER 2 BACKGROUND

2.1 Kinematics of Bipedal Locomotion

Locomotion is a rhythmic stepping motion, which transports the body from one location to another. Bipedal locomotion has been modeled as an inverted pendulum, which is inherently unstable, but the system is stabilized and maintains equilibrium and balance by repetitive stepping (Zatsiorky, Werner et al. 1994). Much work has been done on the kinematics of bipedal locomotion, since the first studies were done over a century and half ago (Weber and Weber 1836) and a terminology for describing the basic kinematics of walking has emerged (Inman, Ralston et al. 1981; Zatsiorky, Werner et al. 1994) (Fig. 2.1). The gait cycle (stride) is defined as a pattern corresponding to a single period of motion, which is further subdivided into two phases: the double support phase and the swing phase. Note that according to this definition the swing phase consists of two single supports. A single step consists of the motion from the heel strike of one foot until the succeeding heel strike of the other foot. The number of steps (respectively strides) performed per unit of time defines the step/stride frequency. The step length is defined as the difference between position of some anatomical point on the weighted foot during the swing phase of a step and position of the same anatomical point on the other foot during the following step, projected onto the anterior-posterior axis. Stride length is similarly defined as the distance covered by a point on one foot over a gait cycle. When walking on a treadmill, distance is measured relative to the moving treadmill. The step length together with the step frequency defines the walking pattern.

Each step of the gait cycle can be further divided into a swing phase and double support stance phase. During the stance phase, both feet are on the ground, but the extended

limb supports the weight of the body and is referred to as the weighted leg (Inman, Ralston et al. 1981). During the swing phase, the unweighted limb swings forward and there are pelvic rotations about a vertical axis and rotation about a horizontal axis (listing), accompanied by flexion of the knee of the non-weight bearing limb (Inman, Ralston et al. 1981). There is also flexion of the knee of the weight-bearing limb in the stance phase of the cycle. The supporting leg is in stance phase at heel strike when the leg is extended.

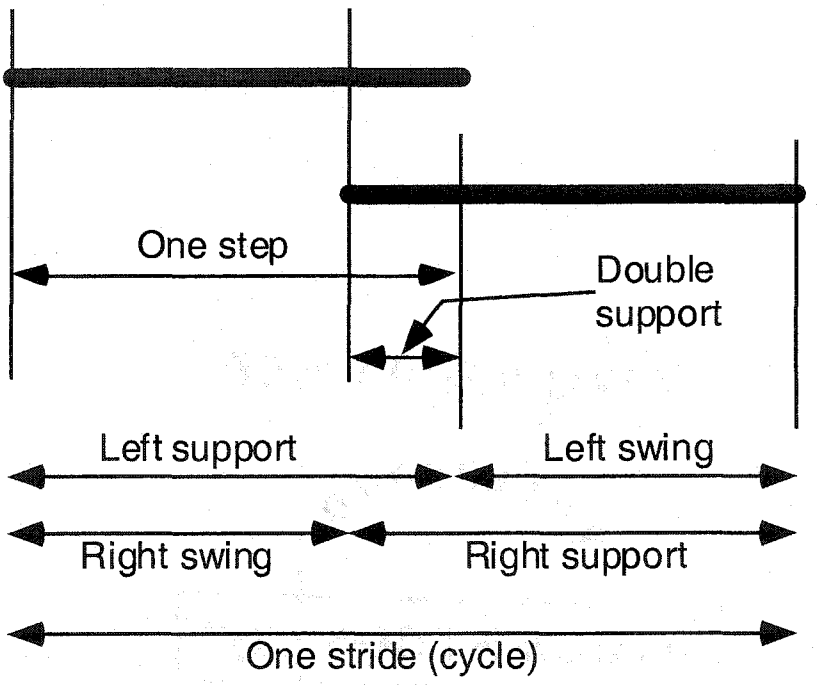

Fig 2.1 Gait stride (cycle) from (Zatsiorky, Werner et al. 1994)

According to these definitions, the walking velocity is given by the product of the step length and step frequency. The components of gait produce a sinusoidal vertical displacement of the center of mass of the body as the subject goes from the stance to the swing phase. The vertical modulation increases with step frequency. Since there are two steps to every stride cycle, the oscillation is at two times the stride rate. Early models of

locomotion have concentrated on the kinematics of the feet and lower limbs and had assumed that the Head Arms and Trunk (HAT) were essentially one link in the pendular structure, to which locomotion had been tied (Winter, MacKinnon et al. 1993; Winter and Eng 1995). The importance of head rotation and gaze stabilization during locomotion had been underestimated.

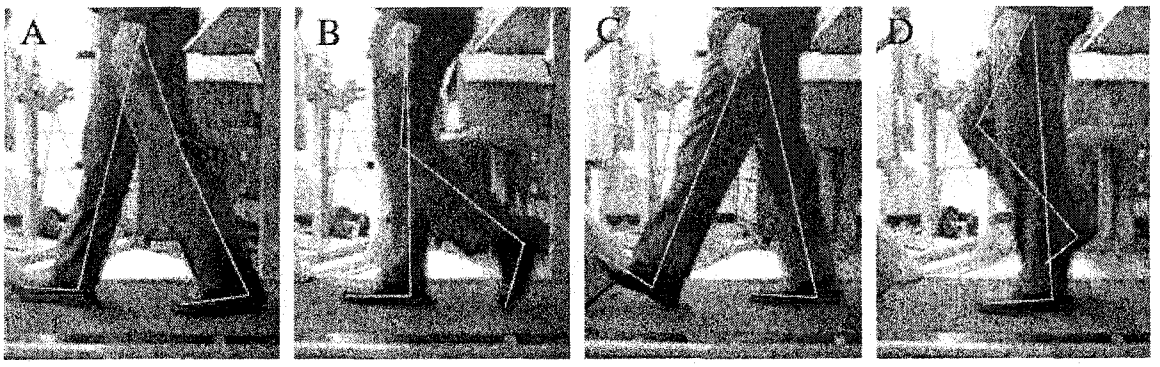

Fig 2.2 Locomotion phases: **A.** Double stance, **B.** Toe-off, **C.** Heel strike, **D.** Single stance (of next step)

2.2 Body and Head Movements During Locomotion

Recently the importance of a "top-down" organization that controls locomotion has been explored. This approach has focused on the idea that there is an organized set of movements during locomotion whose main purpose is to stabilize gaze (Pozzo, Berthoz et al. 1990; Mergner and Rosemeier 1998). As the body moves from the stance to the swing phase, vertical translation of the trunk and trunk rotation are accompanied by head perturbations, which activate the angular and linear vestibulocollic reflexes (aVCR and lVCR). Information about head movements during walking has accumulated rapidly in this decade. This has led to the utilization of head rotation during locomotion as a measure of balance in patients with vestibular abnormalities (Grossman, Leigh et al. 1988; Pozzo,

Berthoz et al. 1991); children (Assaiante and Amblard 1992; Assaiante and Amblard 1993; Ledebt, Bril et al. 1995; Ledebt and Wiener-Vacher 1996), elderly people (Hirasaki, Kubo et al. 1993) and astronauts post flight (Bloomberg, Reschke et al. 1992; Reschke, Bloomberg et al. 1994; Bloomberg, Peters et al. 1997). During walking, the head is stabilized relative to space. It oscillates linearly within a few centimeters, and rotatory motion is confined to a few degrees (Berthoz and Pozzo 1988). Within this small range, the head rotates actively in the pitch (Grossman, Leigh et al. 1988; Pozzo, Berthoz et al. 1990; Crane and Demer 1997; Hirasaki, Moore et al. 1999; Moore, Hirasaki et al. 1999; Imai, Moore et al. 2001). The pitch rotation of the head is believed to compensate for its vertical translation to maintain the stability of gaze (Crane and Demer 1997; Hirasaki, Moore et al. 1999; Moore, Hirasaki et al. 1999; Imai, Moore et al. 2001).

Kinematical trajectories of head and trunk rigid bodies were recorded for slow (0.6 – 1.2 m/s), moderate (1.2 – 1.8 m/s), and fast (1.8 – 2.2 m/s) velocities while walking on treadmill (Hirasaki, Moore et al. 1999). In addition, a single marker was attached to the left heel in order to establish the stride length and the step frequency. The relative contributions of step frequency and stride length to the walking velocity were estimated using the stride length index (SLI) defined as the ratio of the logarithm of the ratio of two stride length over the logarithm of the ratio of two walking velocities multiplied by 100% for two different walking velocities. With increasing walking velocity both the stride length and the step frequency tended to increase monotonically, however for the walking velocities between 1.0 and 1.6 m/s the contribution of the stride length was more significant (SLI > 50%), and outside of this range, the contribution of the step frequency was more significant (SLI < 50%). Although at lower walking velocities the pitching of the head was small and unrelated

to the vertical translation of the head, at higher walking velocities, the pitch rotation of the head was in phase with the vertical translation of the head (pitching down while translating upwards and, conversely, pitching up while translating downwards). Thus, pitching of the head was compensatory to the vertical head translation. Moreover, the intersection of the naso-occipital axes of the head in the two extreme positions during a step cycle remained approximately the same over all step cycles. This point was defined to be the head fixation point (HFP), while the distance from such point to the trunk was denoted as the head fixation distance (HFD). The values of the HFD exhibited significant inter- and small intra-subject variability (Hirasaki, Moore et al. 1999). The relationship of head movement to fore-aft body movement has not been fully explored, either for treadmill or overground locomotion. Neither has it been explored how the head rotates in three dimensions. In this thesis we explore some of these issues.

Recently, a novel representational scheme for describing the linear and angular motions of the body, head and eyes relative to a trajectory frame has been developed (Imai, Moore et al. 2001). Using this representation, it was shown that the body, head and eyes compensate and orient to variations in the GIA during straight walking and turning, consistent with what might be expected if the movements were generated from the vestibular system. In this thesis, we develop the mathematical representations for accomplishing this. We will also investigate parameters of locomotion that have proven to be extremely useful in assessing the compensatory behavior of the head and eyes during locomotion on a treadmill, which include Head Fixation Point (HFP) and associated Head Fixation Distance (HFD) (Pozzo, Berthoz et al. 1990; Hirasaki, Moore et al. 1999; Moore, Hirasaki et al. 1999). We show how these parameters could be connected to the gain of the

vestibulocollic reflex. In this thesis, we also define these parameters in three-dimensional space during overground walking and develop algorithms to study how HFP varies during overground locomotion.

2.3 Kinematical Description of Head Movement

Since head movements during locomotion have now been shown to be a critical part of the stabilizations of gait, it becomes important to understand the kinematics and coordinate system that best describes head rotations. Studies of head rotation imply a possibility that the three-dimensional control of the head movement and posture may be similar to those of the eye: the commands originate in a "velocity-like" form and then a neural integrator is utilized to convert them into positional signals (tonic neurons, hold posture)(Crawford, Martinez-Trujillo et al. 2003). It has been suggested that the neurophysiologic location of such integration may be situated in the midbrain of the interstitial nucleus of Cajal (INC). Unilateral stimulation of the INC resulted in head movements consistent with charging a neural integrator (Klier, Wang et al. 2002). Despite this, the dynamics of head movement during locomotion that relate head linear acceleration and rotational velocity are poorly understood. One of the aims of this thesis was to examine this relationship in two dimensions during overground locomotion with and without head constraints that could modify these dynamics (CHAPTER 5). While rotations have been applied to eye movements, the description of head kinematics is more challenging since the eye is usually described as possessing only three rotational degrees of freedom, whereas for the head six independent variables are required. It therefore becomes important to establish a coordinate frame that will minimize translations of the

coordinate frame when the head is rotated. This requires a fairly exact calibrating procedure to identify the origin and axes associated with head rotation.

One of the first studies to develop a methodology for calibrating head coordinate frames is described in (Medendorp, Melis et al. 1998). They used four landmarks including near auditory canals on the ears and in front of the (closed) eyes (Medendorp, Melis et al. 1998). The recorded coordinates of the landmarks were used to transform the target coordinates into the coordinate frame associated with the primary head position and has been identified as the helical axis approach. This approach is an application of Chasles theorem that states that an arbitrary displacement of a rigid body can be represented as rotation about a certain axis by a certain angle, followed by translation along the same axis by a certain distance (See Appendix B for an intuitive explanation of the theorem). An infrared tracking system was used to record coordinates of markers fixed to the head over an interval of time, and the resulting data was used to determine the parameters of the helical axis. This was done by finding the rotation matrix and translation vector of the head rigid body via a least squares fit (Veldpaus, Woltring et al. 1988), and then converting them to the helical axis parameters, namely the position of the axis in space, as well as the amounts of rotation about-, and translation along- the axis.

The subjects had their trunks fixed in space, while allowing for unrestrained motion of the head. The subjects were instructed to look at 12 eccentric targets, and the trajectories of motion from the central target were analyzed. The distribution of rotation vectors in space was found to obey Donders' law with only small deviations. It was found that the rotation axes for purely horizontal head movements passed near to the midpoint of the two semi-circular canal organs. It was still not clear, however, how the rotation

axes of the head would vary with different head positions and whether the rotations are related to anatomical landmarks associated with the spinal column. In this thesis, we utilize our methodology for obtaining precise coordinates and then determine the coordinate axes as the head is oscillated in roll, pitch, and yaw at different head positions. We also compare the yaw rotations of the head in these positions to the axis of the dens as determined from MRI measurements (Kunin, Delman et al. 2004; Raphan, Kunin et al. 2004). In the next chapter, we consider how the coordinate frames were established.

CHAPTER 3 LANDMARK BASED COORDINATE FRAMES

A first step in characterizing body, head, and eye movements during locomotion is to establish well defined coordinate frames for all these parts and consider them as rigid body motions in space subject to the repetitive stepping by the feet. The coordinate frames for the eye have been established in numerous studies of the vestibuloocular reflex (See Raphan and Cohen, 2002 for review). Head frames have been considered in terms of stereotaxic coordinates in animals and the use of Reid's line in humans (Atlas, Neurology, 1962 #1721). However, an appropriate reference frame for which the head can be considered as a rigid body and a pivot point for head rotation established, as the origin of the head coordinate frame has not been developed. Moreover, a similar coordinate frame for the trunk has not been established. In this Chapter, we will consider how to appropriately define these coordinate frames so that we can quantify their translations and rotations to be related to known body landmarks.

3.1 Trunk Coordinate Frame

The trunk coordinate frame was defined by three points, which lie approximately in the midsagittal plane (Fig 3.1). These are the jugular notch (**a**), the xyphoid process (**b**), and the T1 vertebrae (**c**). These points form a plane from which the origin and axes of the body coordinate frame was determined.

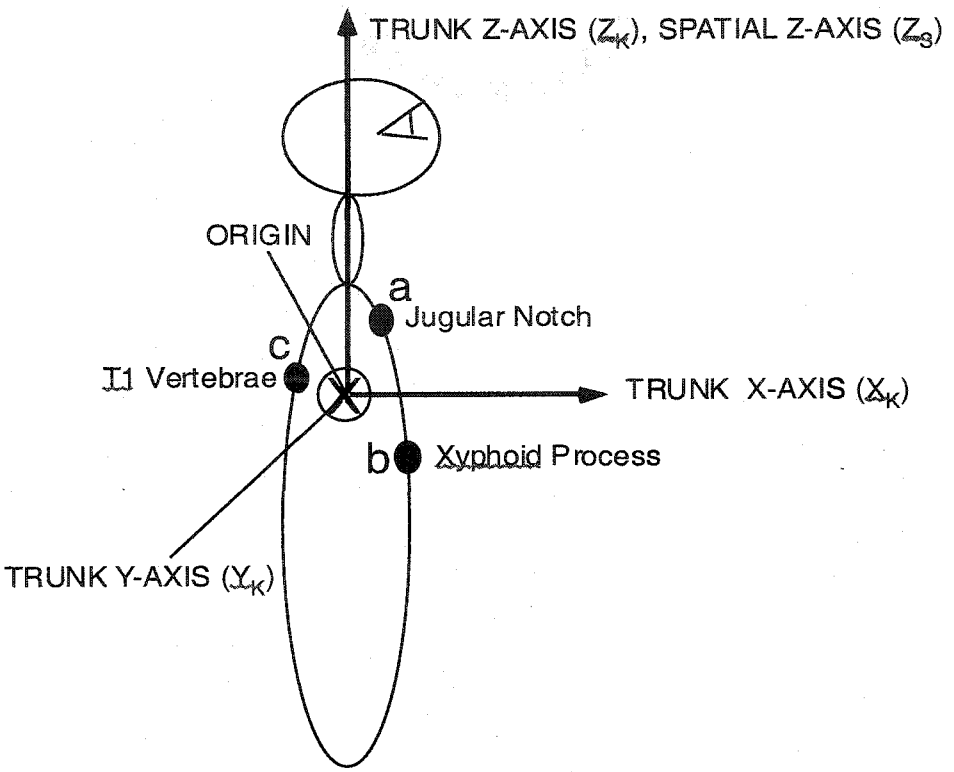

Fig 3.1 Stick figure of side view of the points from which were derived the body coordinate frame. (a) **T1 vertebrae**, (b) **Jugular Notch**, (c) **Xyphoid process.** The direction of the trunk Y-AXIS (Y_K) is shown by the symbol, ⊗, corresponding to a line directed away from the observer. The trunk Z-AXIS (Z_K) is aligned with the spatial vertical axis (Z_S) in primary position.

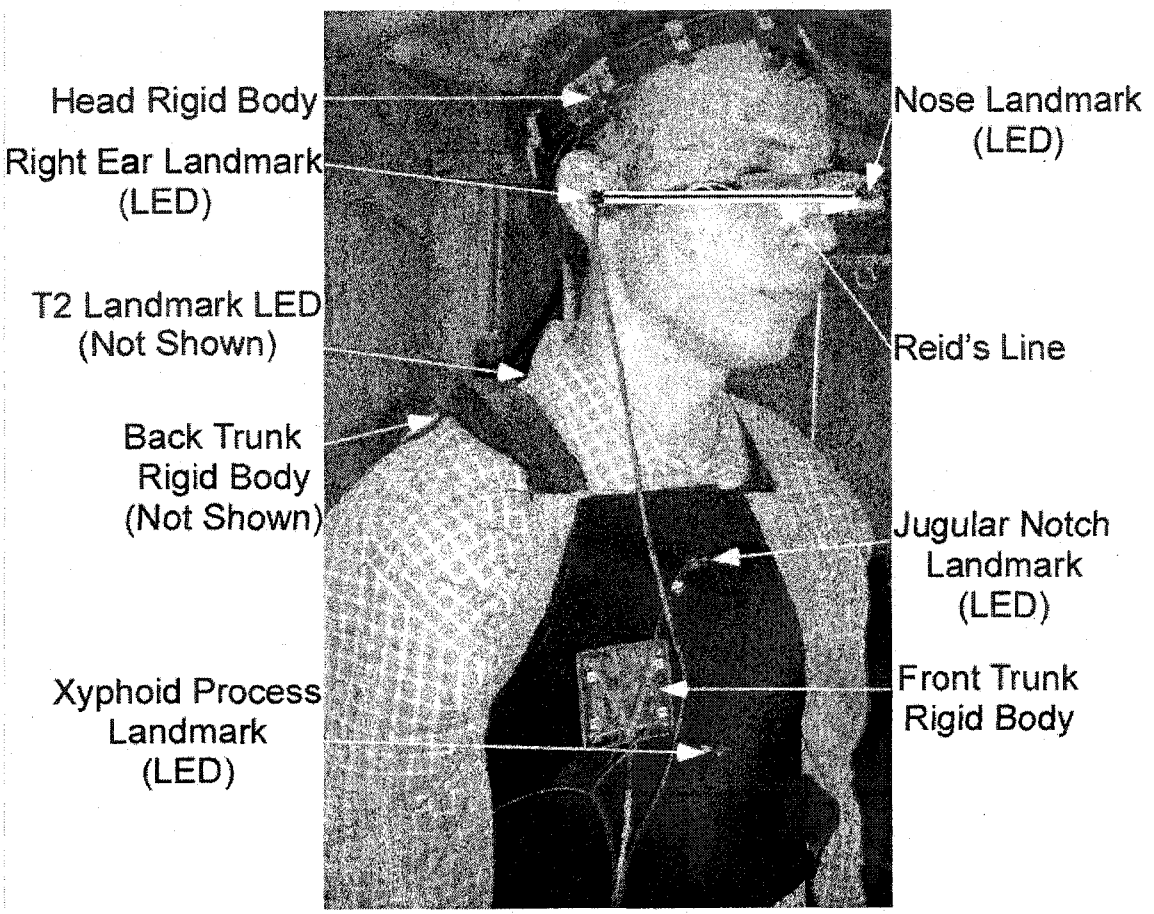

Fig 3.2 Front of Subject in Primary Position (With Permission from Subject)

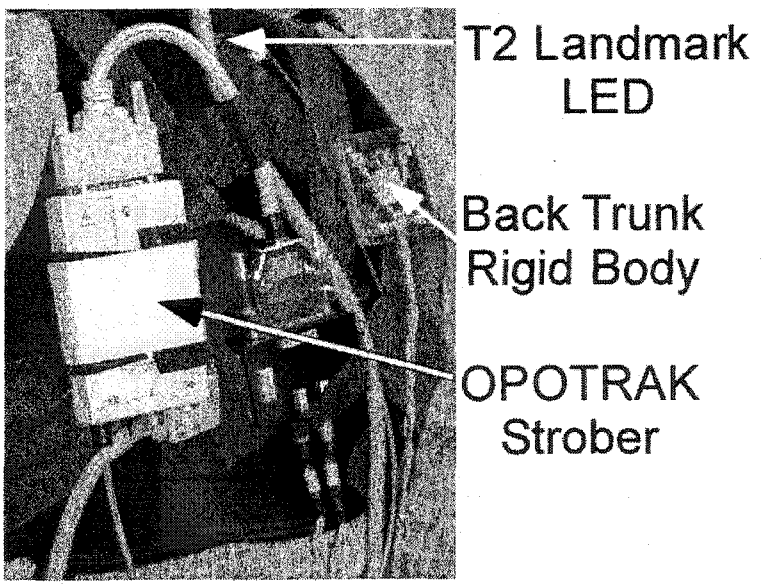

Fig 3.3 Back of Subject in Primary Position (With Permission from Subject)

The origin of the coordinate frame was the average of the three points. We defined primary position of the trunk as that position when the subject was instructed to sit upright in a chair during calibration. Therefore, the **Z**-axis of the trunk coordinate frame was chosen along the spatial vertical. The **X**-axis was established such that it was perpendicular to both the **Z**-axis and the normal to the plane of the landmarks. The positive direction is along the line coming out of the front of the trunk. The **Y**-axis completed the right-handed coordinate triple, whose positive direction is shown by cross, ⊗, corresponding to a line directed away from the observer (Fig 3.1).

3.2 Head Coordinate Frame

The head coordinate frame was also determined from three landmarks based a plane determined the Reid's baseline on either side of the head. The right Reid's baseline extends from the right external auditory meatus (EAM) to the inferior rim of the bony orbit (inferior rim orbit) (Fig 3.4A, **Dashed Line from EAM to inferior rim orbit**). Because of the symmetry of the skull, it was assumed that the two Reid's lines lie in a plane. An extremal point on the nose was chosen such that the plane formed by this point and the two EAM's (Fig 3.4, **f**; Fig 3.4B, **e**, **f**).

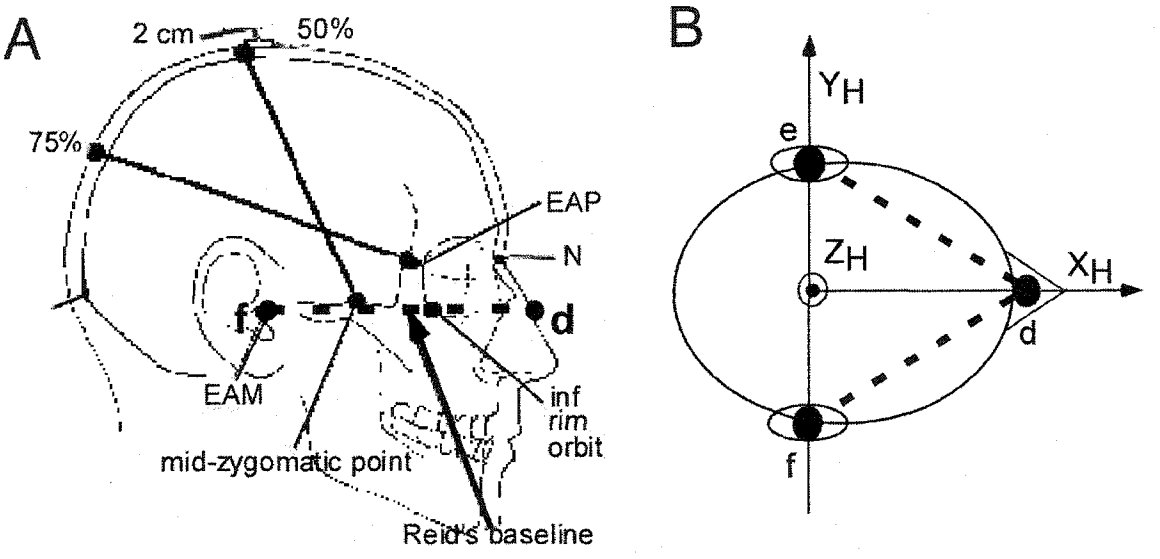

Fig 3.4 Figure of right (A) and Top (B) view of the head and points used to define the head coordinate frame. The dashed line in (A), shown Reid's baseline from the right side view, joining the external auditory meatus (EAM, e) and the point on the nose (d), which is an extension of Reid's baseline. A similar line can be found on the left side, joining points f and d. These points form a plane whose normal is defined as the yaw axis of the head coordinate frame. The line joining points on the two external auditory meatii is the interaural axis and is defined as the Y-axis of the head coordinate frame (YH).

A line orthogonal to the line segment joining points e and f, passing through point d, on the nose is the roll axis of the head coordinate frame (XH). The Z-axis is out of the top of the head and is designated by the symbol ⊙.

The **Y**-axis (Y_H) was defined along the interaural axis with the positive direction from the right to the left EAM. The origin was chosen at the point where the nose landmark projected onto the interaural axis, which was approximately at the midpoint of the line segment joining the points **e** and **f** (Fig 3.4B). The positive **X**-axis (X_H) was along the line from the origin to the nose landmark. The positive **Z**-axis (Z_H) was chosen to complete the right-handed coordinate triple and is designated by the symbol ⊙. We have ignored gross asymmetries of the skull and any steriotaxic coordinate frame would be subject to asymmetries.

3.3 Eye Coordinate Frame

The eye coordinate frame is defined as X_E, the visual axis whose positive direction is toward the observer (Fig 3.5). The Y_E axis is toward the subject's left. The Z_E axis is the axis coming out of the top of the eye. This coordinate frame is used to define the reference position of the eye. The movement of the eye is defined in terms of a rotation in the head coordinate frame (See Above). Eye movements were not recorded or analyzed in this study.

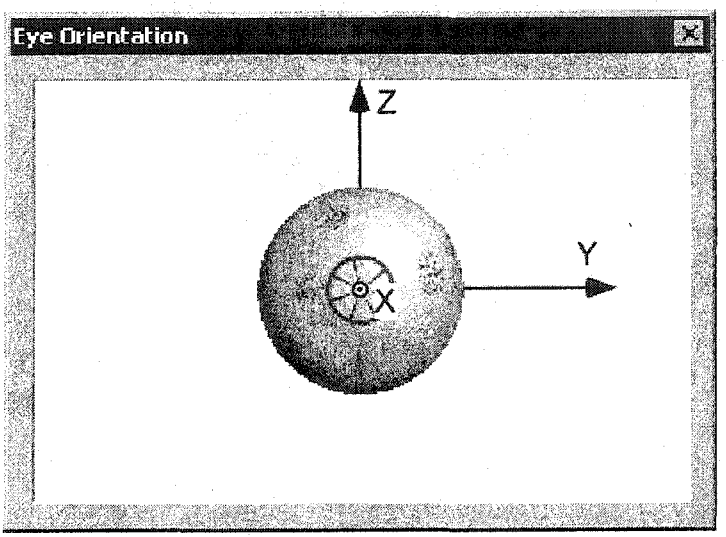

Fig 3.5 The Eye Coordinate Frame

CHAPTER 4 METHODS OF DATA ACQUISITION AND CALIBRATION

Two methods were utilized during the course of this research. One method was used in studying motion of the body and head in two dimensions during over-ground locomotion (the experimental work was done at Boston University by Drs. Raphan, Wall, and Oddsson, and assisted by Kathleen Sienko and Nick Patronik) (Kunin, Wall et al. 2003). A methodology for calibrating head movements in three dimensions was then devised for studying voluntary and reflex induced rotations of the head while making voluntary head movements in three dimensions, walking on a treadmill, overground. The different experiments will be considered below.

4.1 Calibration of Helmet and Sternum (Trunk) During Overground Locomotion for Two Dimensional Studies (Boston University)

In this study, rigid bodies were attached to a helmet worn on the head and approximately positioned over the center of rotation for pitching head movements. The rigid body attached to the sternum (trunk) on the upper chest. Since the analysis of these data was only directed at studying the dynamics of two-dimensional rotations of the trunk and head, the calibration was simplified. For a three dimensional analysis a more elaborate calibration procedure was developed, but its two dimensional character was compared with results obtained using the less rigorous calibration procedure. We consider this procedure next.

4.2 Calibration of Spatial and Landmark-based Coordinate Frames

The spatial coordinate frame and the coordinate frames for the trunk and head were determined using an OPTOTRAK system from Northern Digital, Inc. This system is comprised of a sensor with three cameras that view Infra-Red Light Emitting Diodes (IRED) (Fig 4.1).

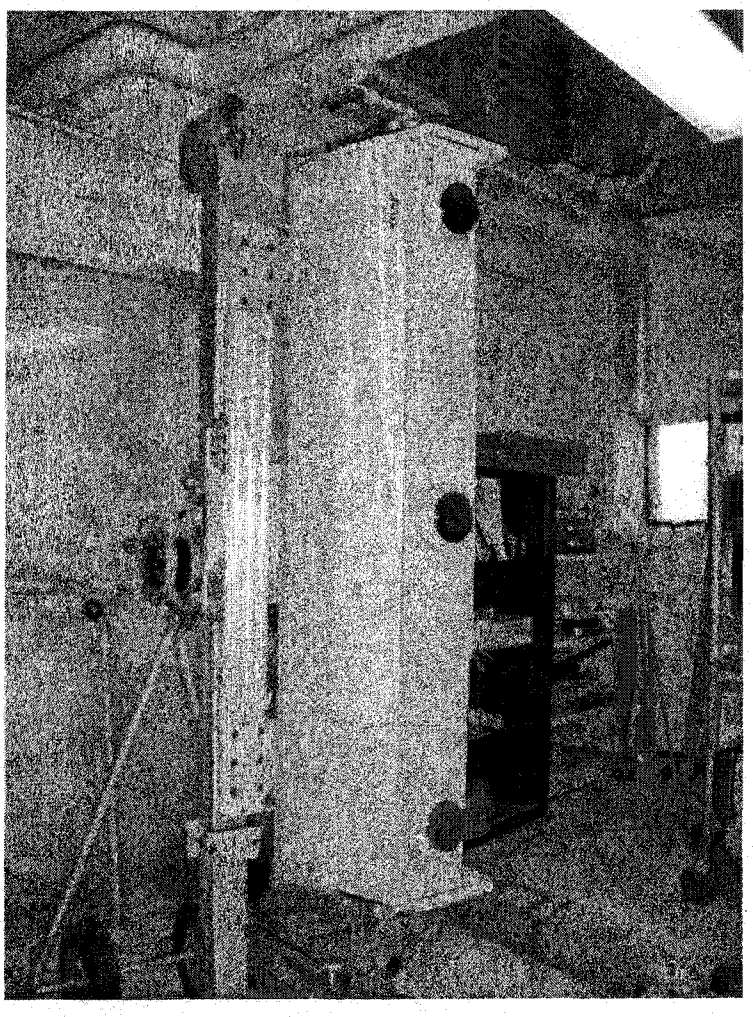

Fig 4.1 Picture of OPTOTRAK Sensor

The viewing angle is approximately 34° when viewed from the side (Fig 4.2B) and the distance covered is approximately 2.44x2.02 m^2 at a viewing distance of 4 m (Fig 4.2A). At viewing distances closer than 2 m, the data obtained are unreliable as the IREDs cannot be viewed (Fig 4.2A, Dotted Lines).

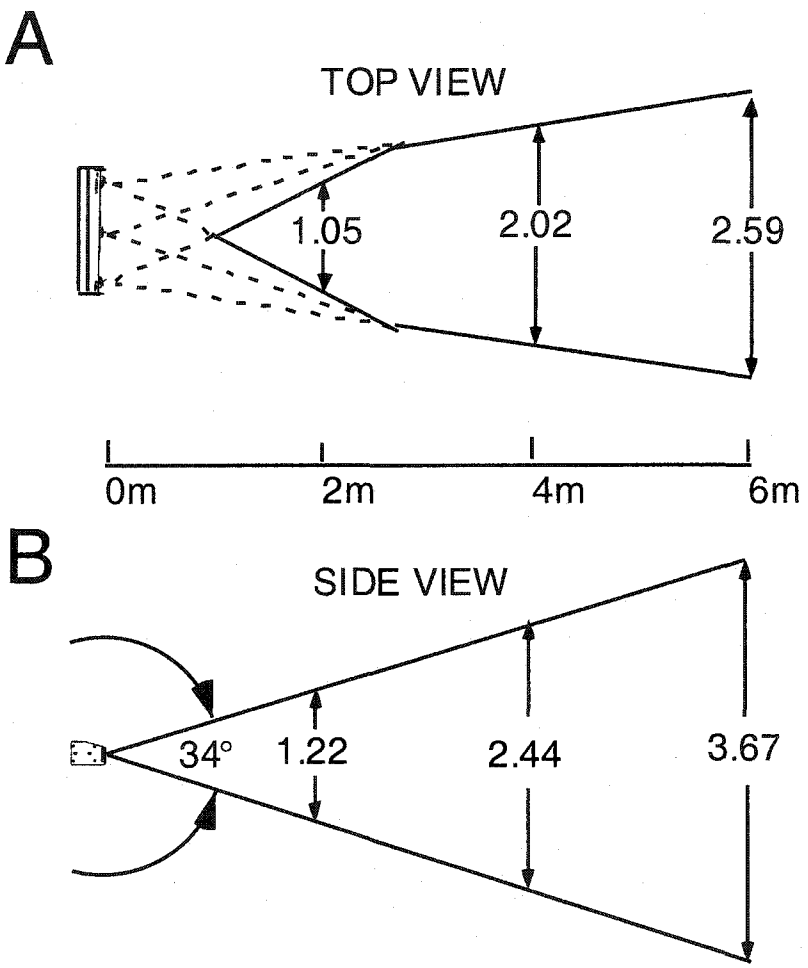

Fig 4.2 Viewing distances for OPTOTRAK sensor as a function of distance. **A.** Top View. **B.** Side View. The dotted lines in A indicate a non-viewing area.

The IREDs are strobed by a high-speed strober capable of pulsing at up to3000 pulses/sec (Fig 4.3).

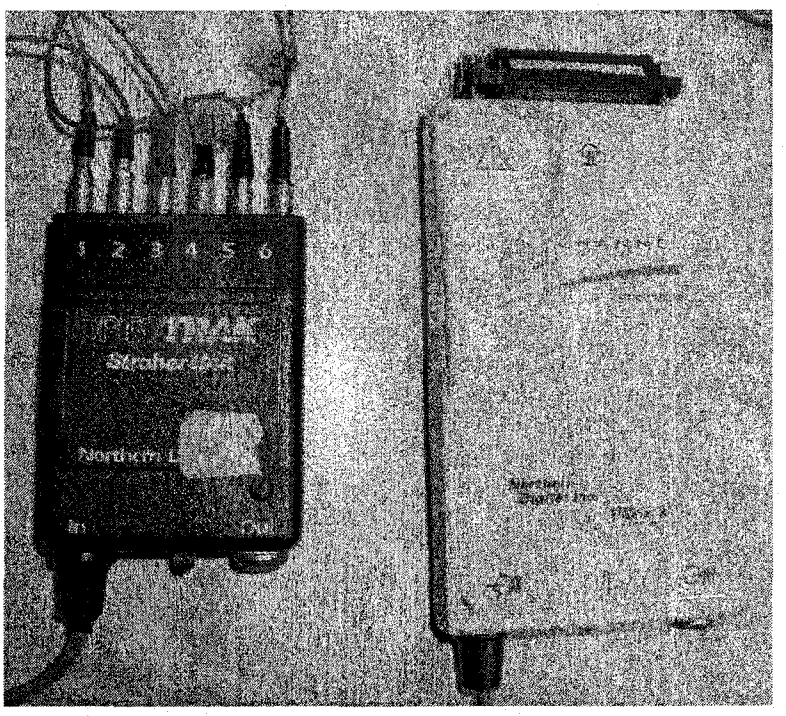

Fig 4.3 Two types of strobers used

Therefore, using up to 26 markers gives a frame rate of 111 frames/sec. We generally use a frame rate of 100 frames/sec, which covers all possible experimental configurations.

4.3 Spatial Frame Determination

The first step in the recording process was to establish a spatial coordinate frame. This was done by building a rigid body of 4 markers (Fig 4.4), which were positioned in a square arrangement with the side length of 24 cm between markers. One of the markers is designated as the origin (marker-4) and two other markers are designated as points through which the X_s (marker-1) and Z_s (marker-3) axes would go through. Marker-2 is used to ensure that the OPTOTRAK software properly creates the rigid body (Northern Digital, Inc). The Y_s axis is normal to the plane of the rigid body, denoted by the ⊗,

forming a right-handed coordinate frame. Once the spatial frame has been established, all marker coordinates are aligned to this frame. The spatial frame rigid body was either placed on the wall or on a treadmill, depending on the experiment being performed.

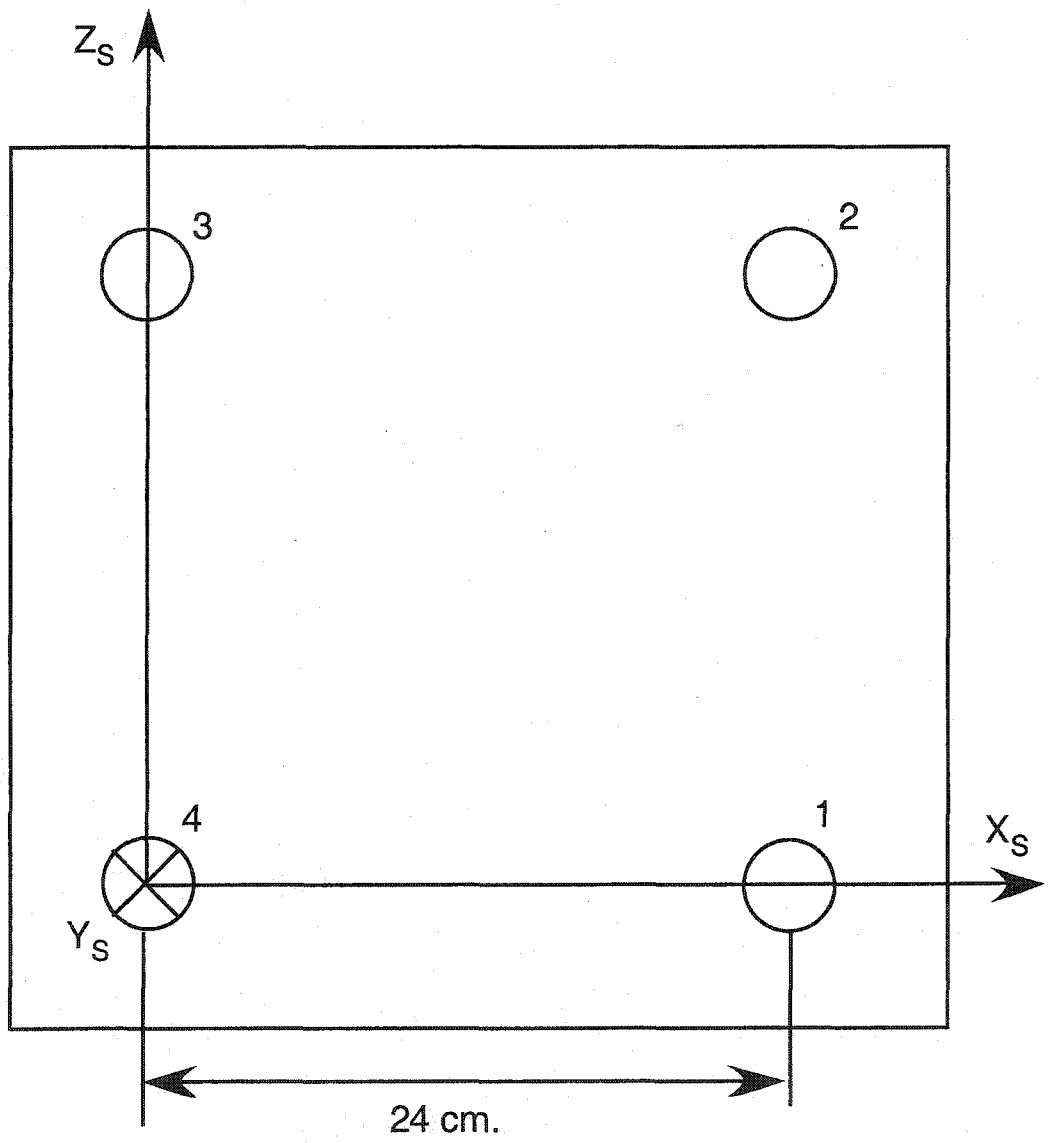

Fig 4.4 The rigid body for the spatial coordinate frame calibration.

4.4 Determination of Trunk and Head Coordinate Frames

The second step in the calibration procedure is to determine the coordinate frames of the trunk and head in terms of the markers that identify the landmarks. Single markers were placed at known anatomical landmark positions on the trunk as described above (Fig 3.1, Fig 3.4). Markers for describing trunk trajectory in experiments following calibration were placed into rigid plastic holders (Fig 4.5). Markers were also placed at the front and two ear inserts on a band-style hearing protector that was embedded in a specially constructed plexiglas holder that contained an eyeglass nose piece that could be easily adjusted for a wide range of subjects (Fig 4.6). When worn, the markers were located at the landmarks that defined the head coordinate frame described above.

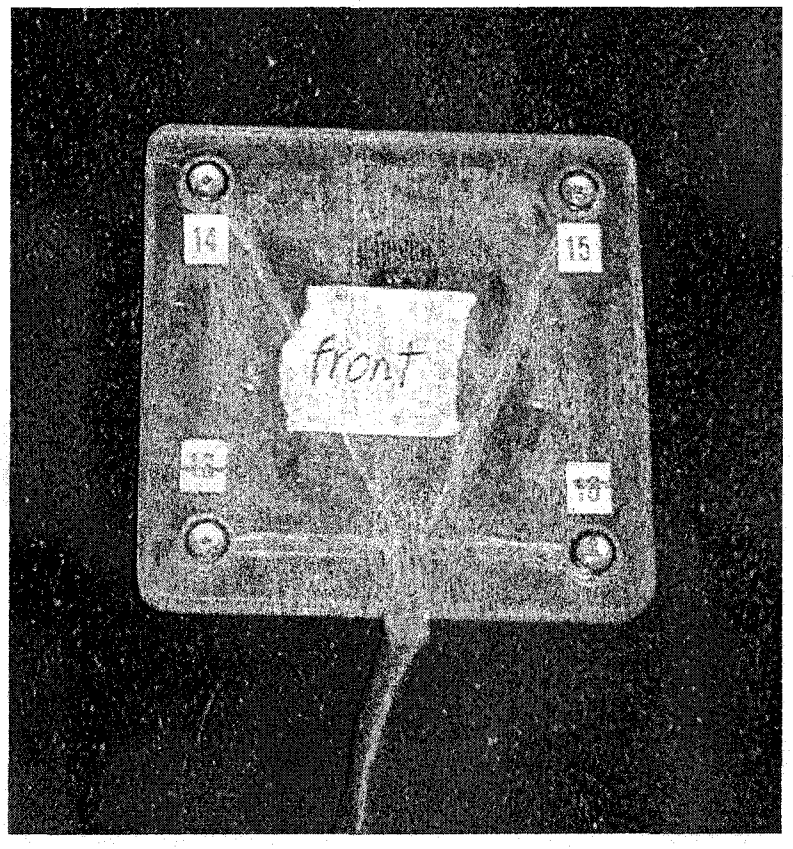

Fig 4.5 Trunk Rigid Body

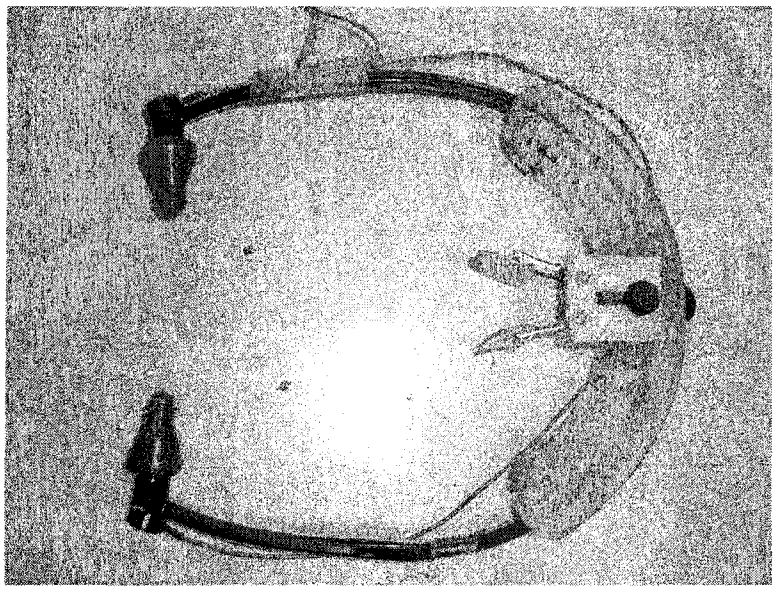

Fig 4.6 Head Calibrator

During calibration, the head-based markers, the trunk landmarks, the rigid bodies for tracking the trunk and head movements were located on the subject. Subjects are then placed on a small platform, which could be manually rotated about a spatial yaw axis of the subject for 30 sec ±200° while the head was held stationary relative to the body (Fig 4.7). Subjects were initially instructed to stand erect looking straight ahead at a visual target at eye level. This position was taken as the primary position for all coordinate frames for that subject. The marker coordinates were determined by a program (6DARCHITECT, Northern Digital, Inc.) during the manual rotation during calibration(Fig 4.7). After acquiring the data on the marker locations, a single rigid body file is constructed by the program that contains the coordinates of every marker location in space. The oscillations that occurred during locomotion were relative to this initial trunk position for each experimental trial.

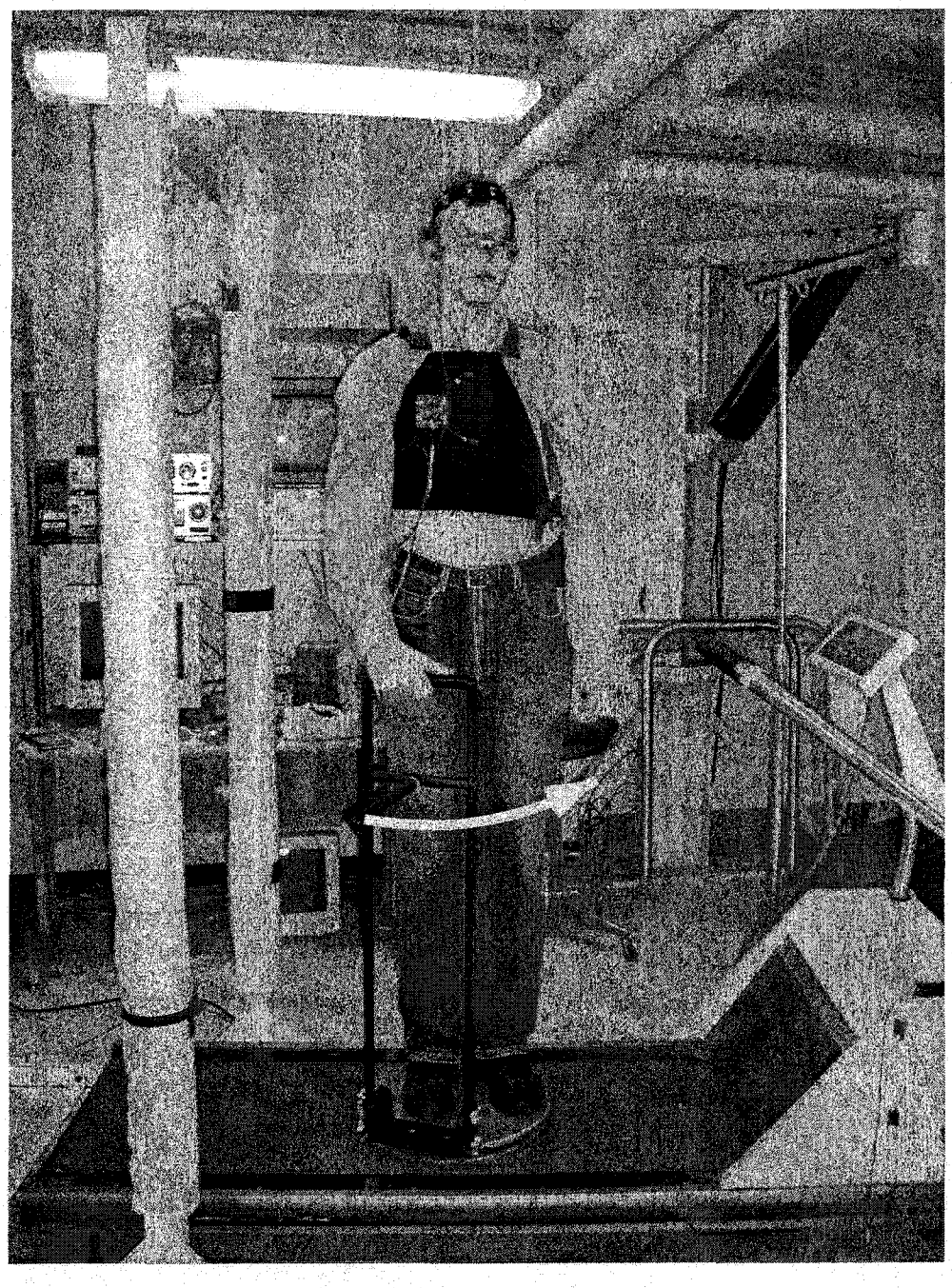

Fig 4.7 Subject Being Rotated for Calibration. Subject stands erect on a small rotating platform and is rotated slowly by hand over the calibration period.

Specialized scripts were written to parse the rigid body file created by 6DARCHITECT, which created separate trunk and head rigid body files. The landmarks coordinates were computed in the new landmark coordinate frame. From this a

transformation was obtained between the spatial and landmark frames for the trunk and head respectively. Files were than generated that contained coordinates of the head and trunk markers in their respective landmark coordinate frames. Following the calibration procedure, the landmarks positions were marked as imaginary and treated as virtual markers during data acquisition when performing experiments. The actual landmark markers were physically removed during the experimental protocol.

4.5 Organization of Files for Data Taking

Data acquisition during calibration and experimentation were organized into a specific file structure to facilitate the experimental procedure (Fig 4.8).

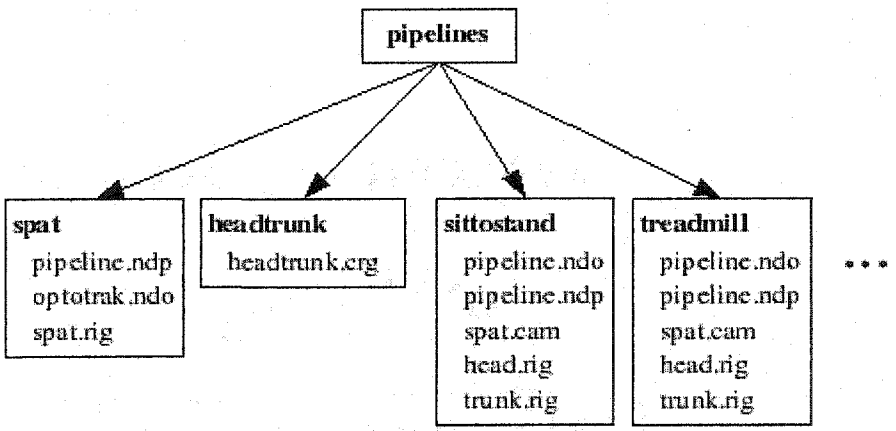

Fig 4.8 Directory Structure of OPTOTRAK TOOLBENCH Template Files associated with specific experiments.

A TEMPLATE directory was created, which contains Template Subdirectories. The subdirectories contain files that describe the equipment configuration for a particular paradigm. For example, the SPAT subdirectory contains pipeline.ndp, optotrak.ndo, and spat.rig. The file pipeline.ndp (Fig 4.9) describes the signal flow from Producers to Collectors (Fig 4.9, Left Panel). For defining the spatial coordinate frame, the pipeline.ndp merely describes how each marker is viewed in a TextViewer as the data are collected (Fig 4.9). The optotrak.ndo file contains information about the number of markers tracked, the port to which the markers are connected, the frame frequency, strobe frequency, the camera file for recording the data, and whether and type of Optotrak Data Acquisition Unit (ODAU) utilized. The optotrak.ndo file also contains the number of trials in the experimental paradigm. In the spatial calibration paradigm, the four markers were connected to Port 1, the frame frequency was 30 Hz, and the OPTOTRAK standard camera file was utilized. The ODAU, which is generally used for analog data acquisition was not utilized in this paradigm, which established the spatial frame.

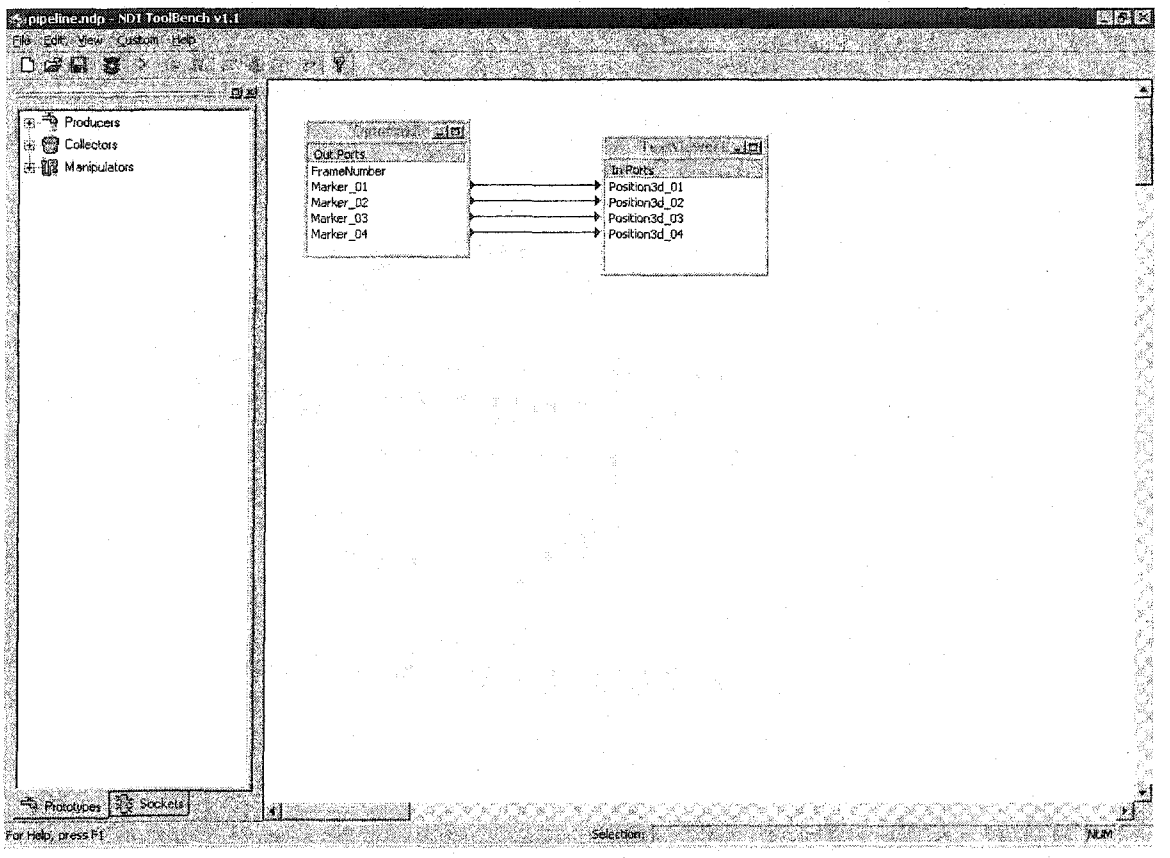

Fig 4.9 Screen Shot for the pipeline.ndp file for performing Spatial Calibration.

The Spat.rig file contains information about the rigid body that is used for defining the spatial coordinate frame.

The HEADTRUNK directory contains the HEADTRUNK.CRG file, which describes the equipment configuration used by 6DARCHITECT in building the head, trunk and landmarks rigid body file. SITTOSTAND and Other Paradigms would have their own associated pipeline.ndp and optotrak.ndo files (Fig 4.8).

4.6 Experimental Procedure Automation

To automate calibration and data taking, each experimental protocol is prepared in an **experiment description file** that is stored in a subdirectory of the Template directory. The experiment (Fig 4.10, Experiment <Root>) has subdirectories for each of the

subjects tested and an associated Spatial Calibration Subdirectory (Fig 4.10). In turn, each Subject subdirectory has subdirectories for each of the paradigms utilized in that experiment (Fig 4.10) that is associated with a paradigm subdirectory in the *template* directory described above. The procedure for calibrating and performing experiments can algorithmically be described and has been implemented as a Perl Script (Fig 4.11). To perform spatial calibration for a particular experiment, the corresponding Template files are copied into a subdirectory, which is referred to as the current spatial calibration subdirectory. Since the Template files contain zero as the number of trials, a single trial is appended to the current *optotrak.ndo* file and are opened by the TOOLBENCH program. The script then sends messages to the TOOLBENCH windows instructing the program to connect to the Optotrak and start pipeline evaluation. At this point we verify the visibility of all markers in the TextViewer window and record positions of the spatial frame rigid body markers into an Optotrak raw data file, r#001.dat. Once recording is complete the main window is closed, and the script invokes ALIGN_A, a program that creates a camera file *spat.cam* based on the files *r#001.dat* and *spat.rig*. These are stored in the SPAT subdirectory of the current experiment.

After the spatial frame calibration and the alignment are completed, the **experiment description file** is read and the script proceeds to the creation of individual subject subdirectories by querying the experimenter for subject ID's, which are then used as subject directory names. The 6DARCHITECT program is then used to create the dynamic rigid body file containing coordinates of all the data taking and calibrating markers. While performing this task, the program is driven by the *headtrunk.crg* macro file, which contains the equipment configuration as well as the rigid body build algorithm

and settings. The script copies this file from the *headtrunk* subdirectory of the template directory as well as the *spat.cam* from the spatial calibration directory to the current subject calibration subdirectory and starts the program, 6DARCHITECT. Once the program starts up, the script sends the messages to the program to open a dialog box prompting the user to select a macro file, and the user chooses the *headtrunk.crg* from the current directory. The user is then required to interact with 6DARCHITECT (See 6DARCITECT Manual) to create and save the rigid body file created from all the markers under the name *headtrunk.rig*.

Once the subject is calibrated, the experiments specified in the experiment description file are run by the script using the TOOLBENCH. This file contains sequence of references to template pipelines used for a particular paradigm, as well as descriptions of the trials to be performed in each paradigm. The template files *optotrak.ndo* and *pipeline.ndp* are copied from the template directory of the relevant paradigm, and then the *optotrak.ndo* file is modified to include the specified trials. After that, the pipeline is opened with the TOOLBENCH and data collection is begun.

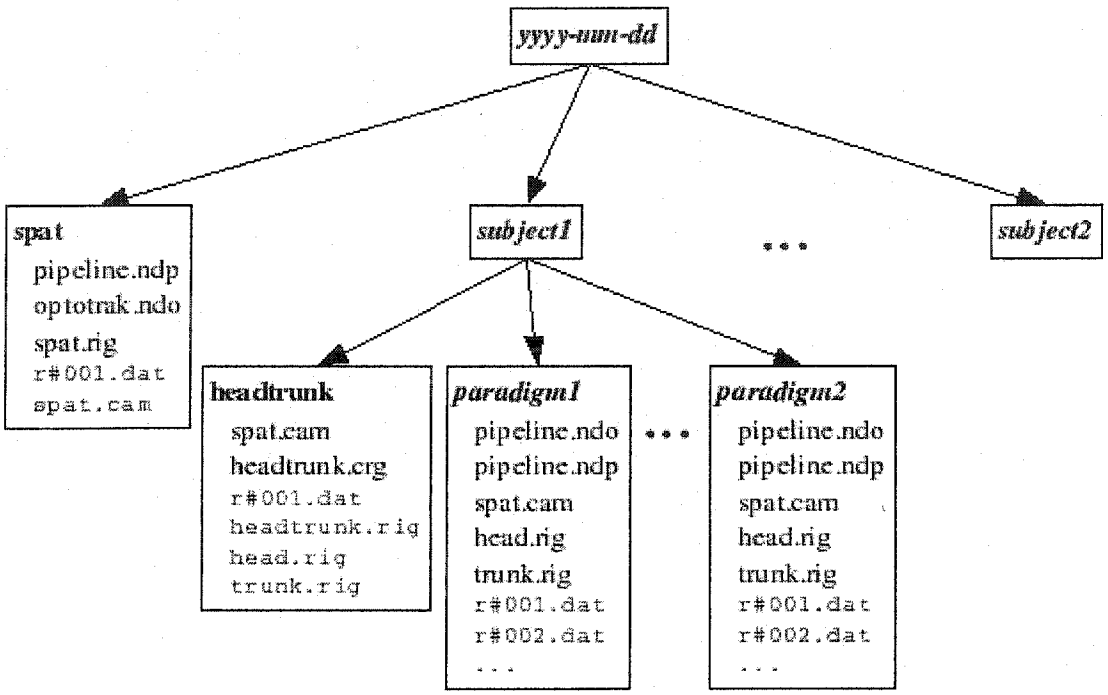

Fig 4.10 Tree-like organization of files during calibration and experimentation

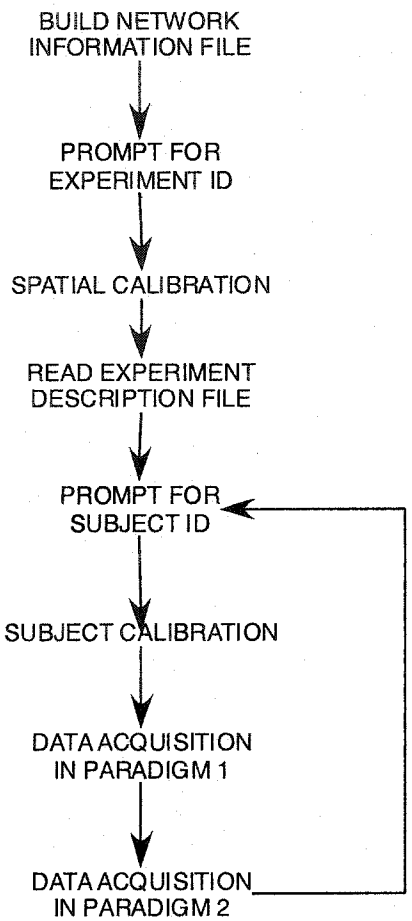

Fig 4.11 Flowchart of the data acquisition process

CHAPTER 5 TWO DIMENSIONAL ANALYSIS OF LOCOMOTION IN THE MIDSAGITTAL PLANE

5.1 Purpose

In this chapter, we examine the relationship between various parameters associated with head movement during walking and show how the vertically projected HFP (Hirasaki, Moore et al. 1999) is related to the gain of the head pitch vs. linear head movement during walking on a treadmill. When walking straight, the head undergoes vertical and fore-aft translations. Theoretically, both of these accelerations could contribute to pitching head movements. In this chapter, we examine both treadmill and overground locomotion to determine whether there were differences in the accelerations and the compensatory responses. We examine the power spectral components of gain and phase as well as the characteristics of the head fixation point.

5.2 Experimental Methods

5.2.1 Treadmill Locomotion

Four normal subjects walked on a linear treadmill while their trunk, head and heel coordinates were recorded using an OPTOTRAK video-based acquisition system (See CHAPTER 3). Their age varies from 30-58. Each subject walked at five velocities, ranging from 0.65 to 1.9 meters/sec. These were repeated twice for each of the following paradigms: walking without head constraint, while fixating a target at approximately 1-1.5 m, while wearing a neck collar constraint, while fixating a target at 20-25 cm, and

with eyes closed. Fig 5.1 shows a subject with soft and stiff collar constraints. Data were transformed from OPTOTRAK (Northern Digital, Inc.) binary format into ASCII and analysed by application software written for this purpose.

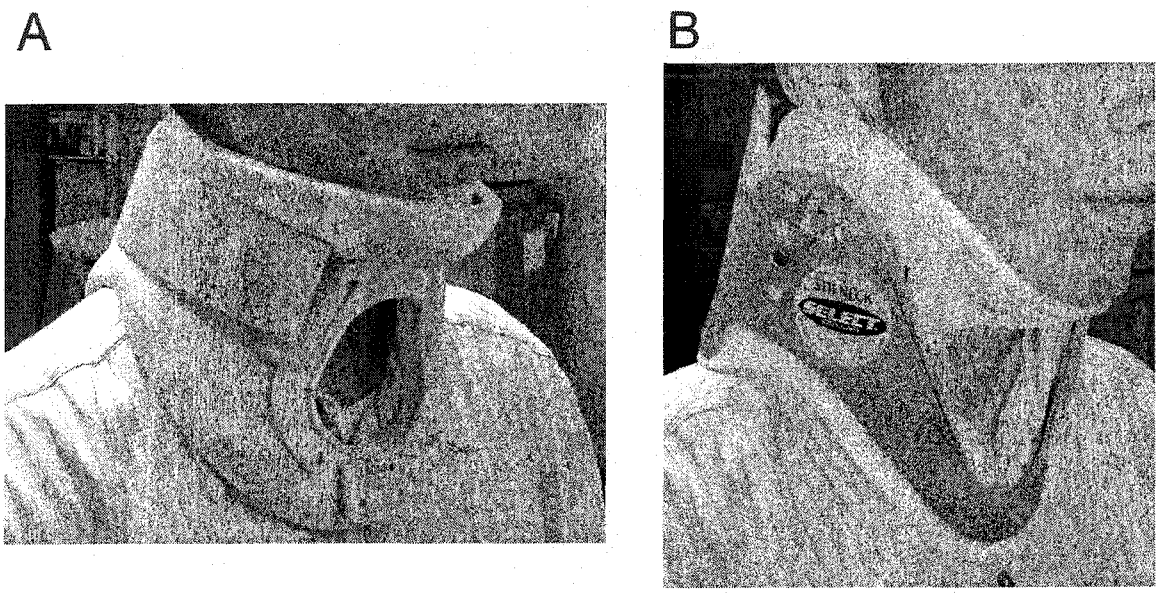

Fig 5.1 A. Subject wearing a soft neck movement-constraining collar, B. subject wearing a stiff neck movement-constraining collar.

5.2.2 Overground Locomotion

Six normal subjects walked over ground while their trunk, head, and shank coordinates were recorded using an OPTOTRAK video-based acquisition system (See CHAPTER 3). Each subject had three trials at slow, medium, and fast walking speeds without head constraint and three with a collar, which partially constrained the head (A collar similar to that shown in Fig 5.1 was used). Data were transformed from OPTOTRAK (Northern Digital, Inc.) binary format into the VMF format and analysed by

application software written for this purpose. Similar experiments were also performed when the subject experienced a forward and backward perturbation on the foot occurred at random times during the locomotion using a high-performance Balance Disturber platform (Boston University) (Fig 5.2). Fifty-four (54) trials per subject were performed.

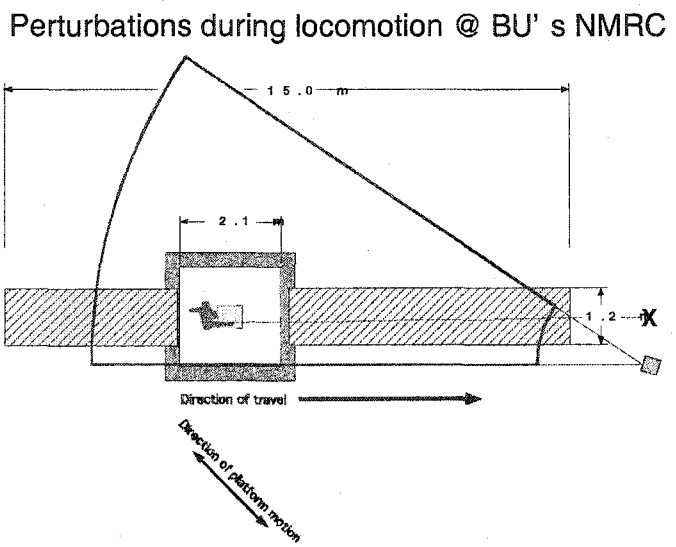

Courtesy of:
Conrad Wall III, MEEI and Lars Oddsson, NMRC, BU

Fig 5.2 Balance Disturber

5.3 Relationship between head vertical and for-aft acceleration

5.3.1 Treadmill locomotion

When vertical acceleration was plotted against fore-aft acceleration during treadmill walking, there was a distinct Lissajous pattern that was elliptical and whose eccentricity was dominated by the vertical acceleration (Fig 5.5).

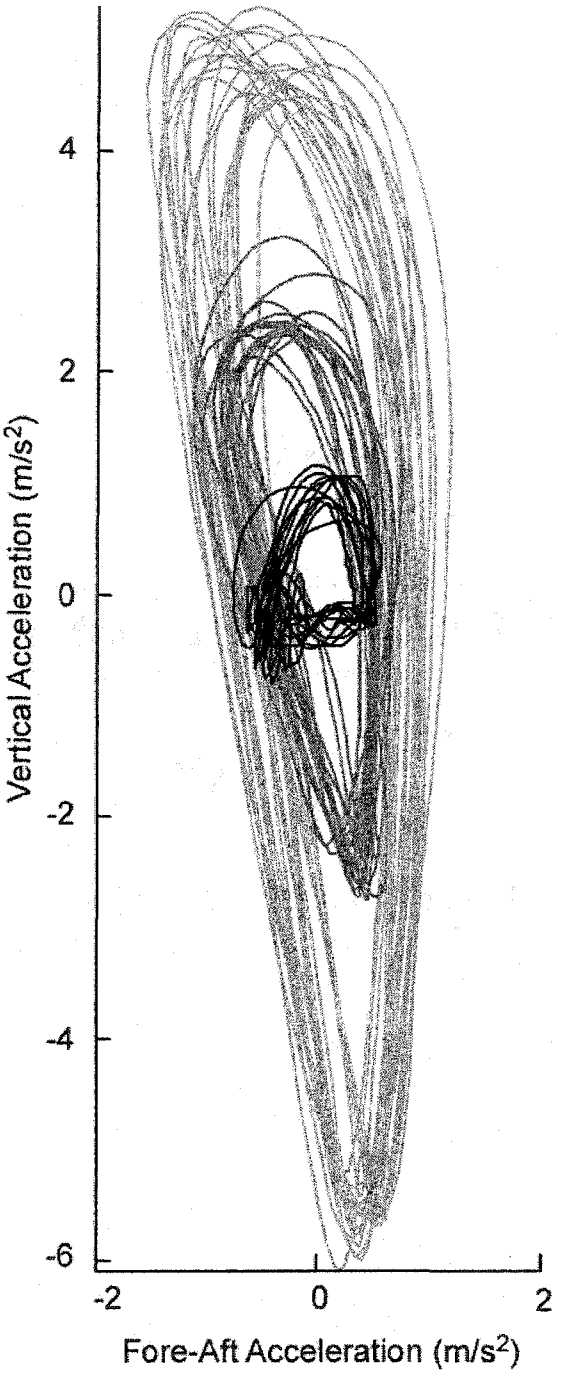

Fig 5.3 Example plot of vertical vs. fore-aft head acceleration during treadmill locomotion for slow (black), medium (dark gray), and fast (light gray) walking velocities.

The tilt of the major axis of the ellipse was close to the vertical. The phase difference $\angle\ddot{x} - \angle\ddot{z}$ was close to 80° for low stepping frequency, increasing to approximately 120° with increased stepping frequency (Fig 5.4). Maximal fore-aft accelerations reached more than 1 m/s^2, which is approximately 0.1 g. This was negligible compared to the vertical acceleration, which reached accelerations of 6 m/s^2 (0.6g) for fast walking velocities and high stepping frequencies.

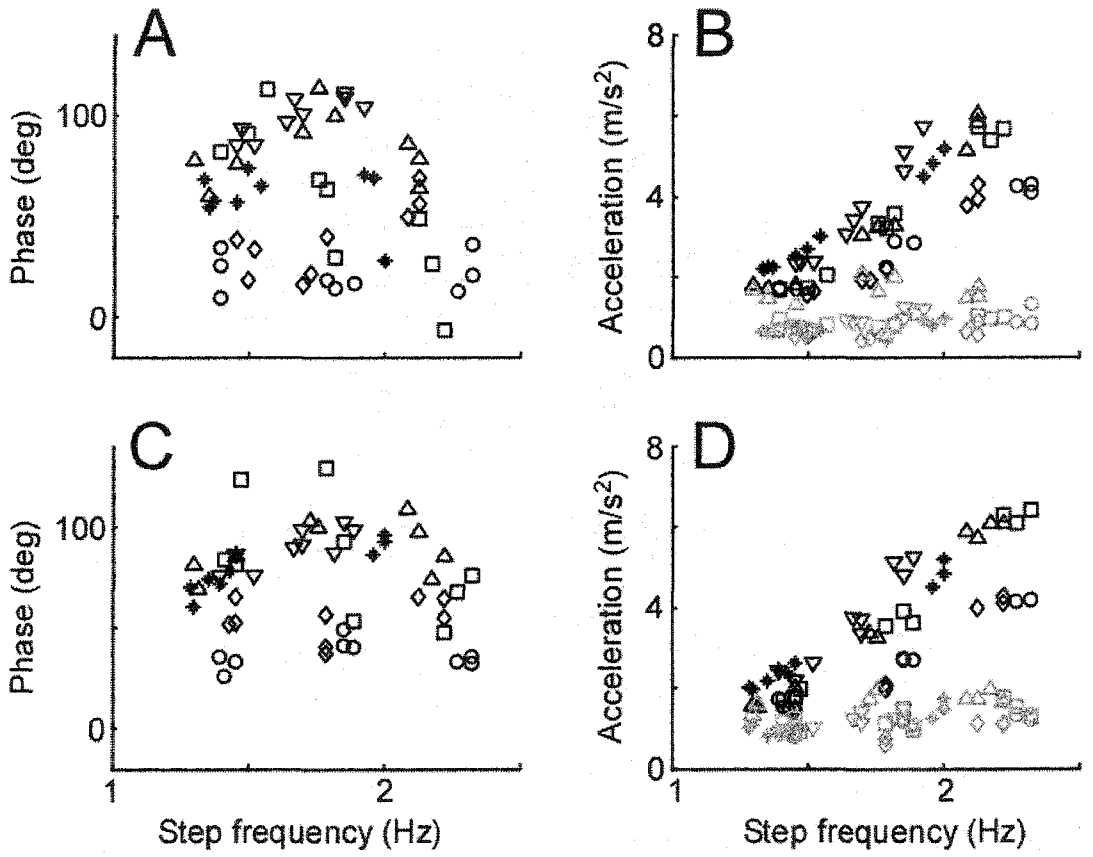

Fig 5.4 Average values of relative phase of the vertical and fore-aft accelerations of the head (A, C) and maximal fore-aft (light gray) and vertical (black) accelerations of the head (B, D), without (A, B) and with (C, D) a neck-restraining collar during treadmill locomotion. Subjects mjd(○), mk(◊), tr(□), and yo(▲).

5.3.2 Overground locomotion

When vertical acceleration was plotted against fore-aft acceleration, there was a similar Lissajous pattern to that obtained during treadmill locomotion. It also was elliptical and the eccentricity was dominated by the vertical acceleration (Fig 5.3).

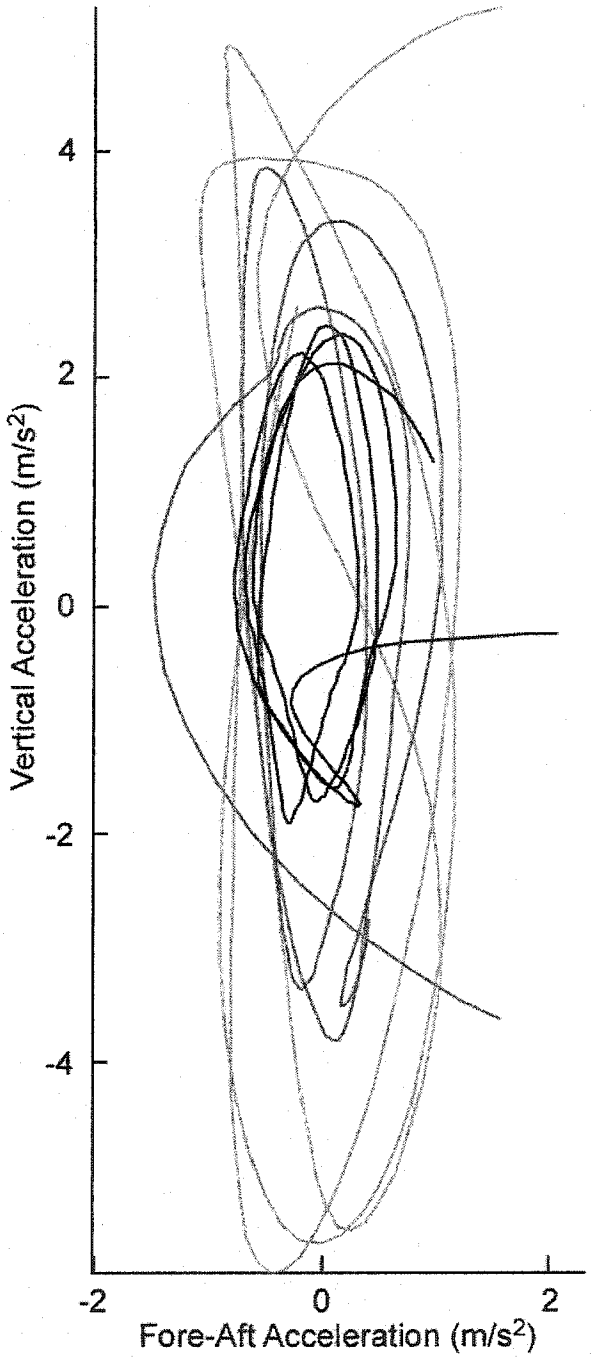

Fig 5.5 Example plot of vertical vs. fore-aft head acceleration during overground locomotion for slow (black), medium (dark gray), and fast (light gray) walking velocities.

The tilt of the major axis of the ellipse was close to the vertical indicating a phase difference between the two accelerations that were close to 90°. Maximal fore-aft

accelerations reached more than 0.5 m/s^2, which is approximately 0.05g. This was negligible compared to the vertical acceleration, which reached accelerations of 5 m/s^2 (0.5g). Because of the dominant acceleration of the vertical component, we neglected the fore-aft acceleration in the generation of the head pitch and only considered how the vertical acceleration impacted head pitch.

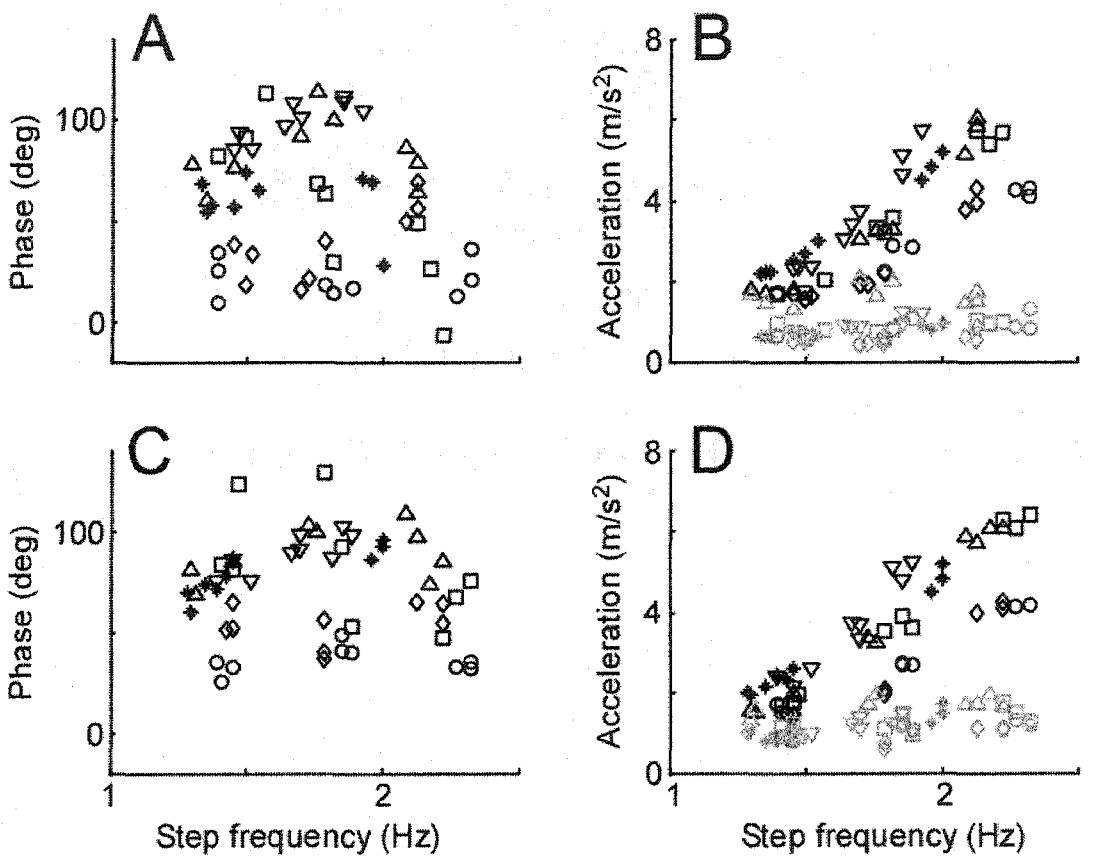

Fig 5.6 Average values of relative phase of the vertical and fore-aft accelerations of the head (A, C) and maximal fore-aft (light gray) and vertical (black) accelerations of the head (B, D), without (A, B) and with (C, D) a neck-restraining collar during overground locomotion.

Our conclusion from these experiments is that there are no clear-cut difference between the phase and magnitudes of the vertical vs. fore-aft accelerations during treadmill and overground locomotion. Because of the dominant acceleration of the vertical component, we neglected the fore-aft acceleration in the generation of the head pitch and only considered how the vertical acceleration impacted head pitch, which we consider next.

5.4 Estimation of Vertically Projected Head Fixation Point

5.4.1 Conceptual Basis and Computation:

The trunk and head coordinate frames are shown in Fig 5.7A, viewed in the midsagittal plane. These coordinate frames are aligned with the spatial coordinate frame in primary position at the start of the locomotion trial. The vertically projected HFP is defined as the point in the pitch plane of the head that optimally approximates the point of coalescence of naso-occipital axes as the head translates and pitches over the walking period (Fig 5.7B). The distance of the HFP from the head when it is in a position having zero pitch is defined as the Vertically-Projected Head Fixation Distance (VP-HFD, Fig 5.7B).

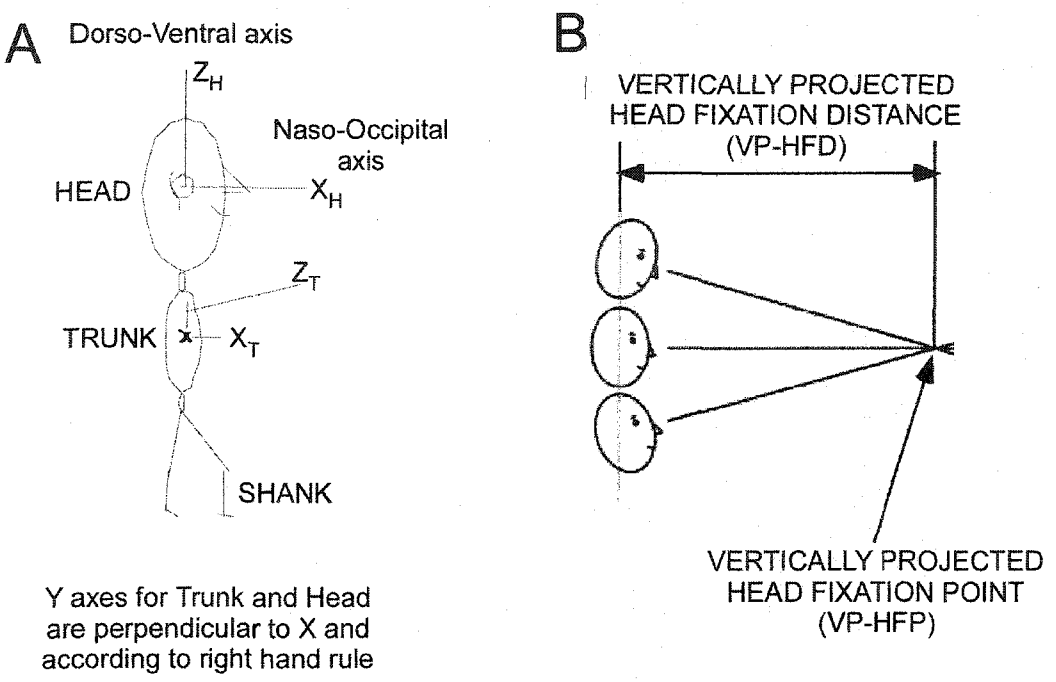

Fig 5.7 **A.** Assignment of coordinate frames. **B.** Operational Definition of Vertically Projected Head Fixation Point and the Distance from the HFP to the Head.

A set of lines in two dimensions representing projections of the naso-occipital axes on the pitch plane is given in the form $\{k_i, b_i\}_{i=1}^{N}$, where each line is given by the function $y = k_i x + b_i$. We find the head fixation distance by determining the x that minimizes the variance of the y's. Note that the following formulas are given for a coordinate system in the 2-dimensional plane with the X-axis directed to the right, and the Y-axis directed upwards, where the positive direction of the angle is the opposite of the positive direction of the angle about a pitch axis. Thus, in order to apply the formulas to the pitch plane data k_i has to be taken as $\tan(-\theta_i)$, where θ_i is the pitch angle of the head in space coordinates.

We approximate the estimator for the variance by:

$$V = \overline{y^2} - \overline{y}^2$$

where

$$\overline{y} = \frac{1}{N}\sum y_i = \frac{1}{N}\left(\sum k_i\right)x + \frac{1}{N}\sum b_i$$

and

$$\overline{y^2} = \frac{1}{N}\sum y_i^2 = \frac{1}{N}\left(\sum k_i^2\right)x^2 + \frac{2}{N}\left(\sum k_i b_i\right)x + \frac{1}{N}\sum b_i^2$$

which yields a parabola, namely

$$N^2\left(\overline{y^2} - \overline{y}^2\right) = x^2\left(N\left(\sum k_i^2\right) - \left(\sum k_i\right)^2\right) + 2x\left(N\left(\sum k_i b_i\right) - \left(\sum k_i\right)\left(\sum b_i\right)\right) + N\left(\sum b_i^2\right) - \left(\sum b_i\right)^2$$

which achieves its minimum at

$$x_{\min} = -\frac{N\left(\sum k_i b_i\right) - \left(\sum k_i\right)\left(\sum b_i\right)}{N\left(\sum k_i^2\right) - \left(\sum k_i\right)^2} \tag{5.1}$$

We also wished to determine whether the HFP was maintained with and without head constraints by a neck collar. Since HFP is a noisy measure of head compensation, the gain of the compensatory lVCR as measured from the correlations between the linear and pitch motions of the head should be related to the VP-HFD. This relationship is considered next.

5.4.2 Relationship Between Head Vertical Translation and Head Pitch: Gain of the Head Movement Reflex (Treadmill Locomotion)

The relationship of head pitch with vertical translation is characterized by a highly periodic stepping apparent in the vertical coordinate of the heel (Fig 5.8G), vertical head translation (Fig 5.8E), and pitch head rotation (Fig 5.8F) while walking on treadmill. (See also Fig 5.18 for overground locomotion).

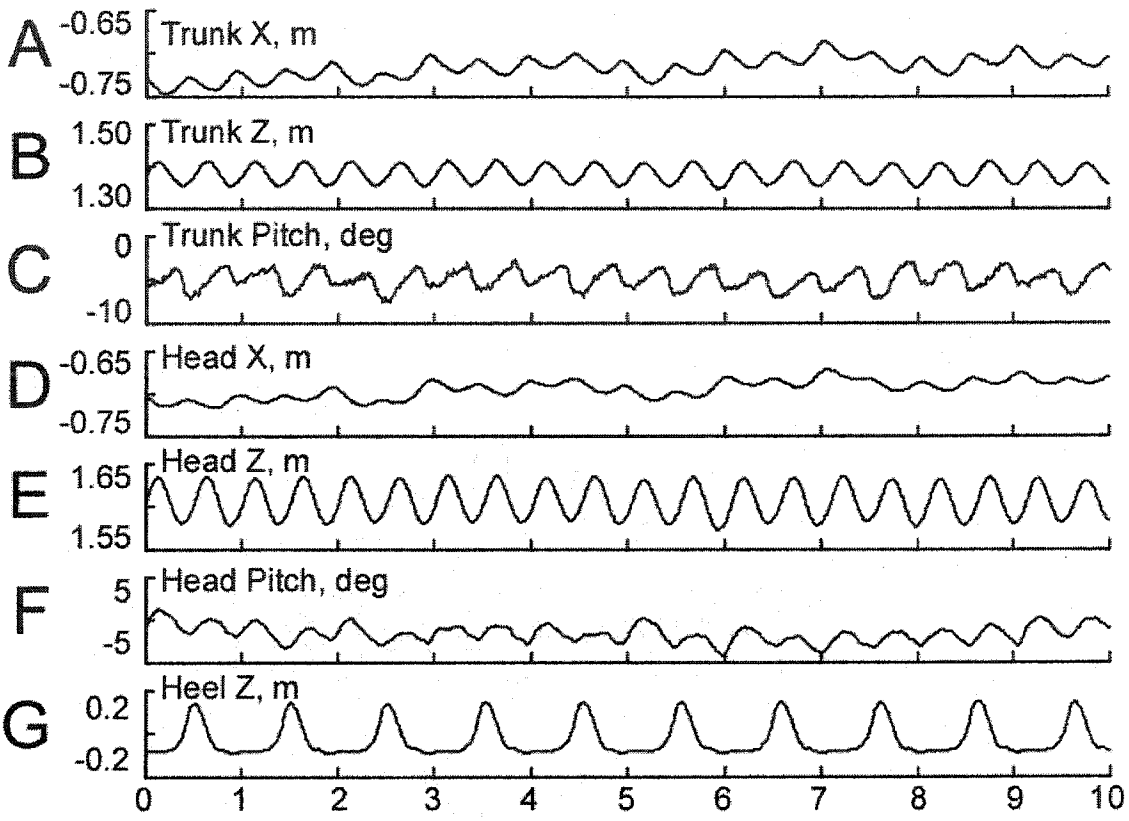

Fig 5.8 Steady state walking on treadmill (Position). All variables re space. A. Trunk X, B. Trunk Z, C. Trunk Pitch, D. Head X, E. Head Z, F. Head Pitch, G. Heel Z.

If the two signals were sinusoids at a single frequency, then each could be represented by an amplitude and relative phase as follows:

$$z = Z_0 \cos \omega_C t \tag{5.2}$$

$$\theta = \theta_0 \cos(\omega_C t - \varphi) \tag{5.3}$$

By differentiating (Eq. 5.2) twice, we obtain the acceleration of the head translation and by differentiating (Eq. 5.3) once, we obtain the angular velocity of the head pitch given as:

$$\ddot{z} = Z_0 \omega_C^2 \cos(\omega_C t - 180^0) \tag{5.4}$$

$$\dot{\theta} = \theta_0 \omega_C \cos(\omega_C t - \varphi - 90^0) \tag{5.5}$$

A simple two-dimensional geometric analysis of the relationship between the vertical head translation and pitch head rotation when they are in phase ($\varphi = 0$) gives:

$$\theta(t) = \tan^{-1} \frac{z(t) - z_0}{x_0} \tag{5.6}$$

where $\theta(t)$ is the pitch angle of the head (positive when looking down) and $z(t)$ is the vertical translation of the head. The point (x_0, z_0) is the head fixation point in the midsagittal plane. For small sinusoidal linear displacements and pitch angles, $\tan\theta \approx \theta$, and (Eq. 5.6) can be replaced by:

$$\theta(t) = \frac{Z_{amp} \cos(\omega_C t) - z_0}{x_0} \tag{5.7}$$

The corresponding phase difference between the vertical acceleration (Eq. 5.4) and the pitch velocity (Eq. 5.5) for this condition would be 90°. Moreover, since $z(t)$ is almost periodic, spectral methods can be utilized to estimate the coherence of the two variables, the phase difference between them and the ratio of head pitch and head linear movement. From this and knowledge of the VP-HFD, we could then compute the gain.

The ratio of the head pitch and head translation can be estimated from the ratio of the cross-power spectrum of the pitch velocity and vertical acceleration and the spectrum of the vertical acceleration. We used nonparametric methods to estimate the spectral content of the signals and their coherence (Schwartz and Shaw 1975; Proakis and Manolakis 1992). The estimates of coherence were computed by first finding the dominant frequency of the locomotion as the frequency at which the value of the cross-spectral density was a maximum. The Matlab (MATLAB, 6.5) CSD function was utilized for this purpose. The data were padded with zeros up to 4096 points in order to generate better resolution for estimating the dominant frequency.

The head acceleration and pitch velocity had cross-correlation signals that were approximately sinusoidal with linearly decreasing amplitudes at slow (Fig 5.9A), medium (Fig 5.10A), and fast (Fig 5.11A) walking speeds These cross-correlations were biased estimates so as not to distort the data far from zero shift (Proakis and Manolakis 1992). This linear decay reflects the finite time interval of data chosen for analysis. The cross-spectral density had a dominant peak at a frequency that was close to the stepping frequency.

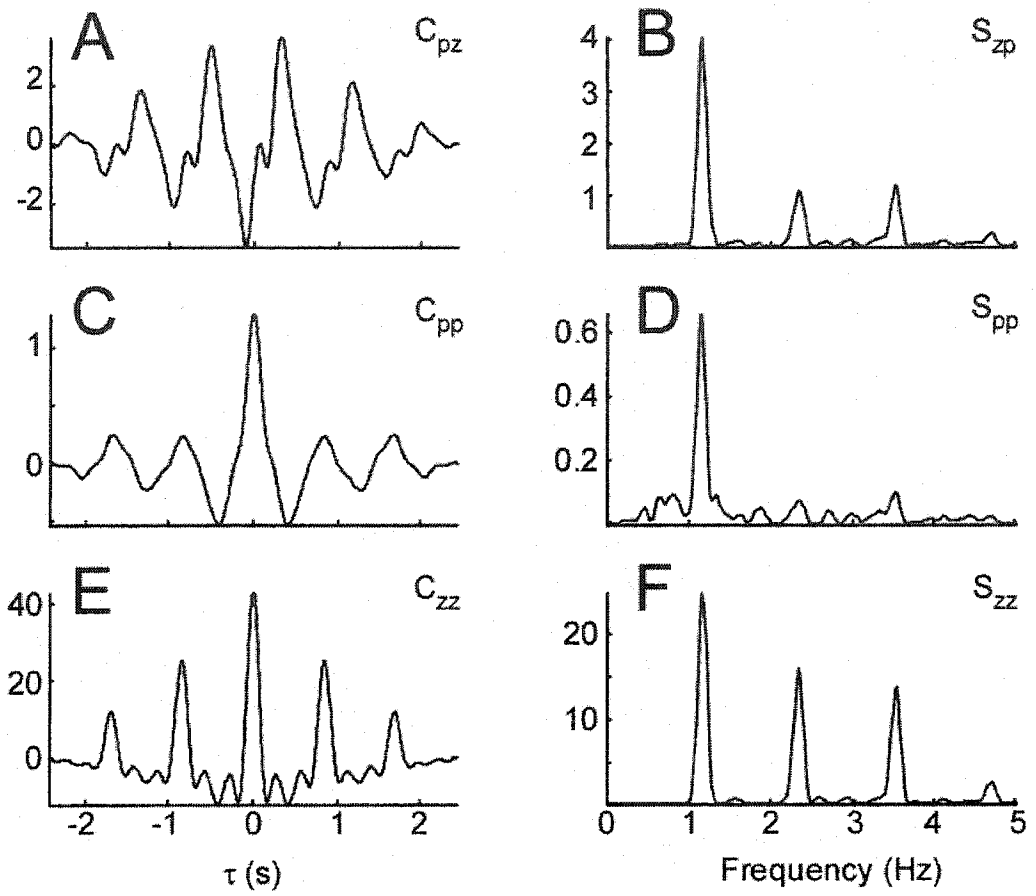

Fig 5.9 Slow treadmill locomotion. Averaged cross- and auto- correlations are presented using the same window size (but not windowed) and overlap as when computing the coherence function. **A.** Cross-correlation of Pitch Velocty with Vertical Acceleration, **B.** Cross-spectrum of Pitch Velocity and Vertical Acceleration, **C.** Autocorrelation of Pitch Velocity, **D.** Power spectrum of Pitch Velocity, **E.** Autocorrelation of Vertical Acceleration, **F.** Power spectrum of Vertical Acceleration.

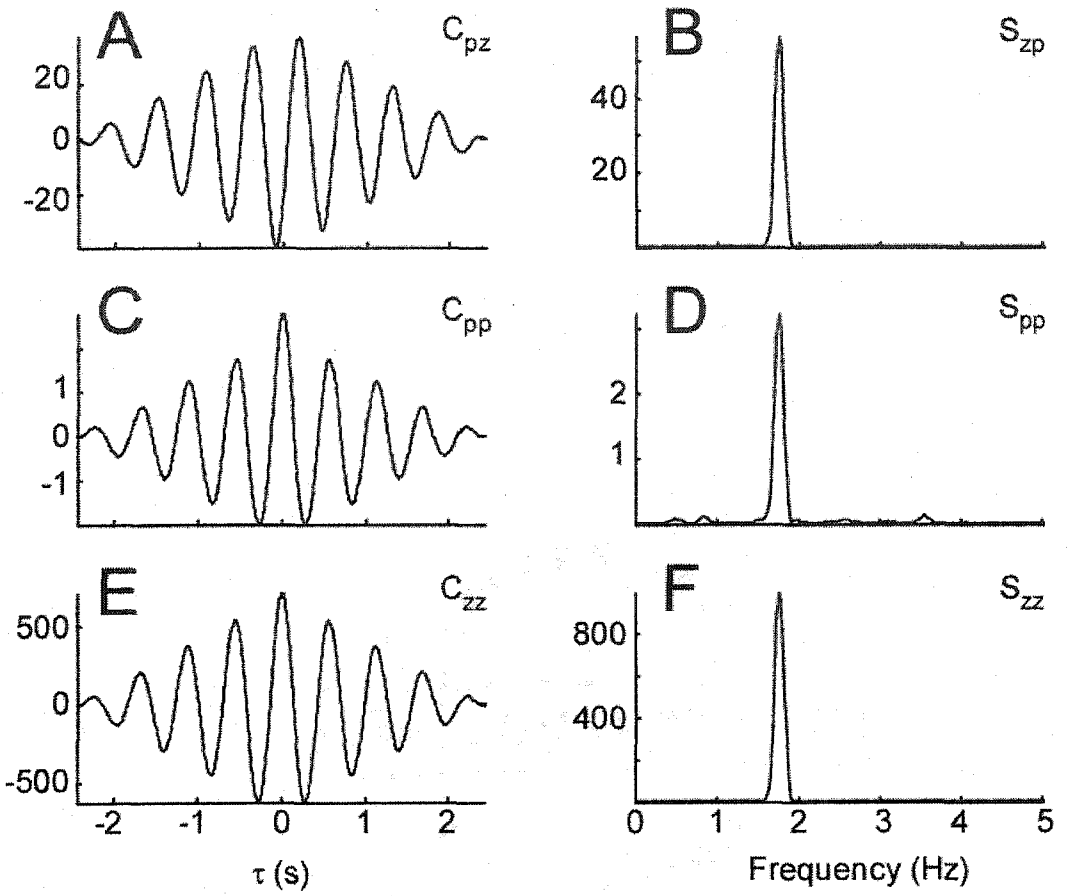

Fig 5.10 Medium velocity treadmill locomotion. Averaged cross- and auto-correlations are presented using the same window size (but not windowed) and overlap as when computing the coherence function. **A.** Cross-correlation of Pitch Velocty with Vertical Acceleration, **B.** Cross-spectrum of Pitch Velocity and Vertical Acceleration, **C.** Autocorrelation of Pitch Velocity, **D.** Power spectrum of Pitch Velocity, E. Autocorrelation of Vertical Acceleration, **F.** Power spectrum of Vertical Acceleration.

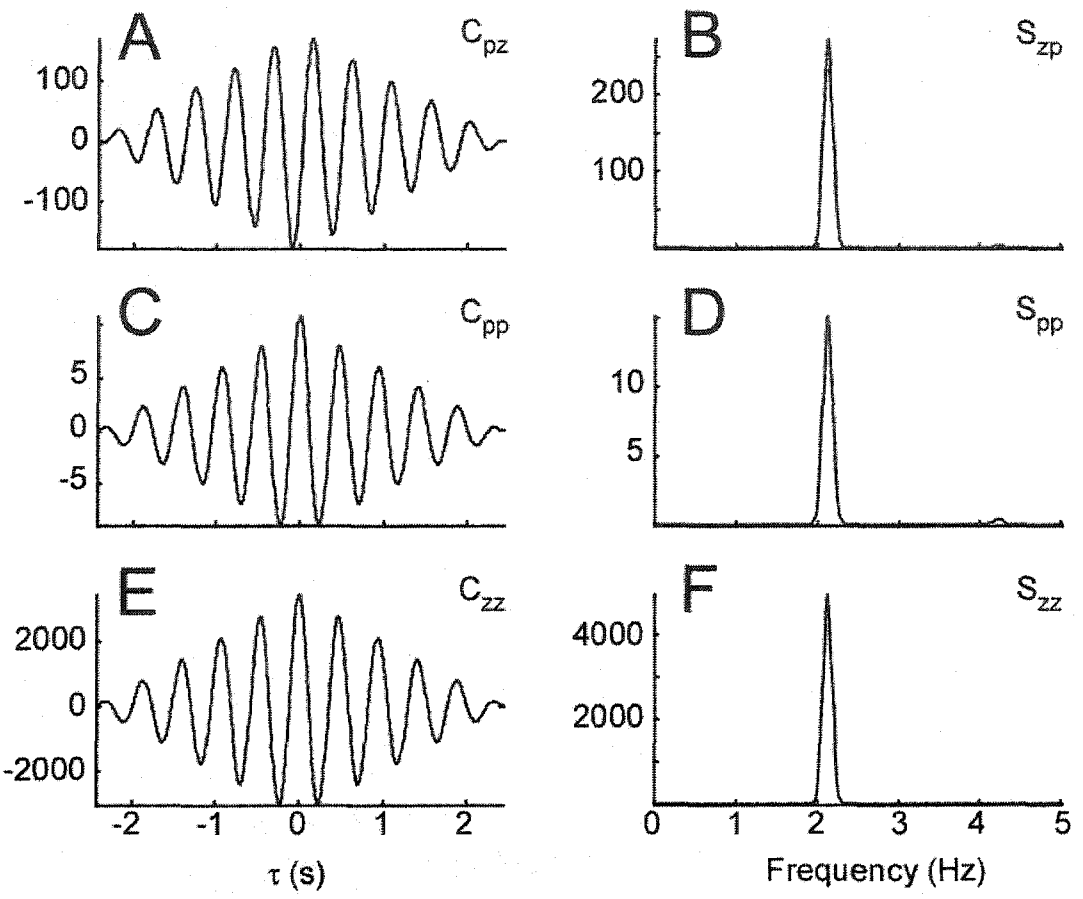

Fig 5.11 Fast treadmill locomotion. Averaged cross- and auto- correlations are presented using the same window size (but not windowed) and overlap as when computing the coherence function. **A.** Cross-correlation of Pitch Velocty with Vertical Acceleration, **B.** Cross-spectrum of Pitch Velocity and Vertical Acceleration, **C.** Autocorrelation of Pitch Velocity, **D.** Power spectrum of Pitch Velocity, **E.** Autocorrelation of Vertical Acceleration, **F.** Power spectrum of Vertical Acceleration.

In order to relate these relationships to the gain, we considered that ideally, head pitch should compensate for the vertical linear movement by a pitch movement that would cause the current naso-occipital to intersect the previous naso-occipital axis at the distance x_{min} (Eq. 5.1). The amount of actual head rotation, however, would produce a nonzero offset of linear displacement of the naso-occipital axis at the idealized head fixation distance. The amount of linear displacement relative to the ideal linear displacement we take as the gain of the reflex. This is a measure of how the lVCR might compensate for the linear translation of the head by a rotation of the head that in turn linearly translates the point along the naso-occipital axis at the head fixation distance in the head coordinate frame. This can be computed analytically as follows:

For small pitch angle of the head, a pitch angle of $\Delta\theta$, would cause an approximate linear displacement, Δz_{rot} due to the head rotation given by:

$$\Delta z_{rot} = x_0 \Delta\theta \tag{5.8}$$

where x_0 is the distance to the HFP. If the actual linear translation of the head is given by Δz, then the gain can be given as:

$$\text{Gain} = \frac{\Delta z_{rot}}{\Delta z} = \frac{\Delta\theta}{\Delta z} x_0 \tag{5.9}$$

This is the ratio of the change in pitch angle and linear head displacement multiplied by the head fixation distance. The gain per unit head fixation distance is given by:

$$\text{Gain/(fixation distance)} = \frac{\Delta z_{rot}}{\Delta z} = \frac{\Delta \theta}{\Delta z} \tag{5.10}$$

If the signals are sinusoidal, the relationships between the amplitudes of the head vertical acceleration and pitch velocity are given by: (Eq. 5.11 and 5.12)

$$\ddot{z}_{\text{ampl}} = Z_0 \omega_C^2 \tag{5.11}$$

$$\dot{\theta}_{\text{ampl}} = \theta_0 \omega_C \tag{5.12}$$

Substituting Z_0 and θ_0 into (Eq. 5.10) yields the gain at the frequency ω_C:

$$\text{Gain/(fixation distance)} = \frac{\dot{\theta}_{\text{ampl}} / \omega_C}{\ddot{z}_{\text{ampl}} / \omega_C^2} = \frac{\dot{\theta}_{\text{ampl}}}{\ddot{z}_{\text{ampl}}} \omega_C \tag{5.13}$$

This Gain at the mean frequency of the cross-spectral density (Stepping Frequency) can be obtained from the cross-spectral density of pitch and vertical acceleration at this frequency as follows (Schwartz and Shaw 1975):

$$\text{Gain/(fixation distance)} = \frac{S_{zp}}{S_{zz}} \omega \tag{5.14}$$

where ω is the mean frequency of the cross-spectral density. S_{zp} is the corresponding value of the cross-power spectral density and S_{zz} is the value of the power spectral density of the vertical head acceleration at the mean radian frequency, ω. The coherence between the vertical acceleration and pitch velocity is given by (Schwartz and Shaw 1975; Proakis and Manolakis 1992):

$$\text{Coherence} = \frac{S_{zp}}{\sqrt{S_{pp}S_{zz}}} \tag{5.15}$$

and was computed using Welch's averaged, modified periodogram method contained in Matlab. The variables z and p were divided into four sections with 50% overlap, and each section was windowed with a Hamming window and four modified periodograms were computed and averaged. Because the number of points in each of the four sections was small, the resulting resolution in frequency for determining the coherence value did not coincide with the dominant frequency of walking. We therefore approximated the coherence at the dominant frequency by linearly interpolating the values of the coherence at the nearest frequency on either side of the dominant frequency of walking.

The results of applying these analytical methods to treadmill locomotion are shown in (Fig 5.12, Fig 5.13, Fig 5.14, and Fig 5.15). When walking normally and fixating a target at 1 m, the gain/HFD declines as a function of stepping frequency (Fig 5.12A). When the gain was normalized by multiplying each value in (Fig 5.12A) by its associated HFD, the gain rose as a function of stepping frequency up to a stepping frequency of 2-2.5 Hz (Fig 5.12B). The phase of the response leads at low stepping

frequencies and declines as the stepping frequency is increased (Fig 5.12C). The coherence between the variables is close to 1 (Fig 5.12D), indicating that there is a small amount of noise and that these variables are highly correlated.

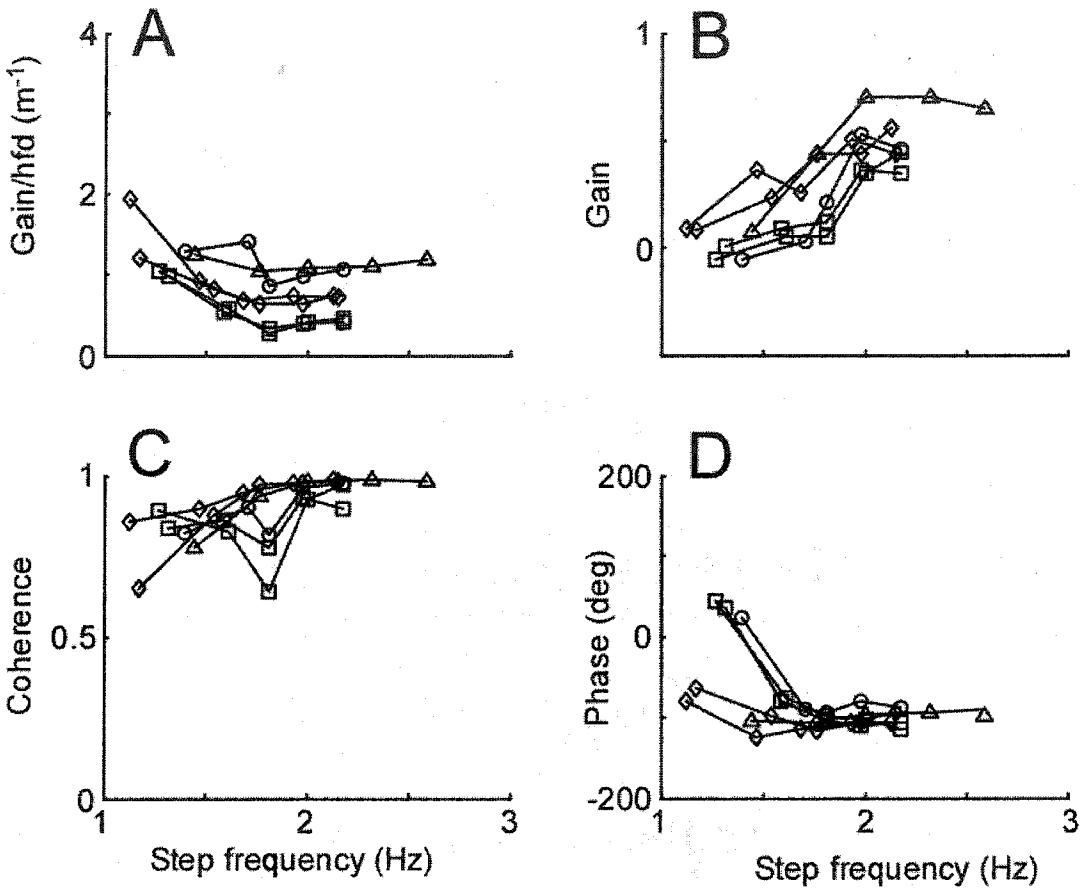

Fig 5.12 **A.** Gain per HFD in as function of Step Frequency while fixating a point at 1m distance. **B.** Gain normalized with respect to HFD for each trial as a function of Step Frequency. **C.** Coherence as a function of Step Frequency, **D.** Phase as a function of Step Frequency

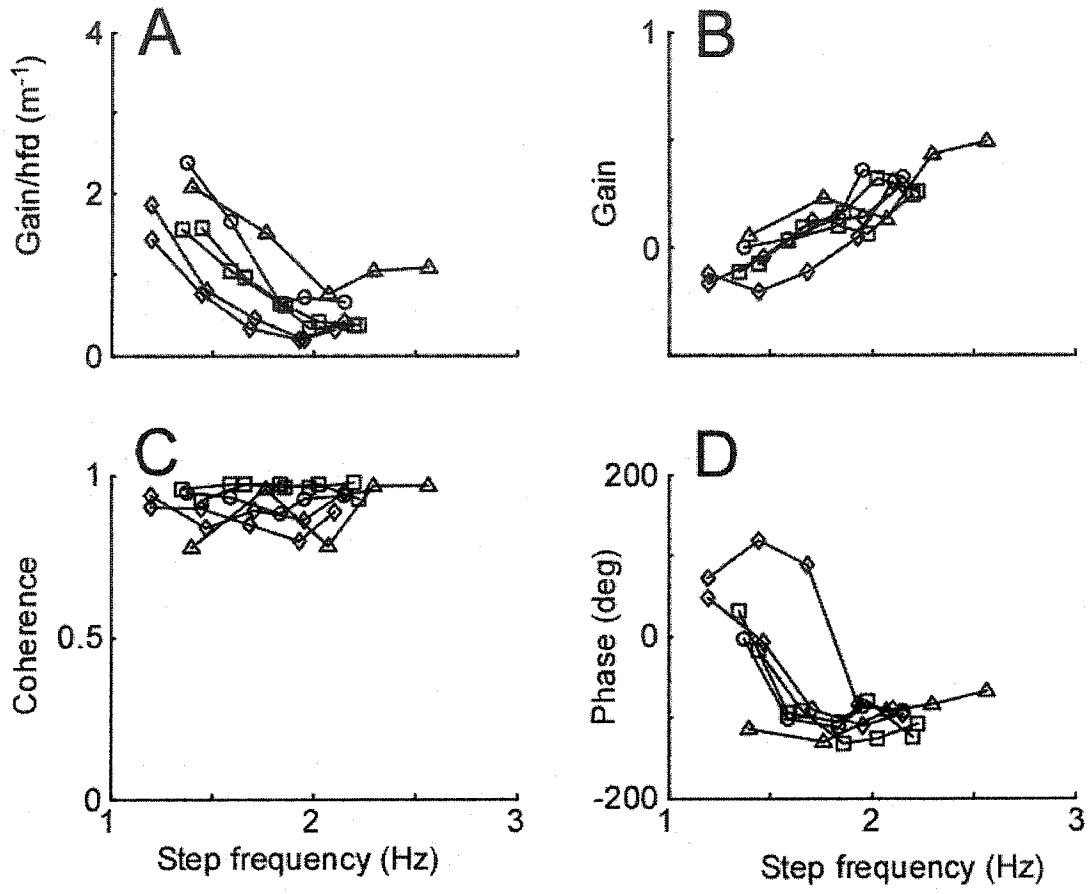

Fig 5.13 **A.** Gain per HFD in as function of Step Frequency while wearing a neck movement constraining collar. **B.** Gain normalized with respect to HFD for each trial as a function of Step Frequency. **C.** Coherence as a function of Step Frequency, **D.** Phase as a function of Step Frequency

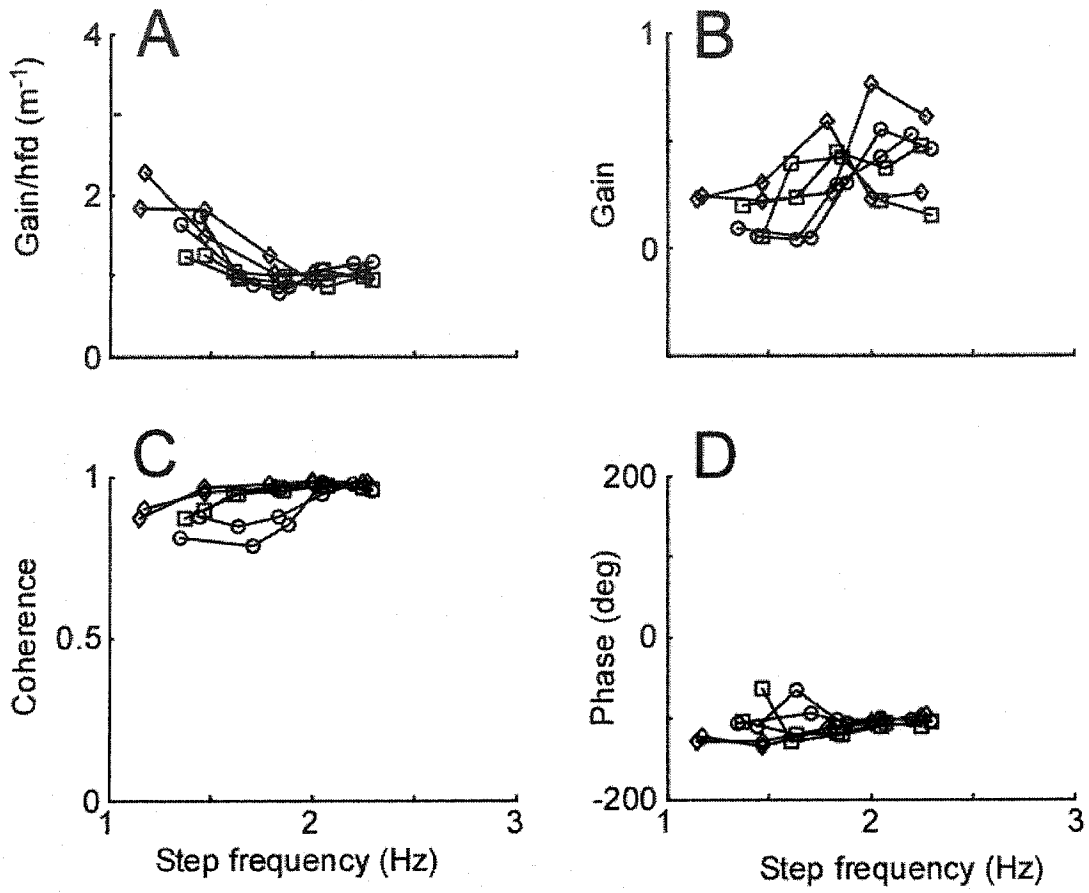

Fig 5.14 **A.** Gain per HFD in as function of Step Frequency while fixating a target at 20 cm. **B.** Gain normalized with respect to HFD for each trial as a function of Step Frequency. **C.** Coherence as a function of Step Frequency, **D.** Phase as a function of Step Frequency

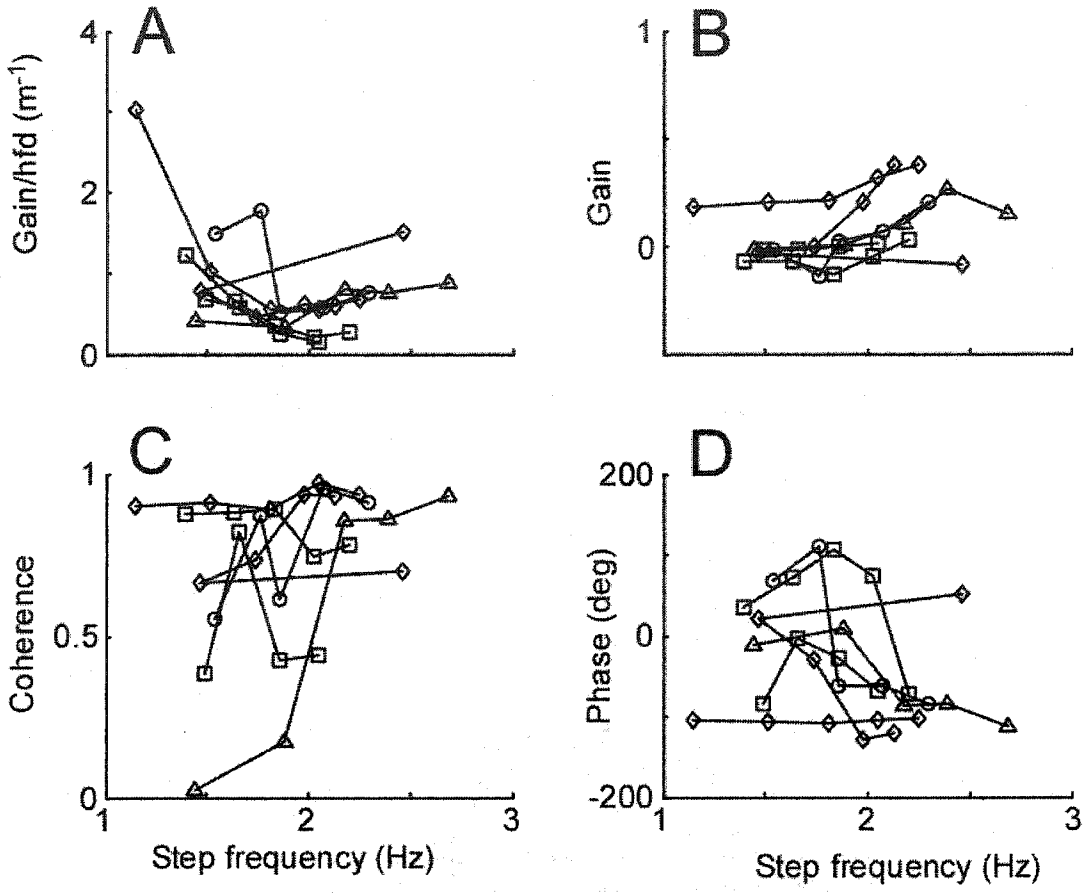

Fig 5.15 **A.** Gain per HFD in as function of Step Frequency In Darkness (eyes closed). **B.** Gain normalized with respect to HFD for each trial as a function of Step Frequency. **C.** Coherence as a function of Step Frequency. **D.** Phase as a function of Step Frequency.

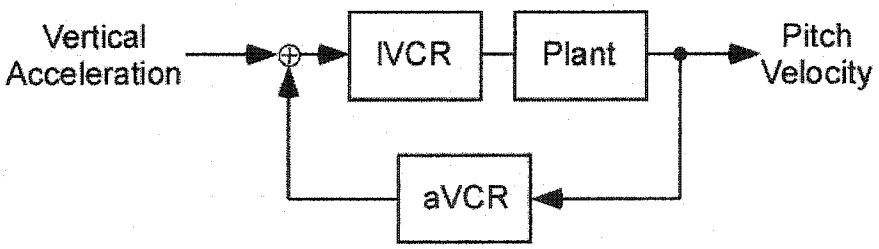

Fig 5.16 Simple Model of the transfer relationship between the Pitch Velocity and Vertical Acceleration.

Similar results were obtained for walking with a collar constraint (Fig 5.13A-D) and walking with a close fixation point (Fig 5.14A-D). When walking in darkness, there was a reduction in gain, indicating that gaze plays an important role in the control of head movements (Fig 5.15A-D). Because the phase varies over 180° as a function of frequency of stepping, the data indicate that the response is related to a higher order system. This would be consistent with a model that drives the plant via the lVCR, with feedback through activation of the aVCR (Fig 5.16). The gain and phase characteristics of a second order model (Fig 5.17) show similar gain and phase behavior. However, there are clear differences. The model reaches a peak gain at the point where the phase goes through zero. The data show a considerable phase advance going through zero considerably before the gain reaches a maximum (Fig 5.17). The coherence also drops off at lower frequencies of stepping, indicating that there is considerable noise in the system. Moreover, there may be some nonlinear factors or higher order terms that cause the phase to drop off more rapidly than a second order model. A complete characterization of this model is beyond the scope of this dissertation and will be considered in future research.

$$H(\omega) = \frac{j\omega T_{Z0}}{(j\omega T_{p0} + 1)(j\omega T_{p1} + 1)}$$

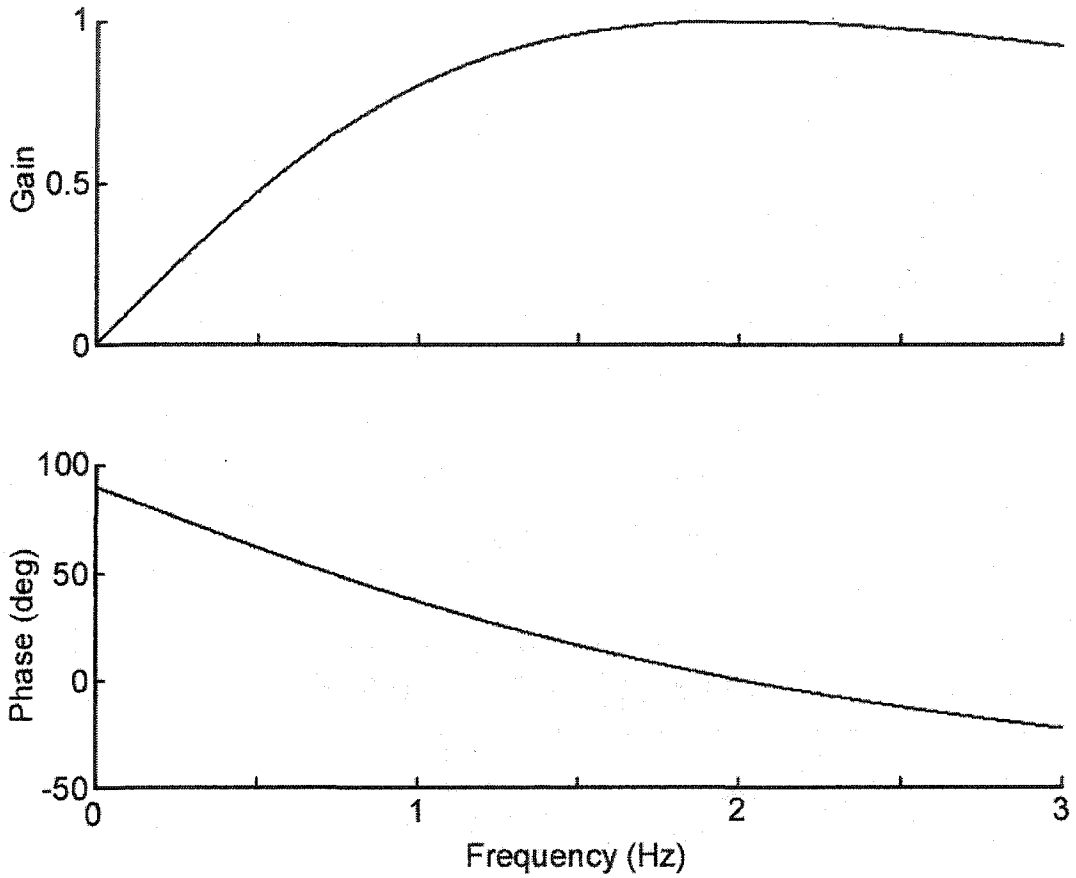

Fig 5.17 Gain and Phase characteristic of a second order model that has global characteristics of the head pitch in response to vertical acceleration

5.4.3 Relationship Between Head Vertical Translation and Head Pitch: Gain of the Head Movement Reflex (Overground Locomotion)

We first consider the relationship of head pitch with vertical translation (Fig 5.18). The locomotion is characterized by a highly periodic stepping as the shank moved up and down (Fig 5.18A), vertical head translation (Fig 5.18F) and pitch head rotation (Fig 5.18G).

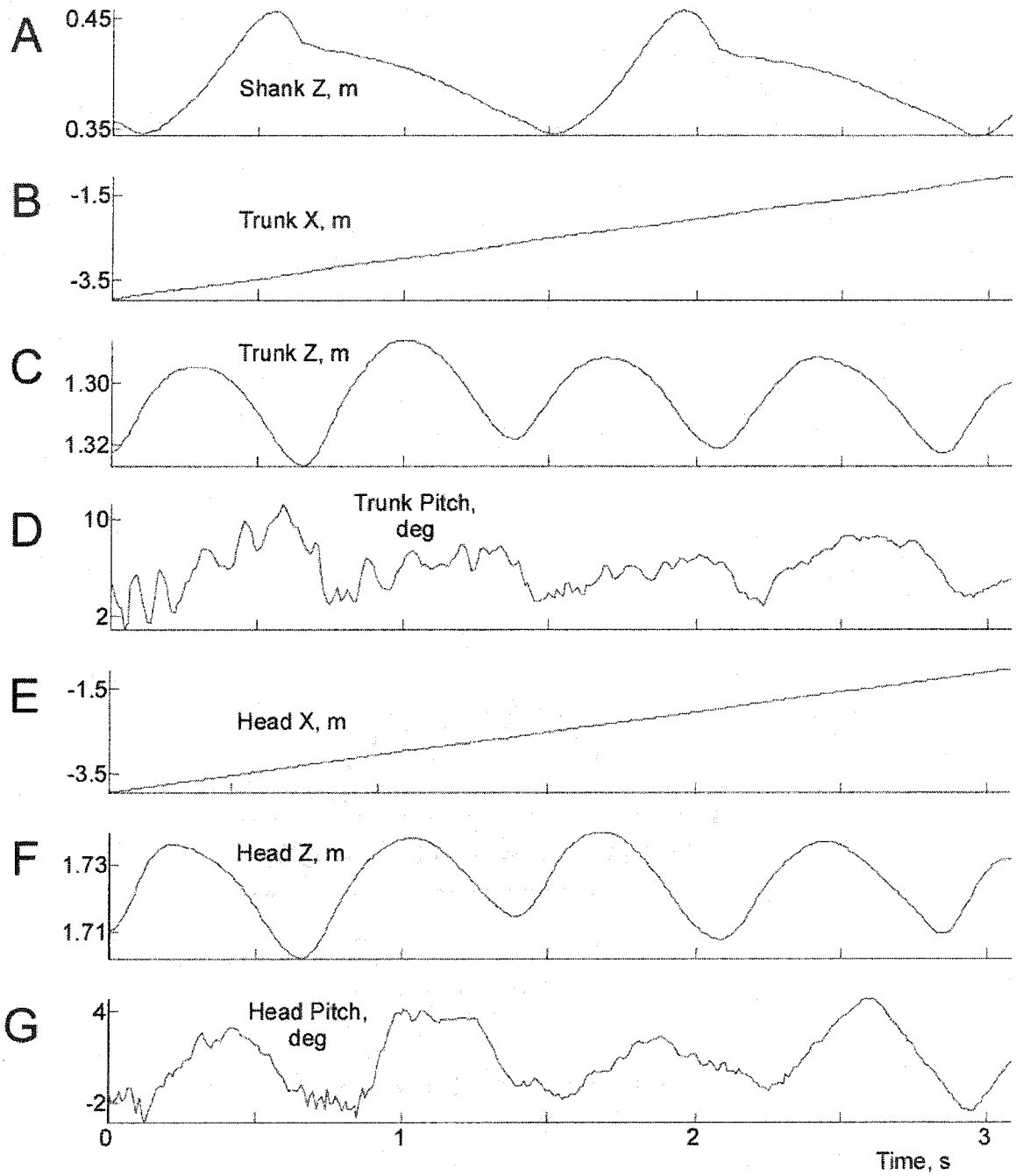

Fig 5.18 Steady state walking overground (Position). All variables re space. **A.** Shank Z, **B.** Trunk X, **C.** Trunk Z, **D.** Trunk Pitch, **E.** Head X, **F.** Head **Z.** and **G.** Head Pitch.

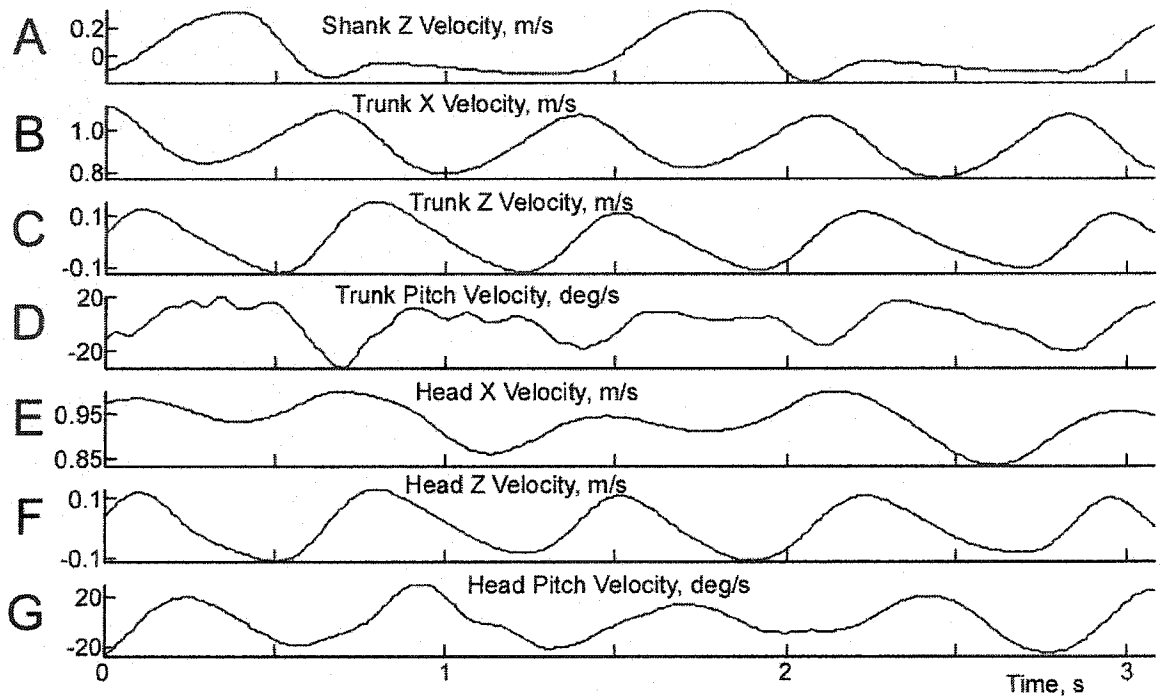

Fig 5.19 Steady state walking over ground (Velocity). All variables re space. **A.** Shank velocity Z, **B.** Trunk Velocity X, **C.** Trunk velocity Z, **D.** Trunk Pitch Velocity, **E.** Head Velocity X, **F.** Head Velocity Z, and **G.** Head Pitch Velocity.

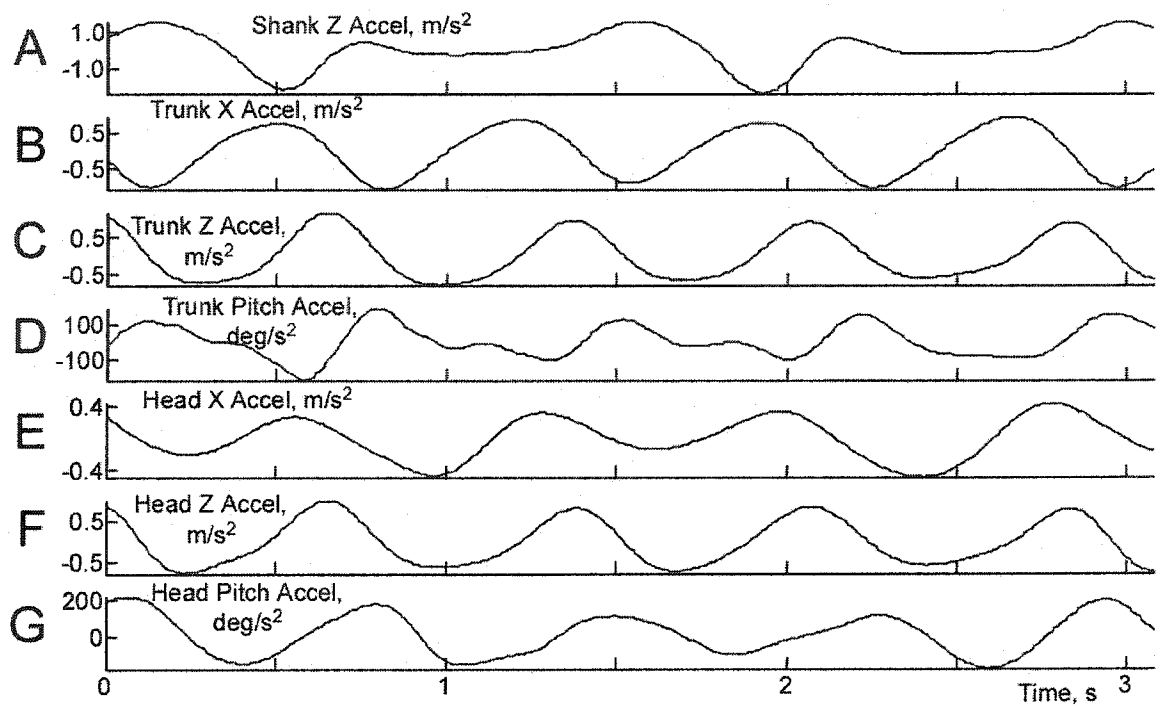

Fig 5.20 Steady state walking over ground (Acceleration). All variables re space. **A.** Shank Acceleration Z, **B.** Trunk Acceleration X, **C.** Trunk Acceleration Z, **D.** Trunk Pitch Acceleration, **E.** Head Acceleration X, **F.** Head Acceleration Z, and **G.** Head Pitch Acceleration.

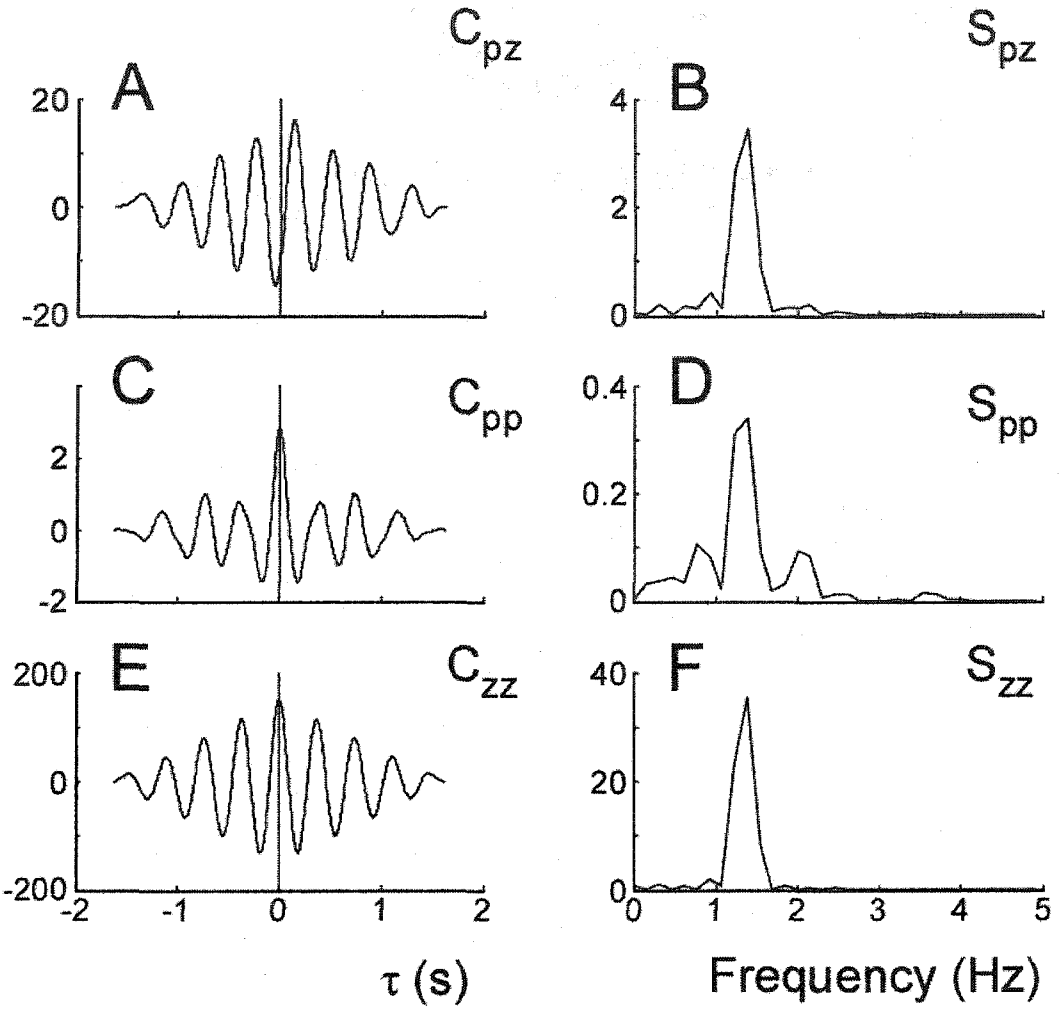

Fig 5.21 **A.** Cross-correlation of Head Pitch Velocity with Head Vertical Acceleration during steady state slow locomotion overground, **B.** Spectrum of Cross-correlation of Head Pitch Velocity with Head Vertical Acceleration, **C.** Auto-correlation of Pitch Velocity, **D.** Power Spectrum of Pitch Velocity, **E.** Auto-correlation of Vertical Acceleration, **F.** Power Spectrum of Vertical Acceleration

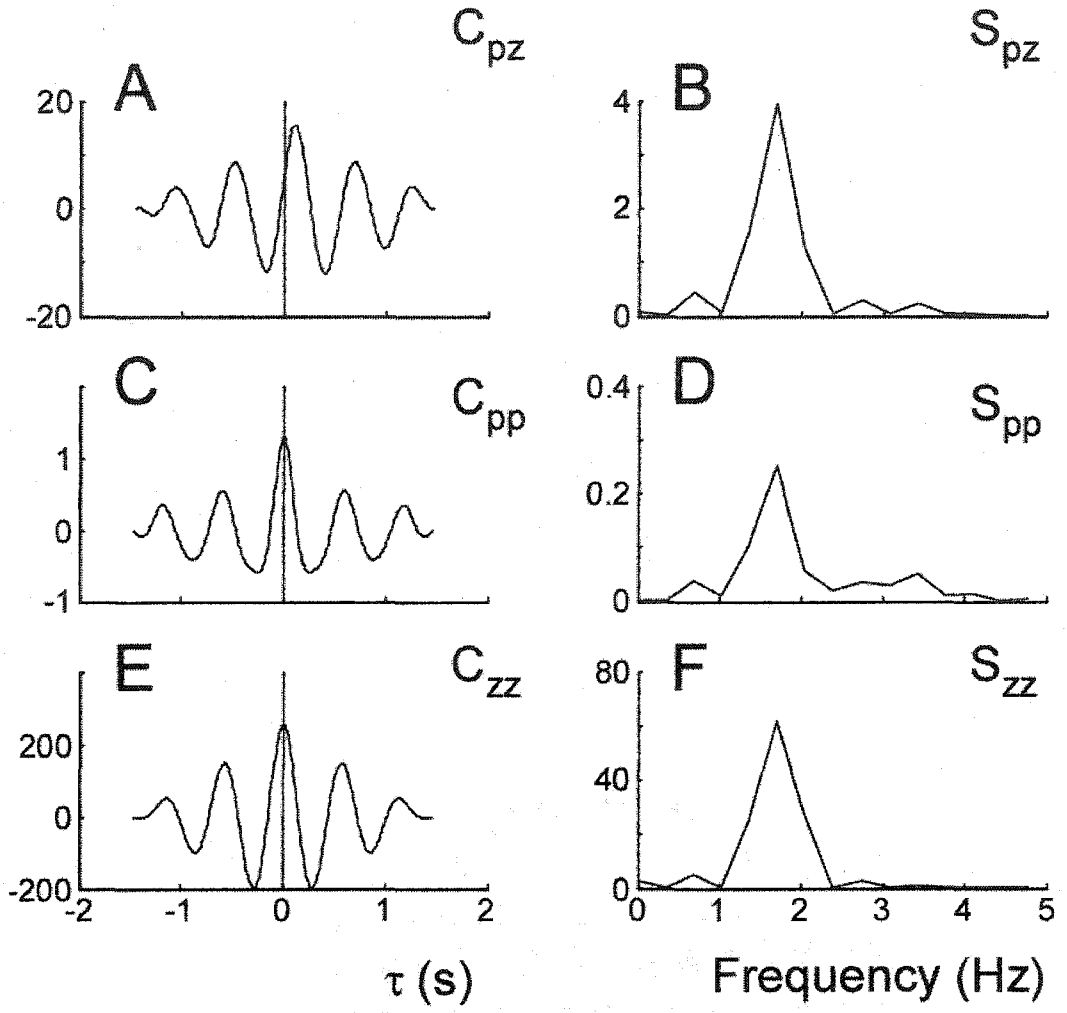

Fig 5.22 **A.** Cross-correlation of Head Pitch Velocity with Head Vertical Acceleration during steady state medium velocity locomotion overground, **B.** Spectrum of Cross-correlation of Head Pitch Velocity with Head Vertical Acceleration, **C.** Auto-correlation of Pitch Velocity, **D.** Power Spectrum of Pitch Velocity, **E.** Auto-correlation of Vertical Acceleration, **F.** Power Spectrum of Vertical Acceleration

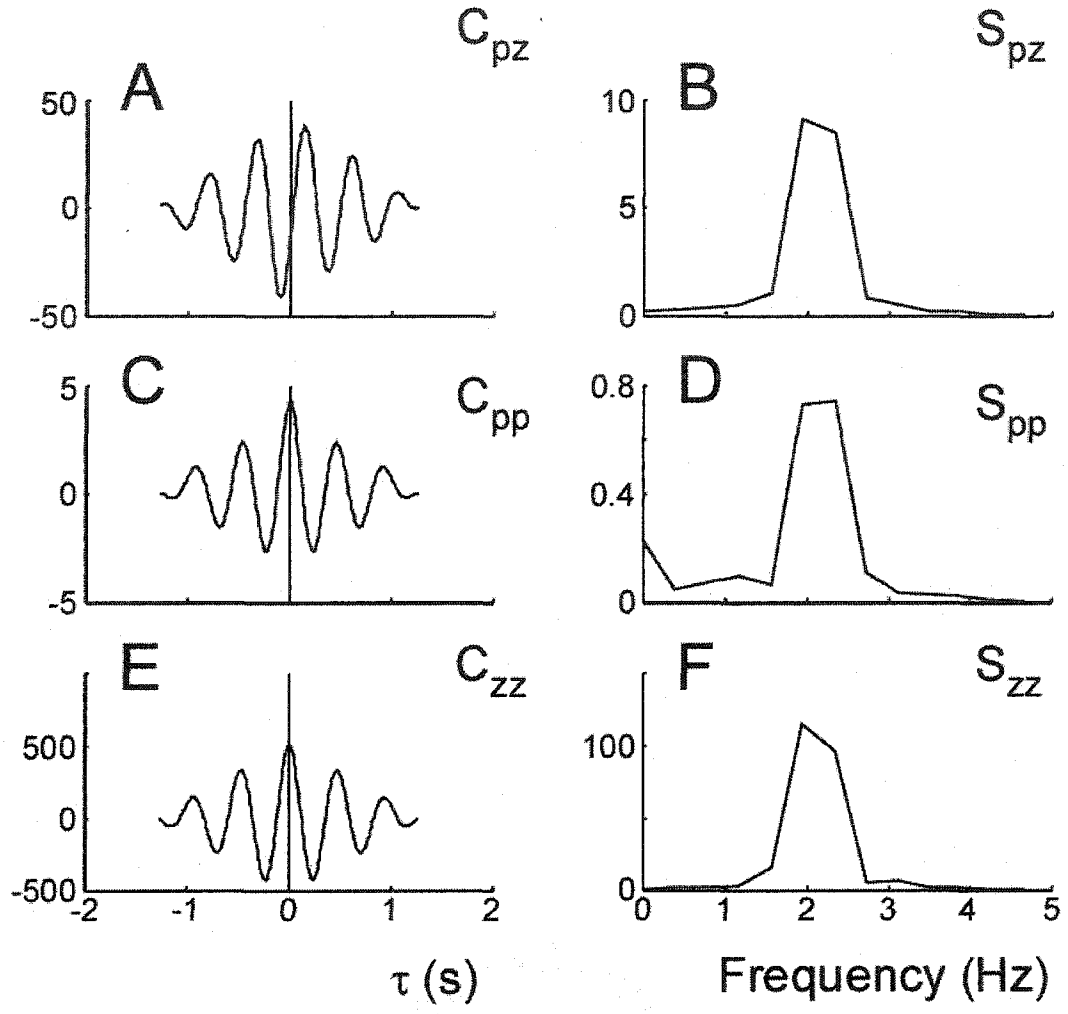

Fig 5.23 **A.** Cross-correlation of Head Pitch Velocity with Head Vertical Acceleration during steady state fast locomotion overground, **B.** Spectrum of Cross-correlation of Head Pitch Velocity with Head Vertical Acceleration, **C.** Auto-correlation of Pitch Velocity, **D.** Power Spectrum of Pitch Velocity, **E.** Auto-correlation of Vertical Acceleration, **F.** Power Spectrum of Vertical Acceleration

Using Equation 5.7, the Gain was approximately 0.2-5 per meter of head fixation distance (Fig 5.24, Fig 5.25 A, C). The coherence at the mean (stepping) frequency was close to 0.95 for all subjects at all walking velocities (Fig 5.24, Fig 5.25 B, D).

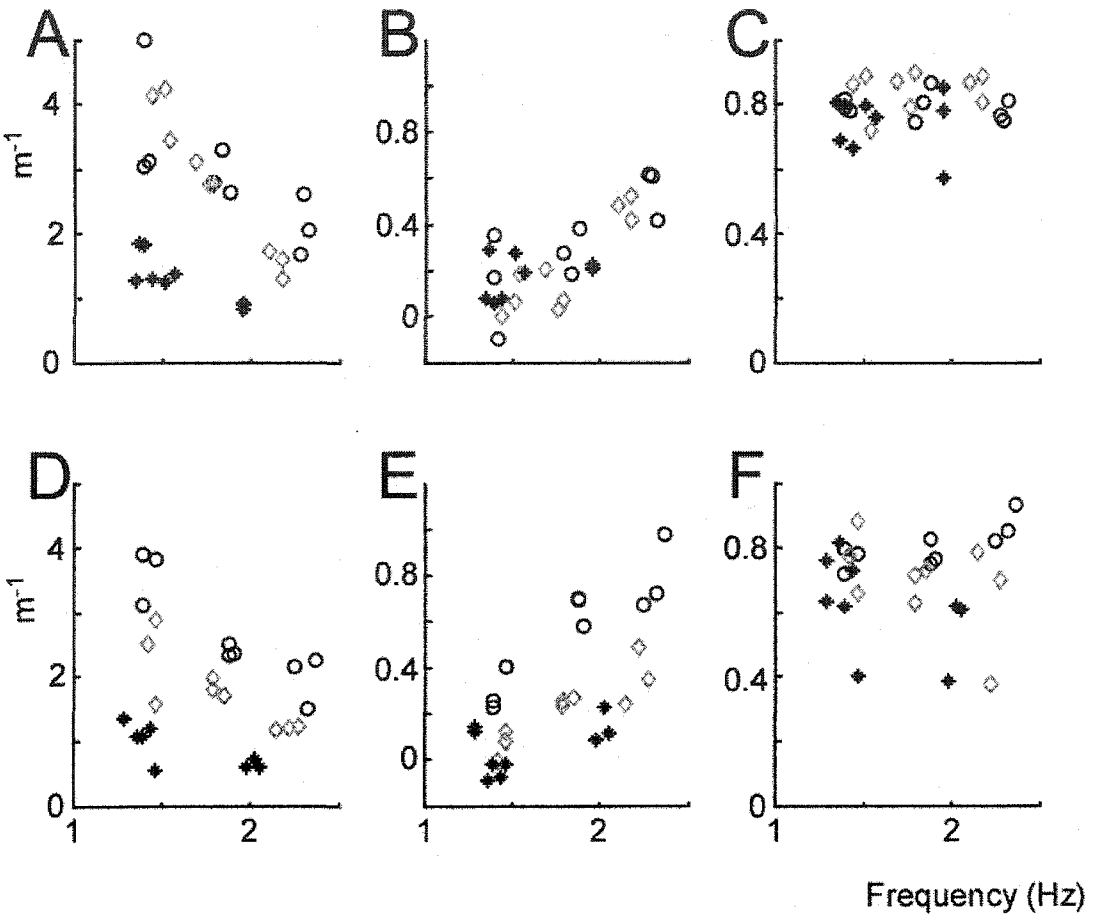

Fig 5.24 Gain per meter of HFD (A, D), Gain (B, E), and Coherence (C, F) without (A, B, C) and with (D, E, F) the neck constraint for overground locomotion. High Coherence subjects.

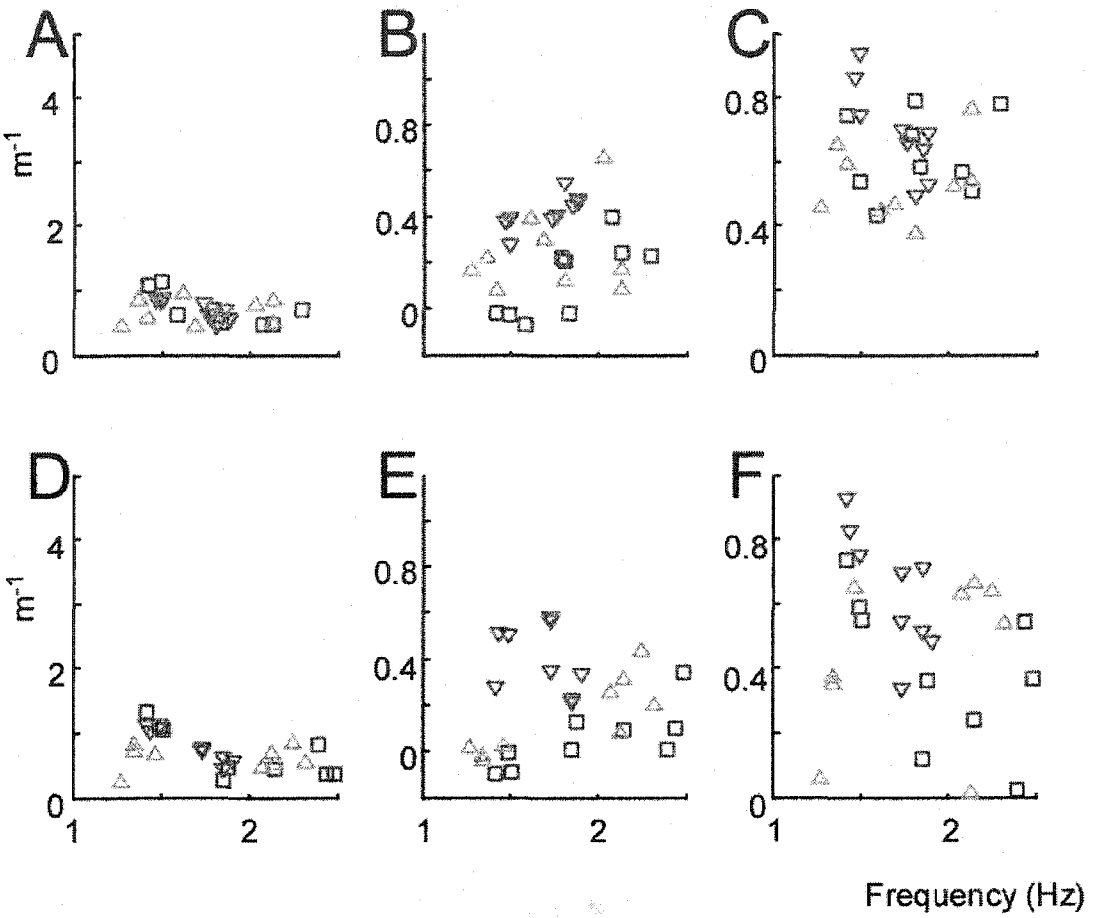

Fig 5.25 Gain per meter of HFD (A, D), Gain (B, E), and Coherence (C, F) without (A, B, C) and with (D, E, F) the neck constraint for overground locomotion. Low Coherence subjects.

In order to estimate the phase relationship from the actual data, we used the mean frequency and fit the original data with sinusoids of that frequency. The estimated phase was computed relative to the ideal of 90°. For slow walking velocities the phase difference was significantly larger than ideal, indicating an average phase lead of 120°±50° without and 157°±18° with the collar (Fig 5.26 A, D). For medium walking velocity the phase is much closer to 90° (Average phase = 82°±59°, without collar;

137°±29° with collar, Fig 5.26 B, E). At the fast walking speed, the phase lagged the ideal without the collar (Average phase = 37°±18°, without collar; 94°±22° with collar, Fig 5.26 C, F). Thus, the phase behavior indicates that the system dynamics are close to second order and may be the result of the feedback due to the aVCR, which tends to stabilize the head in space as the IVCR tends to drive the system towards a stable HFP.

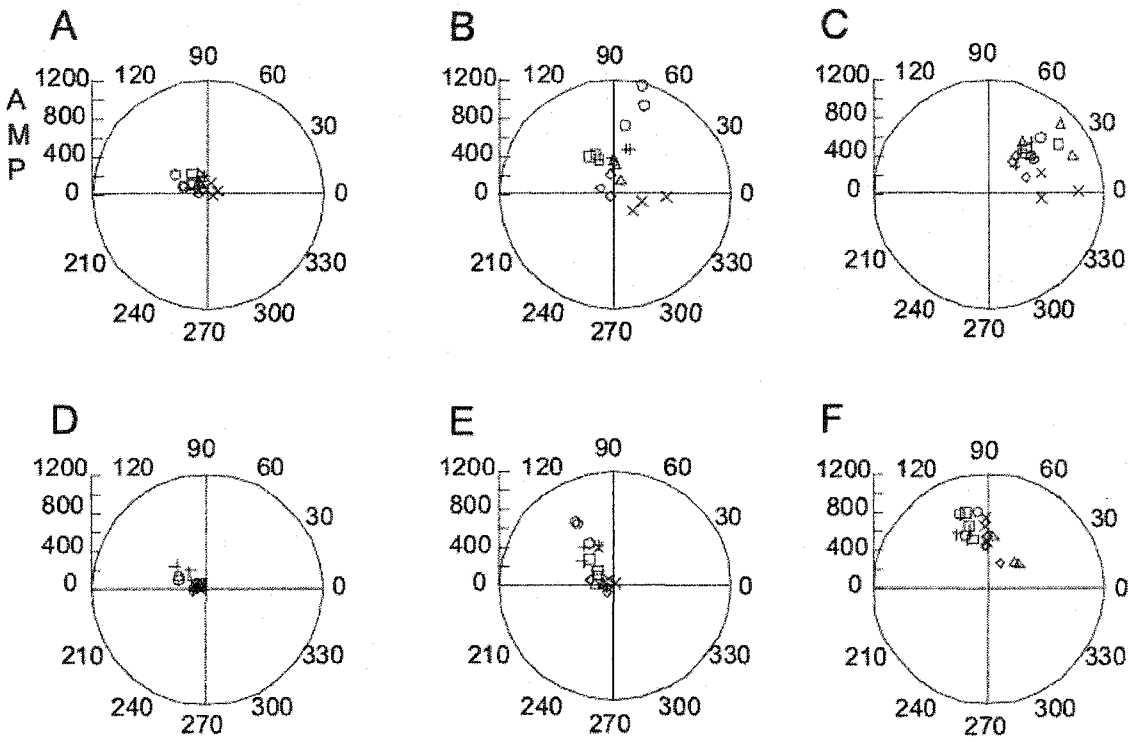

Fig 5.26 Phase of Head Pitch Velocity re Head Vertical Translation at the Dominant Frequency of Walking without (A, B, C) and with (D, E, F) Restraining Collar during slow (A, D), medium (B, E), and fast (C, F) locomotion. Ideal Phase Difference would be 90°. Increases in Step Frequency induced a Phase Lead and increases in Amplitude.

Based on this, we hypothesize that the actual invariant that the system (lVCR) is trying to maintain is the head fixation point and a corresponding VP-HFD. However, one of the reasons we do not observe a perfect head fixation point (zero variance) is the dynamics of the lVCR as well as the dynamic feedback of the aVCR, which tends to maintain the head stable in space. These factors introduce a phase shift of the head pitch angle relative to a given Z translation of the head. Therefore, if we compute the head fixation point and its distance from the head when there is no pitch, using the value of $\theta(t-t_0)$ where t_0 is the phase obtained from the spectral analysis we expect to get an estimate of "true" head fixation point parameter one of the defining characteristics of the lVCR.

We have found that such phase shifting produces a head fixation point whose variance is almost always smaller and whose distance is greater than that of unshifted data. Fig 5.28 also shows that the variation of the phase-adjusted head fixation distance is significantly smaller, which supports our hypothesis that the HFD is invariant parameter of the system).

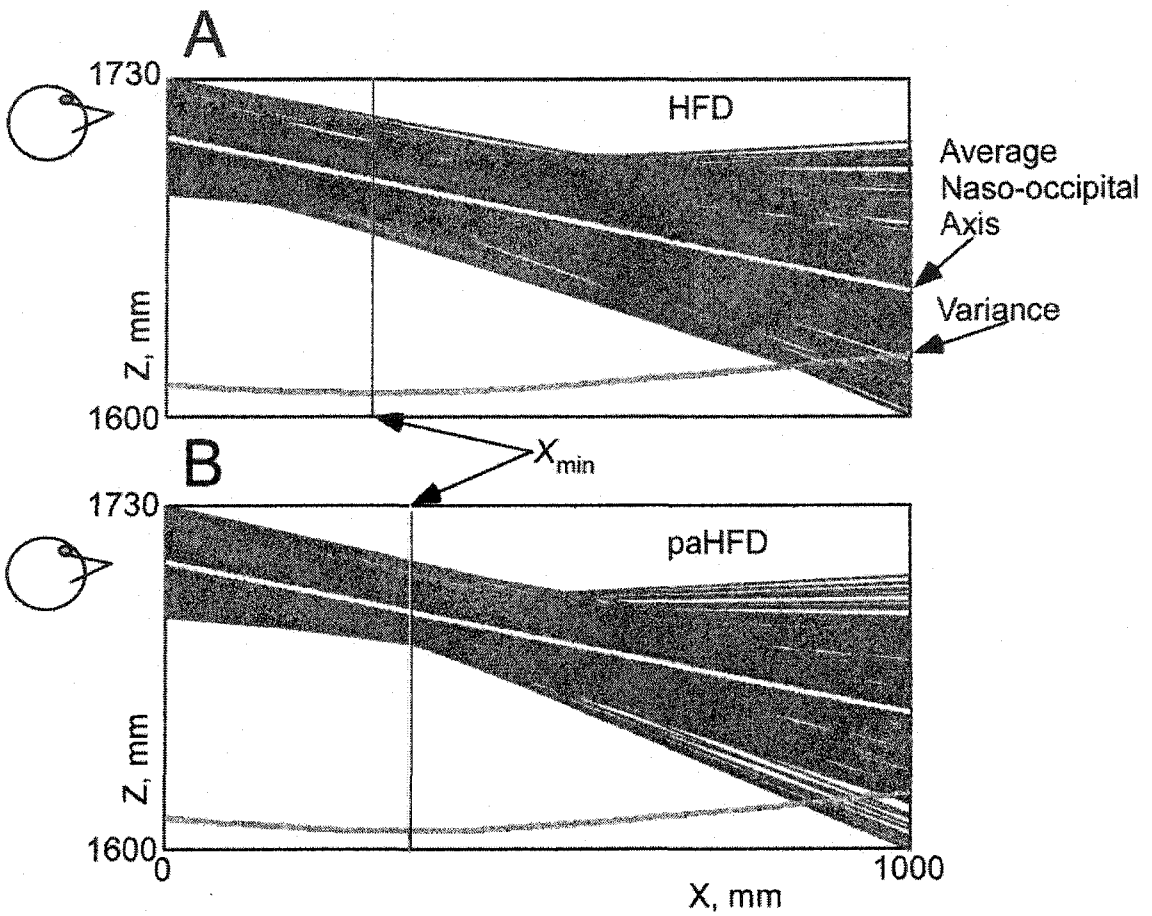

Fig 5.27 Comparison of computed **A.** Head Fixation Point (HFP) and **B.** Phase-Adjusted HFP (paHFP). The paHFP is significantly further from the head than the HFD. This larger value suggests that the previous estimates of ocular rotations to maintain invariant gaze overestimated the contribution of the IVCR and did not consider the dynamics introduced by the aVCR.

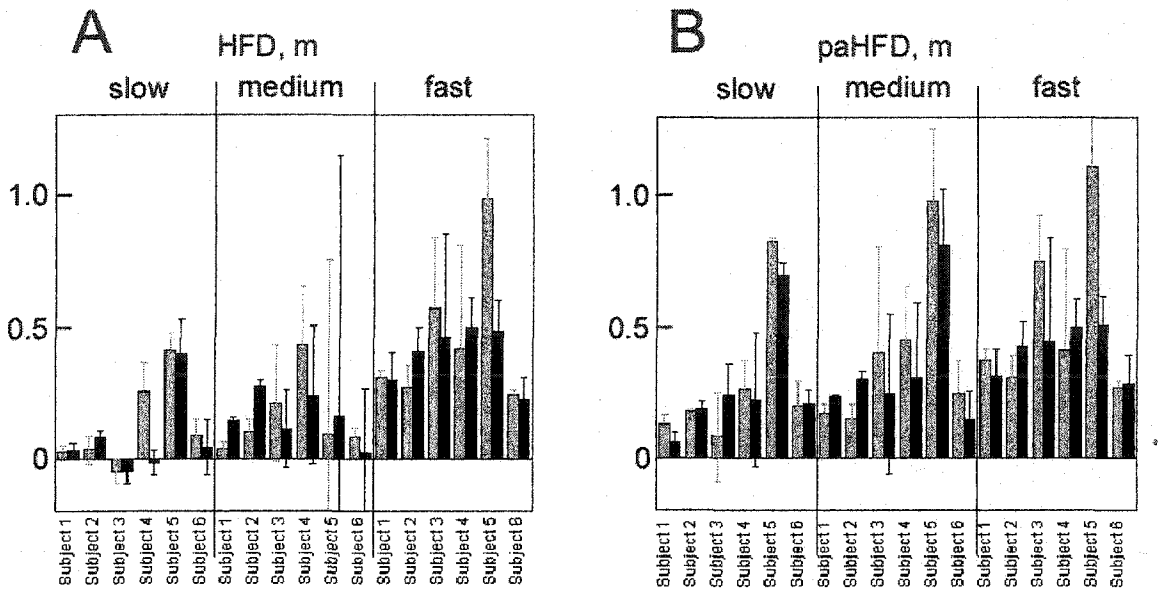

Fig 5.28 Mean HFD (A) and paHFD (B) with (black) and without (light gray) collar for each subject for slow, medium, and fast walking. In both cases the HFD and paHFD increased with walking velocity. The effects of the collar were not significant. With phase adjustment the head fixation distance was more stable

The phase between vertical head acceleration and pitch velocity was also examined during a fore-aft perturbation. Since it was not possible to perform the spectral analysis on the trials involving perturbations due to non-stationary nature of the process, we computed the phase shift by determining its value by the computation of the "minimum variance of the head fixation point." That is, we computed the head fixation points and associated variances for a series of shifts between the vertical translation and pitch rotation data traces. The value of the shift to produce the minimum variance was taken to be phase shift introduced by the lVCR. To demonstrate the phase behavior, each subject was represented by a circle and the average phase was represented by a filled dot on that

circle (Fig 5.29). The gray arc is the standard deviation about the mean for each subject. The dashed radial line is the overall mean phase and the dashed arc on the outer cicle is the standard deviation. With increases in walking velocity the overall mean phase approached zero. It should be noted that because the time period over which the phase was computed during a perturbation was smaller than for continuous walking the variance was larger due to the uncertainty relationships between time of analysis and estimation value. Despite this uncertainty, the overall mean phases were close to 20° without a collar and 0° with a collar.

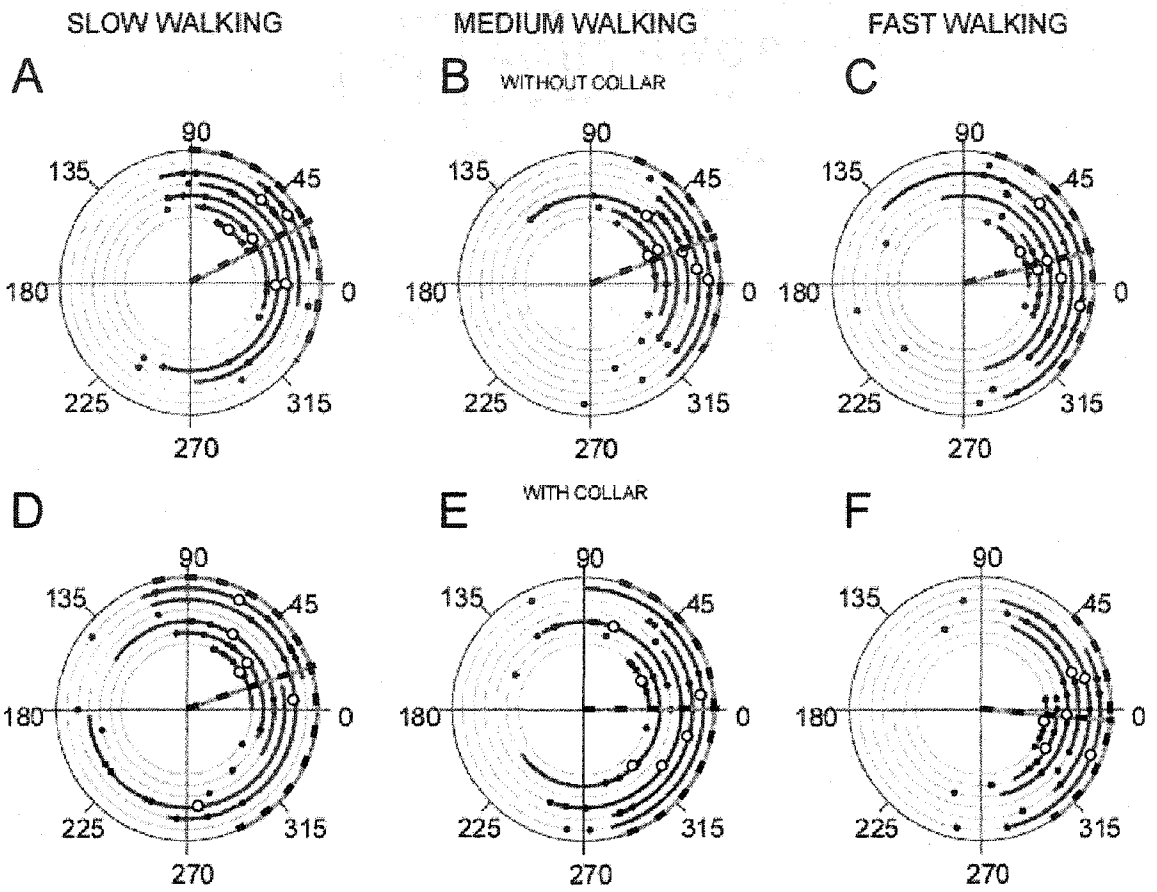

Fig 5.29 Phase between the head vertical translation and pitch rotation during slow (A, D), medium (B, E), and fast (C, F) perturbed locomotion overground without (A, B, C) and with (D, E, F) neck constraint. Each circle represents a different subject. The filled dot represents the mean phase and the arc is the standard deviation about the mean for each subject. The radial dashed line is the overall mean phase and the outer dashed arc is the standard deviation. With increases in walking velocity the overall mean phase approached zero. The collar had the effect of limiting the head rotation and maintaining the phase close to zero for medium and fast walking.

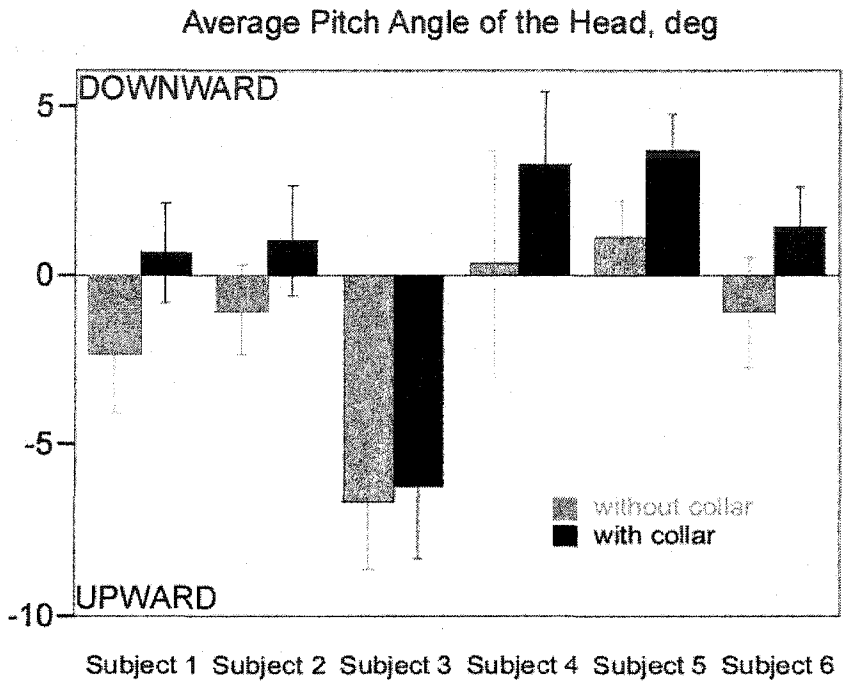

Fig 5.30 Effects of collar constraint on the average Pitch angle of the Head during walking. In order to verify that the collar did in fact provide neck restraint, we computed the average pitch angle of the average naso-occipital axis. The result was that the collar consistently made the subject to look down.

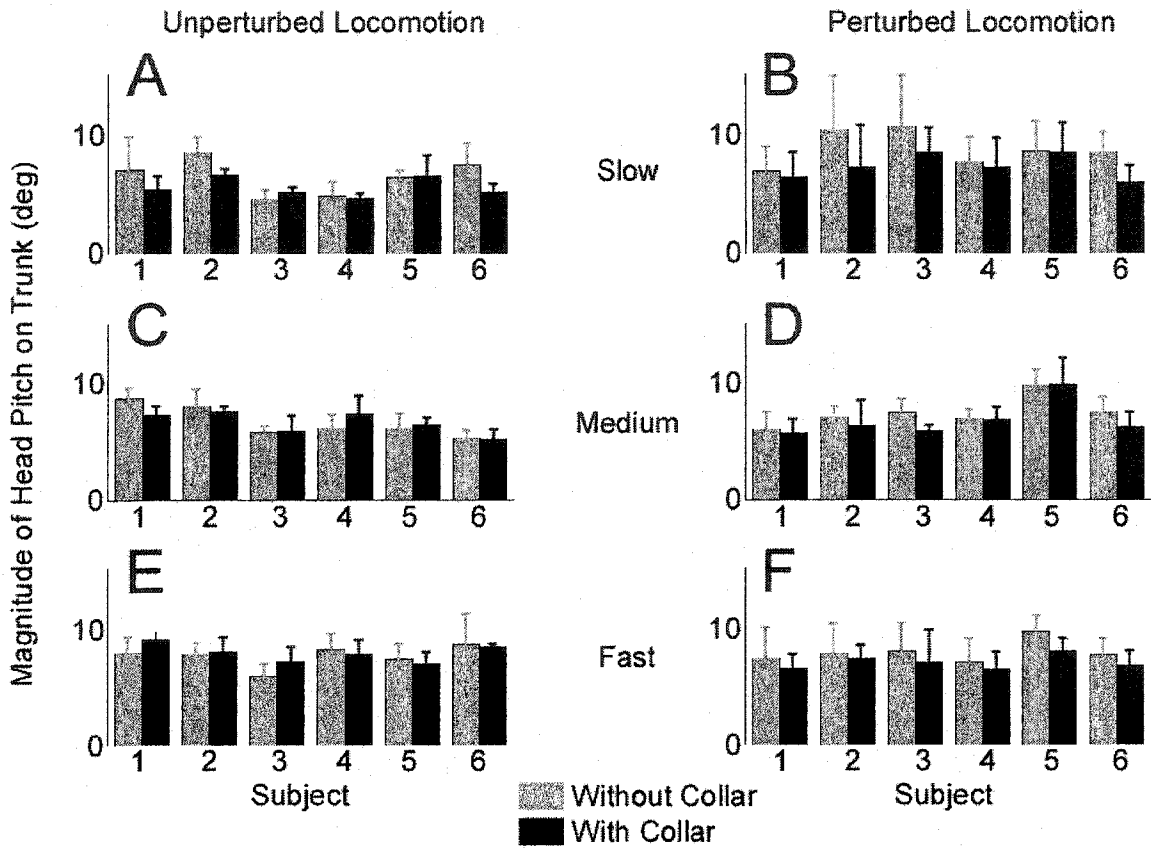

Fig 5.31 Comparison of magnitude of head pitch on trunk during unperturbed (A, C, E) and perturbed (B, D, F) during slow (A, B), medium (C, D), and fast (E, F) locomotion. Since the collar did not significantly affect the magnitude of head pitch, we conclude that the head pitch was maintained by neural control, which overrode the stiffness of the collar.

CHAPTER 6 MATHEMATICAL BASIS FOR DETERMINING ROTATION AXES AND PIVOT POINTS IN THREE DIMENSIONS

In order to gain insight into the three dimensional characteristics of head and trunk movement during walking, we will consider how the head is rotated about some pivot point. This requires estimating an average axis and pivot point for the rotation in three dimensions. The approach that will be taken is to describe the movement of a rigid body by a homogeneous transformation (Fu, Gonzales et al. 1987), which we represent as a matrix, defining what we refer to as a Displacement Matrix. Using this approach, we also determine the axis lines as a function of time as the rigid body follows a certain trajectory. Finally we consider the three dimensional distribution of these axis lines. In CHAPTER 7, we show how this methodology is applied to determining the rotation axes of the head at different head orientations relative to the trunk. In CHAPTER 8, we further show how this methodology can be used to determine the HFP in three dimensions during locomotion.

6.1 Properties of Displacement Matrices (Homogeneous Transformations) and Their Relation to SE(3):

A homogeneous transformation is represented by a 4x4 matrix consisting of 4 submatrices. They represent rotation, translation, perspective, and scaling (Fu, Gonzales et al. 1987). The transformation operates on four-dimensional augmented or homogeneous vectors, which represent vectors in three-dimensional space by augmenting

the vector with a 1 as the last component. That is, for every vector (p_x, p_y, p_z) in three-dimensional space there exists a four-dimensional vector in homogeneous coordinates given by an augmented vector $\mathbf{p} = (p_x, p_y, p_z, 1)$. We will refer to the 4x4 matrix representation of a homogeneous transformation as a "displacement matrix" given as follows:

$$\begin{bmatrix} R_{33} & p_{31} \\ f_{13} & 1x1 \end{bmatrix} = \begin{bmatrix} rotation & translation \\ perspective & scaling \end{bmatrix} \tag{6.1}$$

The 3x3 matrix representing the rotation, R_{33}, can be characterized in terms of Euler angles or axis-angle (Goldstein 1980) (Schnabolk and Raphan 1994) (Raphan 1997). The displacement matrices that we will consider will have the scaling unity and the perspective zero. Therefore, in modeling rotations and translations relative to some coordinate frame, the matrix can be simply given as:

$$\begin{bmatrix} R_{33} & p_{31} \\ 0 & 1 \end{bmatrix} \tag{6.2}$$

where R_{33} is the rotation and p_{31} is the translation. Displacement matrices can be multiplied together to obtain a composite displacement matrix, but the matrix multiplication is not commutative. Thus, these matrices form a non-commutative group under matrix multiplication, which has been called SE(3) (Murray, Li et al. 1994). The submatrices, R_{33}, representing rotations, also form a group under matrix multiplication which has been designated as SO(3).

In modeling the aVOR - lVOR interaction relative to a fixed visual point in space, displacement matrices relative to the head will represent eye movements and head movement will be represented as a displacement matrix relative to space. To find the displacement matrix of the eye relative to space, the two matrices are multiplied. Vectors representing a visual gaze point relative to a space coordinate frame and the visual axis in that coordinate frame can then be computed. Each eye can be treated as a separate entity having its own displacement matrix. Orientations and positions of each eye in three-dimensional space at each instant of time can then be computed in a relatively easy manner (Denavit and Hartenberg 1955).

6.2 Quantitative Description of the Rotational Sub matrix (R33) and Its Relation to Skew Symmetric Matrices

An incremental rotation of a rigid body about the origin a reference coordinate frame can be represented as a skew symmetric matrix given by:

$$\Omega = \begin{pmatrix} 0 & -\omega_3 & \omega_2 \\ \omega_3 & 0 & -\omega_1 \\ -\omega_2 & \omega_1 & 0 \end{pmatrix} \tag{6.3}$$

When the matrix in (Eq. 6.3) operates on a radius vector corresponding to a point, the resultant vector represents an incremental change in the radius vector of the point due to its rotation about the origin of the coordinate system:

$$d\mathbf{q} = \Omega\mathbf{q}dt \tag{6.4}$$

Where $\mathbf{q}$ is radius vector, $d\mathbf{q}$ is the differential change in the vector over some infinitesimal time dt about an axis of the incremental rotation, (ω_1, ω_2, ω_3).

Finite rotations about an axis defined by Ω, can be represented by the matrix exponential of Ω given by:

$$e^{\Omega\theta} = \sum_{i=0}^{\infty} \frac{(\Omega\theta)^i}{i!} \tag{6.5}$$

This matrix will be shown to be related to the sub matrix, R_{33} of (Eq. 6.2), through the formula of Rodriguez (Rodriguez 1840; Raphan 1998) and requires the computation of Ω^i i=0,…,∞. This computation can be simplified by considering Ω^2 and $\omega\omega^T$ as follows:

$$\Omega^2 = \begin{pmatrix} -\omega_2^2 - \omega_3^2 & \omega_1\omega_2 & \omega_1\omega_3 \\ \omega_1\omega_2 & -\omega_1^2 - \omega_3^2 & \omega_2\omega_3 \\ \omega_1\omega_3 & \omega_2\omega_3 & -\omega_1^2 - \omega_2^2 \end{pmatrix} \tag{6.6}$$

and

$$\boldsymbol{\omega}\boldsymbol{\omega}^T = \begin{pmatrix} \omega_1^2 & \omega_1\omega_2 & \omega_1\omega_3 \\ \omega_1\omega_2 & \omega_2^2 & \omega_2\omega_3 \\ \omega_1\omega_3 & \omega_2\omega_3 & \omega_3^2 \end{pmatrix} \tag{6.7}$$

Requiring

$$\|\omega\|^2 = \omega_1^2 + \omega_2^2 + \omega_3^2$$

the matrix, Ω^2, can be given in terms of ω as:

$$\Omega^2 = \boldsymbol{\omega}\boldsymbol{\omega}^{\mathrm{T}} - \|\boldsymbol{\omega}\|^2 I \tag{6.8}$$

By multiplying the matrix by itself, the third power of the matrix can be expressed as:

$$\Omega^3 = \Omega\Omega^2 = \Omega(\boldsymbol{\omega}\boldsymbol{\omega}^{\mathrm{T}} - \|\boldsymbol{\omega}\|^2 I) = (\boldsymbol{\omega}\times\boldsymbol{\omega})\boldsymbol{\omega}^{\mathrm{T}} - \Omega\|\boldsymbol{\omega}\|^2 I = -\|\boldsymbol{\omega}\|^2\Omega \tag{6.9}$$

Since the finite rotation, $e^{\Omega\theta}$, is dependent on the product $\Omega\theta$, we can divide Ω so that $\|\boldsymbol{\omega}\| = 1$ and correspondingly scale θ, to maintain $\Omega\theta$ invariant. The i^{th} power can then be expressed using only the square of the matrix as follows:

$$\Omega^i = \begin{cases} \Omega & \text{if} \quad i = 4k+1 \\ \Omega^2 & \text{if} \quad i = 4k+2 \\ -\Omega & \text{if} \quad i = 4k+3 \\ -\Omega^2 & \text{if} \quad i = 4k+4 \end{cases} \tag{6.10}$$

which can also be expressed as follows:

$$\Omega^i = (-1)^{\left\lfloor \frac{i+1}{2} \right\rfloor + 1} \Omega^{2-i \bmod 2}, i = 1,.... \tag{6.11}$$

(Eq. 6.11) can now be substituted into (Eq. 6.5), which can be written as two sums over even and odd powers of Ω respectively and is given as:

$$e^{\Omega\theta} = \sum_{i=0}^{\infty} \frac{(\theta\Omega)^i}{i!} = I + \sum_{i=1}^{\infty} \frac{(\theta\Omega)^{2i}}{(2i)!} + \sum_{i=0}^{\infty} \frac{(\theta\Omega)^{2i+1}}{(2i+1)!} \tag{6.12}$$

In order to simplify (Eq. 6.12), we will substitute (Eq. 6.11) into (Eq. 6.12) using simplified formulae for Ω^{2i} and Ω^{2i+1}. Making use of the following relationships:

$$\begin{aligned} &2i \bmod 2 = 0 \\ &\left\lfloor \frac{2i+1}{2} \right\rfloor = i \\ &2i+1 \bmod 2 = 1 \\ &\left\lfloor \frac{2i+2}{2} \right\rfloor = i+1 \end{aligned} \tag{6.13}$$

formulae for Ω^{2i} and Ω^{2i+1} can be obtained from (Eq. 6.11) and (Eq. 6.13) as follows:

$$\begin{aligned}\Omega^{2i} &= (-1)^{i+1}\Omega^2 \\ \Omega^{2i+1} &= (-1)^i\Omega\end{aligned} \tag{6.14}$$

Substituting (Eq. 6.14) into the sums in (Eq. 6.12), the first sum of (Eq. 6.12) is given as:

$$\sum_{i=1}^{\infty}\frac{(\Omega\theta)^{2i}}{(2i)!} = \sum_{i=1}^{\infty}(-1)^{i+1}\frac{\theta^{2i}}{(2i)!}\Omega^2 = -\Omega^2(\cos\theta - 1) \tag{6.15}$$

Similarly the second sum reduces to

$$\sum_{i=0}^{\infty}\frac{(\Omega\theta)^{2i+1}}{(2i+1)!} = \sum_{i=0}^{\infty}(-1)^i\frac{\theta^{2i+1}}{(2i+1)!}\Omega = \Omega\sin\theta \tag{6.16}$$

Substituting (Eq. 6.15) and (Eq. 6.16) into (Eq. 6.12) yields the Rodrigues formula:

$$e^{\Omega\theta} = I + \Omega\sin\theta + \Omega^2(1-\cos\theta) \tag{6.17}$$

In order to establish that the matrix $e^{\Omega\theta}$ is a rotation matrix, it has to be verified that it satisfies the properties of SO(3), which are:

1) The transpose of the matrix is equal to its inverse.
2) The determinant of the matrix is +1

The transpose of the matrix, $e^{\Omega\theta}$, is given as:

$$\begin{aligned}(e^{\Omega\theta})^{\mathrm{T}} &= I + \Omega^{\mathrm{T}}\sin\theta + (\Omega^2)^{\mathrm{T}} \\ &= I - \Omega\sin\theta + \Omega^2(1-\cos\theta) \\ &= I + \Omega\sin(-\theta) + \Omega^2(1-\cos(-\theta)) \\ &= e^{-\Omega\theta}\end{aligned} \tag{6.18}$$

Multiplying the matrix by its transpose, results in the following:

$$
\begin{aligned}
(e^{\Omega\theta})^{\mathrm{T}} e^{\Omega\theta} &= \left(I - \Omega\sin\theta + \Omega^2(1-\cos\theta)\right)\left(I + \Omega\sin\theta + \Omega^2(1-\cos\theta)\right) \\
&= I + \Omega\sin\theta + \Omega^2(1-\cos\theta) - \Omega^2\sin^2\theta - \Omega^3\sin\theta(1-\cos\theta) \\
&+ \Omega^2(1-\cos\theta) + \Omega^3(1-\cos\theta)\sin\theta + \Omega^4(1-\cos\theta)^2 \\
&= I + \Omega^2(1-\cos\theta - \sin^2\theta + 1 - \cos\theta - 1 + 2\cos\theta - \cos^2\theta) = I
\end{aligned}
\tag{6.19}
$$

Since the product is the identity, the transpose is the inverse.

From (Eq. 6.18) and (Eq. 6.19), it follows that the determinant of the exponential map $\left|e^{\Omega\theta}\right| = \pm 1$. Since $\left|e^{\Omega 0}\right| = |I| = 1$ and that the determinant map is continuous it follows that $\left|e^{\Omega\theta}\right| = 1$. Thus, the exponential of $\Omega\theta$, $e^{\Omega\theta}$, is a rotation matrix.

It can also be shown that for each rotation matrix, R, given by

$$
R = \begin{bmatrix} r_{11} & r_{12} & r_{13} \\ r_{21} & r_{22} & r_{23} \\ r_{31} & r_{32} & r_{33} \end{bmatrix} \tag{6.20}
$$

there exists an exponential map, $e^{\Omega\theta}$, i.e., that the map is surjective.

Since

$$
\begin{aligned}
e^{\Omega\theta} &= I + \Omega\sin\theta + \Omega^2(1-\cos\theta) \\
&= \begin{pmatrix} 1-v_\theta(\omega_2^2+\omega_3^2) & \omega_1\omega_2 v_\theta - \omega_3 s_\theta & \omega_1\omega_3 v_\theta + \omega_2 s_\theta \\ \omega_1\omega_2 v_\theta + \omega_3 s_\theta & 1-v_\theta(\omega_1^2+\omega_3^2) & \omega_2\omega_3 v_\theta - \omega_1 s_\theta \\ \omega_1\omega_3 v_\theta - \omega_2 s_\theta & \omega_2\omega_3 v_\theta + \omega_1 s_\theta & 1-v_\theta(\omega_1^2+\omega_2^2) \end{pmatrix}
\end{aligned} \tag{6.21}
$$

$$
= \begin{pmatrix} \omega_1^2 v_\theta + c_\theta & \omega_1\omega_2 v_\theta - \omega_3 s_\theta & \omega_1\omega_3 v_\theta + \omega_2 s_\theta \\ \omega_1\omega_2 v_\theta + \omega_3 s_\theta & \omega_2^2 v_\theta + c_\theta & \omega_2\omega_3 v_\theta - \omega_1 s_\theta \\ \omega_1\omega_3 v_\theta - \omega_2 s_\theta & \omega_2\omega_3 v_\theta + \omega_1 s_\theta & \omega_3^2 v_\theta + c_\theta \end{pmatrix} \tag{6.22}
$$

where $c_\theta = \cos\theta$, $s_\theta = \sin\theta$, and $v_\theta = 1-\cos\theta$. It follows from (Eq. 6.22) that

$$
\theta = \cos^{-1}\left(\frac{r_{11}+r_{22}+r_{33}-1}{2}\right) \tag{6.23}
$$

and

$$
\boldsymbol{\omega} = \begin{pmatrix} \omega_1 \\ \omega_2 \\ \omega_3 \end{pmatrix} = \frac{1}{2\sin\theta}\begin{pmatrix} r_{32}-r_{23} \\ r_{13}-r_{31} \\ r_{21}-r_{12} \end{pmatrix} \tag{6.24}
$$

proving the surjectivity of the exponential map and establishing the Euler-Rodrigues relationships (Rodriguez 1840). It should be noted that the skew symmetric matrix, which describes the angular velocity is also known as the exponential coordinates of the rotation.

6.3 Exponential Coordinates for General Displacements

We now consider how exponential coordinates can be found for more general rigid body motions, in which the body translates as well as rotates about the origin of the reference coordinate frame. In this more general case, motion of a point can be described by an ordered pair of distinct mathematical objects, (d, R). The element d represents a vector from the origin of an inertial frame to the origin of the moving rigid body and R is the rotation of the rigid body relative to the inertial frame. The latter is referred to as its orientation. As for rotations, the ordered pairs (d, R) also form a group, which has been called the Special Euclidean group, SE(3). The group operation for SE(3) is the composition of the rigid body transformations such that:

$$(d_1, R_1)(d_2, R_2) = (R_1 d_2 + d_1, R_1 R_2) \tag{6.25}$$

Since the composition of two rotations is a rotation, and the application of a rotation operator on a vector is a vector, the group operation is closed. From the associativity of the group of rotations and vector addition, it can be shown that the group operation defined for SE(3) is also associative. The identity element of the group is ((0,0,0), I). For

every element (d_1, R_1) there exists an inverse, $(-R_1d_1, R_1^T)$, which produces the group identity when multiplied by (d_1, R_1) either on the left or on the right. Thus SE(3), the displacements of a rigid body, form a group.

A vector $\mathbf{q}$ from the origin of a reference frame to some point in the rigid body will change by $\mathbf{dq}$, due to an infinitesimal rotation, Ω and translation, $\mathbf{v}$, over time, *dt*. This can be given as:

$$d\mathbf{q} = (\Omega\mathbf{q} + \mathbf{v})dt \tag{6.26}$$

(Eq. 6.26) can be expressed as a 4x4 matrix, similarly to (Eq. 6.1):

$$\Xi = \begin{pmatrix} \Omega & \mathbf{v} \\ 0 & 0 \end{pmatrix} \tag{6.27}$$

where Ξ is the twist associated with an infinitesimal displacement of the rigid body. As for infinitesimal rotations, this matrix can now be converted to exponential coordinates by considering $e^{\Xi\delta}$, where Ξ is analogous to and is a generalization of the infinitesimal rotation matrix and δ is a generalization of the angle. As for the case of pure rotations, it

will be assumed Ξ will be divided by a factor such that $\|\boldsymbol{\omega}\| = 1$ and δ will be scaled to maintain the product $\Xi\delta$ invariant. Any vector $\mathbf{v}$, then satisfies the following equation:

$$\boldsymbol{\omega} \times (\boldsymbol{\omega} \times \mathbf{v}) = \Omega^2 \mathbf{v} = \boldsymbol{\omega}\boldsymbol{\omega}^{\mathrm{T}} \mathbf{v} - \mathbf{v} = (\boldsymbol{\omega} \cdot \mathbf{v})\boldsymbol{\omega} - \mathbf{v} \tag{6.28}$$

and can be simplified to give:

$$\mathbf{v} = (\boldsymbol{\omega}^{\mathrm{T}} \mathbf{v})\boldsymbol{\omega} - \boldsymbol{\omega} \times (\boldsymbol{\omega} \times \mathbf{v}) \tag{6.29}$$

Substituting (Eq. 6.29) into (Eq. 6.27)

$$\Xi = \begin{pmatrix} \Omega & h\boldsymbol{\omega} \\ 0 & 0 \end{pmatrix} + \begin{pmatrix} 0 & \mathbf{u} \\ 0 & 0 \end{pmatrix} \tag{6.30}$$

where $h = \boldsymbol{\omega} \cdot \mathbf{v}$ and $\mathbf{u} = -\boldsymbol{\omega} \times (\boldsymbol{\omega} \times \mathbf{v})$

Such decomposition simplifies the expression for the i^{th} power of Ξ:

$$\Xi^i = \begin{pmatrix} \Omega^i & 0 \\ 0 & 0 \end{pmatrix} + \begin{pmatrix} 0 & \Omega^{i-1}\mathbf{u} \\ 0 & 0 \end{pmatrix} \text{ for } i = 2,\ldots \tag{6.31}$$

Since

$$\Xi^2 = \begin{pmatrix} \Omega & \mathrm{v} \\ 0 & 0 \end{pmatrix}\begin{pmatrix} \Omega & \mathrm{v} \\ 0 & 0 \end{pmatrix} = \begin{pmatrix} \Omega^2 & \Omega\mathbf{v} \\ 0 & 0 \end{pmatrix} \tag{6.32}$$

$$\Xi^{i+1} = \begin{pmatrix} \Omega & \mathbf{v} \\ 0 & 0 \end{pmatrix}\begin{pmatrix} \Omega^i & \Omega^{i-1}\mathbf{v} \\ 0 & 0 \end{pmatrix} = \begin{pmatrix} \Omega^{i+1} & \Omega^i\mathbf{v} \\ 0 & 0 \end{pmatrix} = \begin{pmatrix} \Omega^{i+1} & \Omega^i\mathbf{u} \\ 0 & 0 \end{pmatrix} \tag{6.33}$$

which allows the following expression for the exponential of the matrix Ξδ:

$$
\begin{aligned}
e^{\Xi\delta} &= \sum_{i=0}^{\infty} \frac{(\Xi\delta)^i}{i!} \\
&= I + \delta \begin{pmatrix} \Omega & h\boldsymbol{\omega} \\ 0 & 0 \end{pmatrix} + \delta \begin{pmatrix} 0 & \mathbf{u} \\ 0 & 0 \end{pmatrix} + \sum_{i=2}^{\infty} \frac{\delta^i}{i!} \left(\begin{pmatrix} \Omega^i & 0 \\ 0 & 0 \end{pmatrix} + \begin{pmatrix} 0 & \Omega^{i-1}\mathbf{u} \\ 0 & 0 \end{pmatrix} \right) \\
&= \begin{pmatrix} \sum_{i=0}^{\infty} \frac{\delta^i}{i!} \Omega^i & 0 \\ 0 & 1 \end{pmatrix} + \delta \begin{pmatrix} 0 & h\boldsymbol{\omega} \\ 0 & 0 \end{pmatrix} + \sum_{i=1}^{\infty} \frac{\delta^i}{i!} \begin{pmatrix} 0 & \Omega^{i-1}\mathbf{u} \\ 0 & 0 \end{pmatrix} \\
&= \begin{pmatrix} e^{\Omega\delta} & 0 \\ 0 & 1 \end{pmatrix} + \delta \begin{pmatrix} 0 & h\boldsymbol{\omega} \\ 0 & 0 \end{pmatrix} + \begin{pmatrix} 0 & -\sum_{i=1}^{\infty} \frac{\delta^i}{i!} \Omega^{i-1}\Omega(\boldsymbol{\omega}\times\mathbf{v}) \\ 0 & 0 \end{pmatrix} \\
&= \begin{pmatrix} e^{\Omega\delta} & \boldsymbol{\omega}\boldsymbol{\omega}^T\mathbf{v}\delta + (I - e^{\Omega\delta})(\boldsymbol{\omega}\times\mathbf{v}) \\ 0 & 1 \end{pmatrix}
\end{aligned}
\tag{6.34}
$$

The displacement matrix, $e^{\Xi\delta}$, is seen to have a form given as:

$$
e^{\Xi\delta} = D = \begin{bmatrix} \mathrm{R} & \mathrm{d} \\ 0 & 1 \end{bmatrix} \tag{6.35}
$$

where R is the rotational part and d is the translational part of the displacement, D. The rotational part of the twist Ξ can be found from R using the Euler-Rodriguez equations:

(Eq. 6.23) and (Eq. 6.24). The translational part of the twist can be found from the system of linear equations:

$$\left(\omega\omega^{\mathrm{T}}\theta + (I - e^{\Omega\theta})\Omega\right)\mathrm{v} = \mathrm{d} \tag{6.36}$$

Once the exponential coordinates for displacement are obtained, the axis of rotation in Euclidean space can be deduced from the differential equation that governs motion of a point on the rigid body:

$$\dot{\mathbf{q}} = \Omega\mathbf{q} + \mathbf{v} \tag{6.37}$$

Substituting (Eq. 6.29) into (Eq. 6.37) gives

$$\dot{\mathbf{q}} = \Omega(\mathbf{q} - \omega \times \mathbf{v}) + \omega^{\mathrm{T}}\mathbf{v}\omega \tag{6.38}$$

If the vector $\mathbf{q}$ is chosen as $\mathbf{q}_0 = \omega \times \mathbf{v}$ the first component of (Eq. 6.38) vanishes and the infinitesimal displacement is solely along ω, the axis of the displacement.

To analyze body, head and eye movements in three dimensions, it will be necessary to find smooth displacements of these body parts in space from noisy samples of the displacement matrices.

6.4 Algorithm for filtering and estimating Displacements

We first consider a proposed methodology for filtering displacements using twists and exponential coordinates. Let D_{-n}, $D_{-n+1},\ldots,D_0,\ldots,D_{n-1},D_n$ be a sequence of displacements given in a global coordinate frame, sampled from a small portion of the rigid body trajectory. We will assume that the sampled trajectory is "smooth," so that incremental displacements between, D_k and D_{k+1}, could be approximated by a single incremental displacement matrix e^{Ξ}, obtained from the twist Ξ for k ranging from –n to n-1. We can now define a matrix B over the window –n,...0,...n, relative to the spatial frame of reference, such that each D_k can be obtained as this incremental displacement from B:

$$D_k \approx e^{k\Xi}B \tag{6.39}$$

The incremental displacement, $\Delta_k = D_k D_{-k}^{-1}$, could then be approximated as:

$$\Delta_k \approx e^{k\Xi}B\left(e^{-k\Xi}B\right)^{-1} = e^{k\Xi}BB^{-1}\left(e^{-k\Xi}\right)^{-1} = e^{2k\Xi} \tag{6.40}$$

and

$$\Delta_k \approx e^{2k\Xi} \tag{6.41}$$

independent of B. To find the matrix, Ξ that gives the "best" approximation over the range of displacement matrices, D_{-n}, $D_{-n+1},\ldots,D_0,\ldots,D_{n-1},D_n$, we propose a procedure that is similar to minimizing the mean squared error for fitting one-dimensional data. The value of the displacement matrix at some sample, D_k, can be multiplied by the inverse of the predicted displacement, $(e^{k\Xi}B)^{-1}$. If the data were predicted perfectly by the approximation, then the matrix multiplication should be the identity transformation, I. Therefore, an appropriate error at each sample displacement is the norm of the difference between the matrix product $D_k(e^{k\Xi}B)^{-1}$ and the identity matrix I. Thus, the total error, E, can be defined as:

$$E = \sum_{k=-n}^{n} \left\| D_k \left(e^{k\Xi} B\right)^{-1} - I \right\|^2 \tag{6.42}$$

where an appropriate norm $\| \cdot \|$, for matrices can be chosen (Blum 1972; Press, Teukolsky et al. 1992). The matrices Ξ and B that minimize E can then be determined.

A straightforward minimization procedure for finding B and Ξ would involve utilization of nonlinear optimization techniques (Press, Teukolsky et al. 1992). The minimization procedure could be simplified, however, by minimizing the residual norm (Blum 1972) for the incremental displacement, Δ_k as follows:

$$\sum_{k=1}^{n} \left\| \Delta_k \cdot \left(e^{2k\Xi} \right)^{-1} - I \right\|_2^2 \rightarrow \min \tag{6.43}$$

Since each Δ_k is a displacement in its own right, it is generated by some twist, which is a function of Δ_k, denoted by $\Xi(\Delta_k)$. Thus, instead of minimizing (Eq. 6.43), we can minimize the function *T*, given by:

$$T = \sum_{k=1}^{n} \left\| \Xi(\Delta_k) - 2k\Xi \right\|_2^2 \tag{6.44}$$

The optimal estimate of Ξ in the least squares sense can be given as follows (See Appendix A):

$$\Xi = \frac{3}{n(n+1)(2n+1)} \sum_{k=1}^{n} \Xi(\Delta_k) \tag{6.45}$$

The original sum, (Eq. 6.43), can serve as a measure for the goodness of fit:

$$\sum_{k=1}^{n} \left\| \Delta_k e^{-2k\Xi} - I \right\|_2^2 \tag{6.46}$$

Obtained in this way, the optimal twist estimate Ξ yields both the angular velocity estimate ω, and pivot point estimate, which can be found as

$$\mathbf{q}_0 = \boldsymbol{\omega} \times \mathbf{v} \tag{6.47}$$

where $\mathbf{v}$ is the differential translation part of the twist. This point in three-dimensional space $\mathbf{q}_0$, is a point on the rotational axis corresponding to the incremental displacement given by e^{Ξ}.

6.5 Algorithm for Determining Closest Point to a Set of Lines (Virtual Intersection Point)

We now consider the problem of finding an approximate intersection point in three dimensions for lines in space. We define this point as the *virtual intersection point* of the lines in three dimensions. When the lines represent axes lines of rotation, we will refer to the virtual intersection point as the *virtual pivot point*. An example of a virtual intersection point would be the point of intersection of all naso-occipital axes over a window of displacements. For real data, there is no single intersection point and therefore, an estimate of an approximate intersection point must be defined. A virtual pivot point would be the point about which the head rotates. These applications will be considered in detail in CHAPTER 7 and CHAPTER 8.

The methodology is based on finding the nearest point to a set of lines in three-dimensional space using the usual metric for finding the distance from a point to a line. The virtual intersection point is that point, which minimizes the sum of the square distances to each of the lines.

Lines in space will be given in parametric form by specifying a point P in three dimensional space relative to some global coordinate frame and a direction vector $\mathbf{v}$ (with $\|\mathbf{v}\| = 1$). The line is defined as a set of points $\{P+t\mathbf{v} \mid -\infty < t < \infty\}$ and denoted as $(P, \mathbf{v})$. The point, P is not unique, since any point on the line is appropriate, but the vector, $\mathbf{v}$, is unique up to a direction.

Let Q be a point in the three-dimensional space and $\mathbf{d}(t)$ a vector directed from Q towards a point on the line $(P, \mathbf{v})$. That is $\mathbf{d}(t) = P + t\mathbf{v} - Q$. Let the distance from Q to the

line be the minimum of $\|\mathbf{d}(t)\|$. From elementary analytical geometry it follows that the minimum is attained for the vector $\mathbf{d}$ both perpendicular to $\mathbf{v}$ and lying in the common plane of the line and the point Q. That is

$$\overrightarrow{PQ} + \mathbf{d} = (\overrightarrow{PQ} \cdot \mathbf{v})\mathbf{v} \tag{6.48}$$

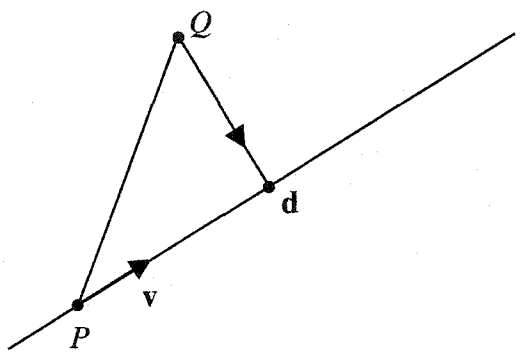

Thus, $\mathbf{d}$ can be found as:

$$\begin{aligned} \mathbf{d} &= -(Q-P) + \big((Q-P)\cdot \mathbf{v}\big)\mathbf{v} \\ &= -(Q-P) + (Q\cdot \mathbf{v} - P\cdot \mathbf{v})\mathbf{v} \\ &= -Q + (Q\cdot \mathbf{v})\mathbf{v} - \big(-P + (P\cdot \mathbf{v})\mathbf{v}\big) \end{aligned} \tag{6.49}$$

Since the last term of the sum in (Eq. 6.49) depends only on the line parameterization, and is not affected by location of the point Q, it will be convenient to denote

$$\begin{aligned} C &= -\left(-P + (P \cdot \mathbf{v})\mathbf{v}\right) \\ d &= -Q + (Q \cdot \mathbf{v})\mathbf{v} + C \end{aligned} \tag{6.50}$$

Note that C is the point on the line closest to the origin of the coordinate system. This allows for a "normalized" representation of lines.

Given a system of n lines $(P_1, \mathbf{v}_1)$, $(P_2, \mathbf{v}_2)$,...,$(P_n, \mathbf{v}_n)$, not all parallel in three-dimensional space, there exists a point Q which minimizes the sum of squared distances to each line, i.e. if $\mathbf{d}_k$ is the distance vector from Q to the line $(P_k, \mathbf{v}_k)$, then $E = \frac{1}{2}\sum_{k=1}^{n} \|\mathbf{d}_k\|^2$ is minimized. Such a condition on the lines is referred to as their having general position. Substituting $C_{ki} = P_{ki} - v_{ki} P_k^{\mathrm{T}} \mathbf{v}_k$, E can be expressed as:

$$E = \frac{1}{2}\sum_{k=1}^{n}\sum_{i}\left(v_{ki}\sum_{j} v_{kj} Q_j - Q_i + C_{ki} \right)^2 \tag{6.51}$$

which attains the minimum when all partial derivatives of E with respect to the components of Q vanish. That is $\frac{\partial E}{\partial Q_m} = 0$ for $m = 1,2,3$ which leads to the following system of equations:

$$\frac{\partial S}{\partial Q_m} = \sum_{k=1}^{n} \left[\left(v_{km} \sum_{j \neq m} v_{kj} Q_j + v_{km}^2 Q_m - Q_m + C_{km} \right)(v_{km}^2 - 1) + \sum_{i \neq m} \left(v_{ki} \sum_{j \neq m} v_{kj} Q_j + v_{ki} v_{km} Q_m - Q_i + C_{ki} \right) v_{ki} v_{km} \right] = 0 \tag{6.52}$$

where regrouping the terms yields:

$$\frac{\partial S}{\partial Q_m} = \sum_{k=1}^{m} \left[\underbrace{\left((v_{km}^2 - 1)^2 + v_{km}^2 \sum_{i \neq m} v_{ki}^2 \right)}_{(a)} Q_m + \underbrace{(v_{km}^2 - 1) v_{km} \sum_{j \neq m} v_{kj} Q_j}_{(b)} + (v_{km}^2 - 1) C_{km} + \underbrace{v_{km} \sum_{i \neq m} v_{ki}^2 \sum_{j \neq m} v_{kj} Q_j}_{(c)} - v_{km} \sum_{i \neq m} v_{ki} Q_i + v_{km} \sum_{i \neq m} v_{ki} C_{ki} \right] \tag{6.53}$$

When $\mathbf{v}_k$ is normalized, (a) can be simplified to

$$(v_{km}^2 - 1) - v_{km}^2 (v_{km}^2 - 1)^2 = 1 - v_{km}^2 \tag{6.54}$$

and the sum of (b) and (c) is zero. The system of equation becomes:

$$\sum_{k=1}^{n} \left[(1 - v_{km}^2) Q_m - v_{km} \sum_{i \neq m} v_{ki} Q_i \right] = \sum_{k=1}^{n} \left[(1 - v_{km}^2) C_{km} - v_{km} \sum_{i \neq m} v_{ki} C_{ki} \right] \tag{6.55}$$

for $m = 1,2,3$

In matrix form this equation can be written as:

$$\left(\sum_{k=1}^{n} V_k^2 \right) Q = \sum_{k=1}^{n} V_k^2 C_k \tag{6.56}$$

or

$$Q = \left(\sum_{k=1}^{n} V_k^2 \right)^{-1} \sum_{k=1}^{n} V_k^2 C_k \tag{6.57}$$

where

$$V_k^2 = \begin{pmatrix} -v_{k2}^2 - v_{k3}^2 & v_{k1}v_{k2} & v_{k1}v_{k3} \\ v_{k1}v_{k2} & -v_{k1}^2 - v_{k3}^2 & v_{k2}v_{k3} \\ v_{k1}v_{k3} & v_{k2}v_{k3} & -v_{k1}^2 - v_{k2}^2 \end{pmatrix} \tag{6.58}$$

which is similar to (Eq. 6.6).

While Q is the virtual intersection point, there are points on the lines that are closest to Q. This distribution of points is a measure of the relationship of the lines to the virtual intersection point and is considered next.

6.6 Computation of Distribution of Points on the Lines Closest to the Virtual Intersection Point

Let Q_k denote the point on the k-th line closest to the virtual intersection point Q, whose coordinates are given relative to Q. These points can be found using Eq 6.49. We now wish to determine parameters that define this three-dimensional distribution. Conceptually, this can be done by first finding the direction along which the distribution has the greatest variance and its associated variance. Second, the plane orthogonal to this direction is found and the direction of maximum variance of the points projected into this plane and the associated variance is found. Third, the remaining direction orthogonal to the previous two directions is found and the variance of the points projected onto this line is found. The vectors along the three directions are the principal component directions

and is the conceptual basis for the Karhunen-Loeve transformation ((Tou and Gonzalez 1974), which is a method for finding an orthonormal basis for distributions along principal components. This orthonormal basis and associated variances can be determined by finding the extrema of the sum of squares of the dot products $(\langle \mathbf{v}, Q_k \rangle)^2$, for a vector $\mathbf{v}$ of unit length. Formally, this can be represented as:

$$\sum \mathbf{v}^T Q_k Q_k{}^T \mathbf{v} \rightarrow \max$$

The maximum is achieved along the eigenvector, $\mathbf{v}_1$ of the matrix $\Sigma Q_k Q_k{}^T$, corresponding to the largest eigenvalue. This eigenvalue gives the variance of the distribution along the first principal component. Similarly, the next eigenvalue gives the variance of the distribution in the subspace orthogonal to $\mathbf{v}_1$, and is along the second principal component $\mathbf{v}_2$. The final eigenvalue is the variance along the final principal component, $\mathbf{v}_3$.

6.7 Test of the Algorithm Using Artificial Rotations of a Gimbaled System

The proposed algorithms for determining a pivot point from rigid body displacement were initially tested using a gimbaled system that could be rotated by hand about yaw and pitch axes (Fig 6.1). Two groups of 3 markers were also mounted on the base and movable axis of the gimbaled system (Fig 6.1). One of the LED's on the base was located at the pivot point, which was fixed relative to the other rigid bodies, but moved less than a millimeter in space for all pitch rotations. The gimbal was oscillated in pitch with different amplitudes and at three frequencies.

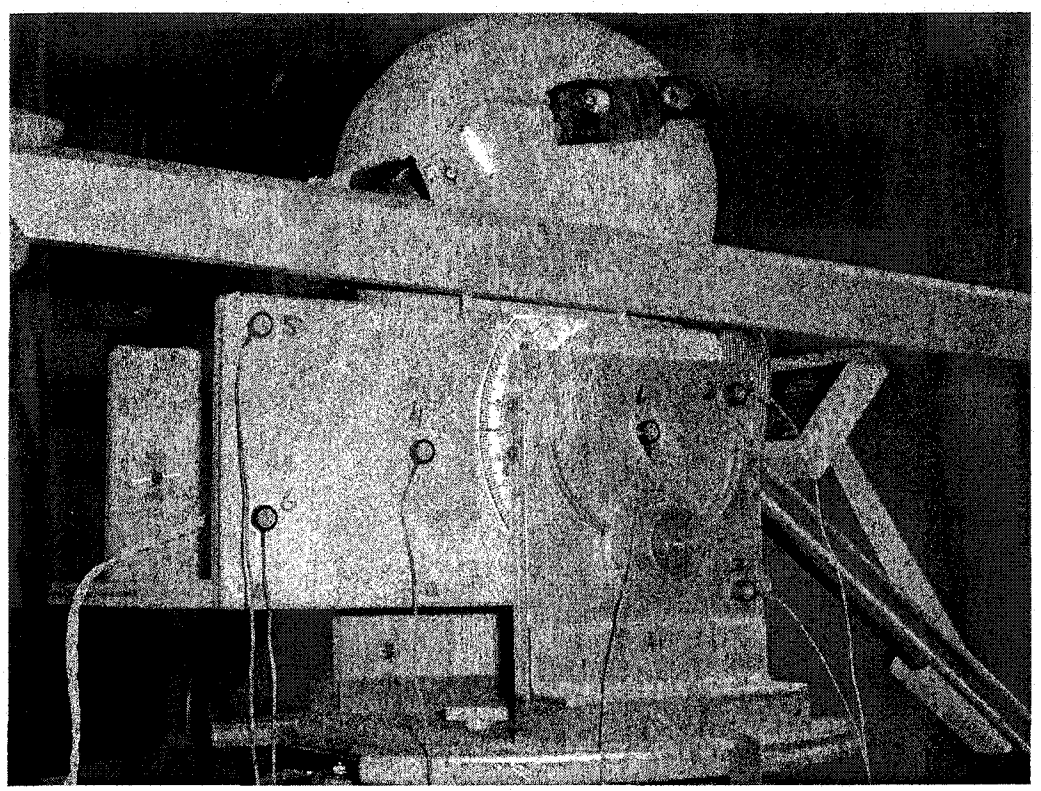

Fig 6.1 Gimbaled system

The data were transformed to ASCII files using a toolbench program as groups of data giving linear translation of the rigid body and rotation as a quaternion. These specified the coordinate transformations of moving group of markers with respect to a coordinate system attached to the base markers. In addition, coordinates of the pivot marker (Marker 1, Fig 6.1) were computed in the moving coordinate frame (i.e. attached to the markers on the moving part). We implemented a program (form_trans) that converted the ASCII files into VMF files representing the linear translation and rotation as axis-angle of each rigid body captured by the OPTOTRAK software. The VMF analysis program (VMF_anlz) was then utilized to display those files for inspection of the transformation parameters in their dependence on the time variable. The Displacement Matrices were constructed from these components.

Instantaneous axis-lines of rotation were computed and transformed into the moving coordinate frame using equations of the previous section. In order to verify accuracy, we then computed the distance of each of the instantaneous axis-lines to the known coordinates of the pivot marker. The resulting histogram is shows that majority of the axis lines are within 3mm of the pivot marker (Fig 6.2). The rightmost bin of the histogram counts the axis lines whose distance from the known pivot point was greater than 100 mm. The reason for this inaccuracy is that this algorithm is sensitive to the angular velocity of the rigid body. A low angular velocity results in less accurate estimate of the axis line. Moreover, since the rigid body in this experiment was oscillated rather than rotated in the same direction, it was impossible to obtain meaningful estimates near the point of the trajectory where the motion is reversed, since such sequence of displacements cannot be approximated by a single incremental displacement. This problem was dealt with by excluding parts of trajectory where the angular velocity is below some threshold.

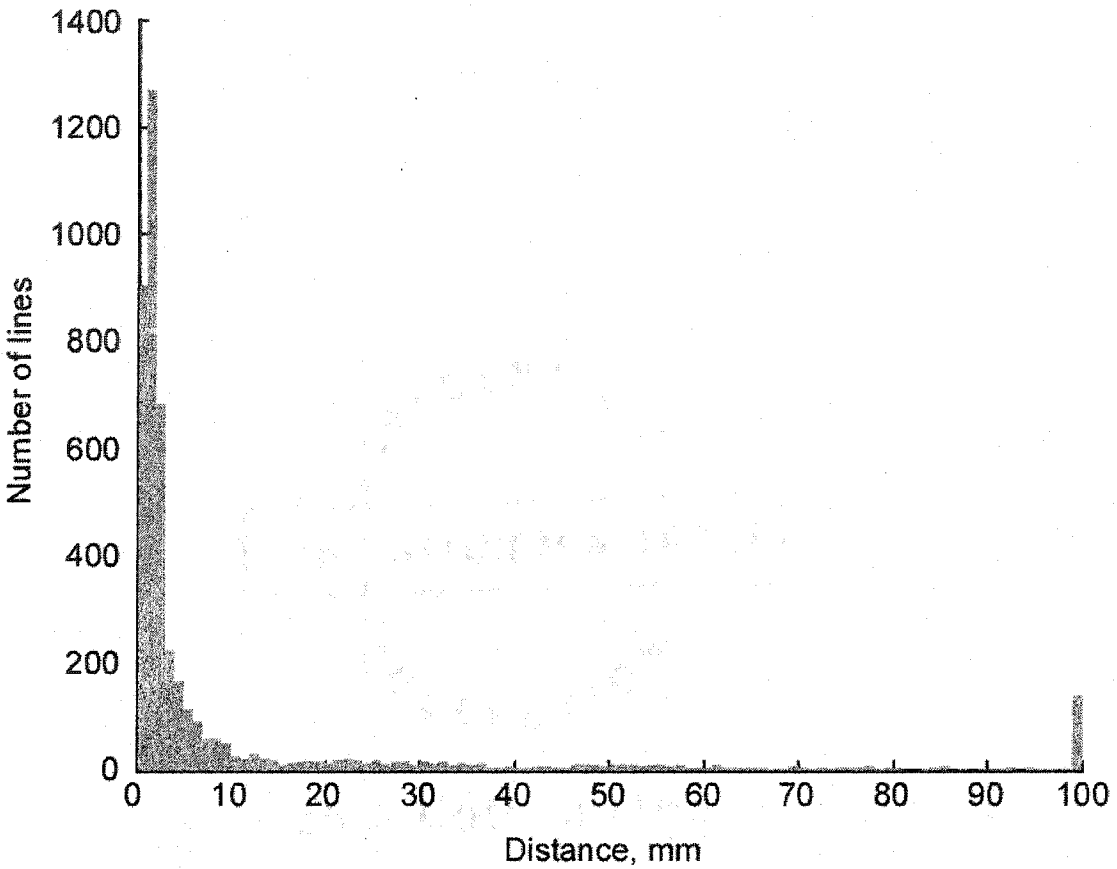

Fig 6.2 Histogram of the distances of instantaneous axis-lines from the pivot marker

CHAPTER 7 EXPERIMENTAL DETERMINATION OF HEAD ROTATION AXES FROM VOLUNTARY OSCILLATION OF THE HEAD ON TRUNK AT DIFFERENT HEAD ORIENTATIONS

7.1 Head coordinate system established based on voluntary rotations

Data of the positions of two rigid bodies, the head and trunk, were studied in five normal humans. The experiments were approved by the Institutional Review Board at Mount Sinai School of medicine and at the City University of New York and were performed in accordance with the ethical standards established in the 1964 Declaration of Helsinki. Subjects gave their informed consent prior to the inclusion in the study. Privacy and anonymity of the data associated with the subjects were maintained at all times during the course of the study.

Using the Toolbench program (Northern Digital, Inc), the head displacement was generated relative to the trunk coordinate frame. All subjects performed rolling, pitching, and yawing head movements voluntarily for 10 s each in the primary position of the head. The results of the fitting for each head shaking are assembled in Table 7-1, Table 7-2, Table 7-3, and Table 7-4.

Table 7-1 Rotation axes in head coordinates for subject MJD

Type	v_x	v_y	v_z	P_x	P_y	P_z
Rolling	0.8554	-0.0031	-0.5180	UN	-0.2	-64.6
Pitching	-0.0088	0.9998	0.0190	-19.7	UN	-48.4
Yawing	0.2505	0.0037	0.9681	-6.2	-1.5	UN

Table 7-2 Rotation axes in head coordinates for subject MM

Type	v_x	v_y	v_z	P_x	P_y	P_z
Rolling	0.9177	0.1009	-0.3842	UN	-5.9	-59.9
Pitching	-0.0155	0.9997	-0.0170	-7.6	UN	2.2
Yawing	-0.0243	-0.0112	0.9996	-11.8	-0.7	UN

Table 7-3 Rotation axes in head coordinates for subject PJ

Type	v_x	v_y	v_z	P_x	P_y	P_z
Rolling	0.9799	0.0770	-0.1838	UN	-0.7	-72.9
Pitching	-0.0729	0.9956	0.0591	-5.4	UN	-45.0
Yawing	0.2177	-0.0261	0.9757	-20.1	-6.5	UN

Table 7-4 Rotation axes in head coordinates for subject XLZ

Type	v_x	v_y	v_z	P_x	P_y	P_z
Rolling	0.8949	-0.0195	-0.4458	UN	-1.8	-81.6
Pitching	0.0232	0.9971	-0.0719	-18.2	UN	-45.4
Yawing	0.0732	0.0211	0.9971	-12.0	2.7	UN

where v_x, v_y, v_z are the direction cosines of a vector along the average axis and P_x, P_y, and P_z are the coordinates of a point on the axis, which defines the axis-line. Since the rotation axis were fairly well aligned with the corresponding landmark coordinate axes, the pivot point along the axis of head rotation is not capable of being localized and was denoted as UN in the table.

The average rotation axes for roll, pitch, and yaw relative to the head frame are shown in Fig 7.1. The coordinates of the averaged rotation axes are summarized in the following table

Table 7-5 Averaged rotation axes

Type	v_x	v_y	v_z
Rolling	0.9213	0.0392	-0.3869
Pitching	-0.0185	0.9998	-0.0027
Yawing	0.1301	-0.0032	0.9915

From the table, the average roll, pitch, and yaw rotation axes (Roll Rot Axis, Pitch Rot Axis, Yaw Rot Axis) are shown in (Fig 7.1A).

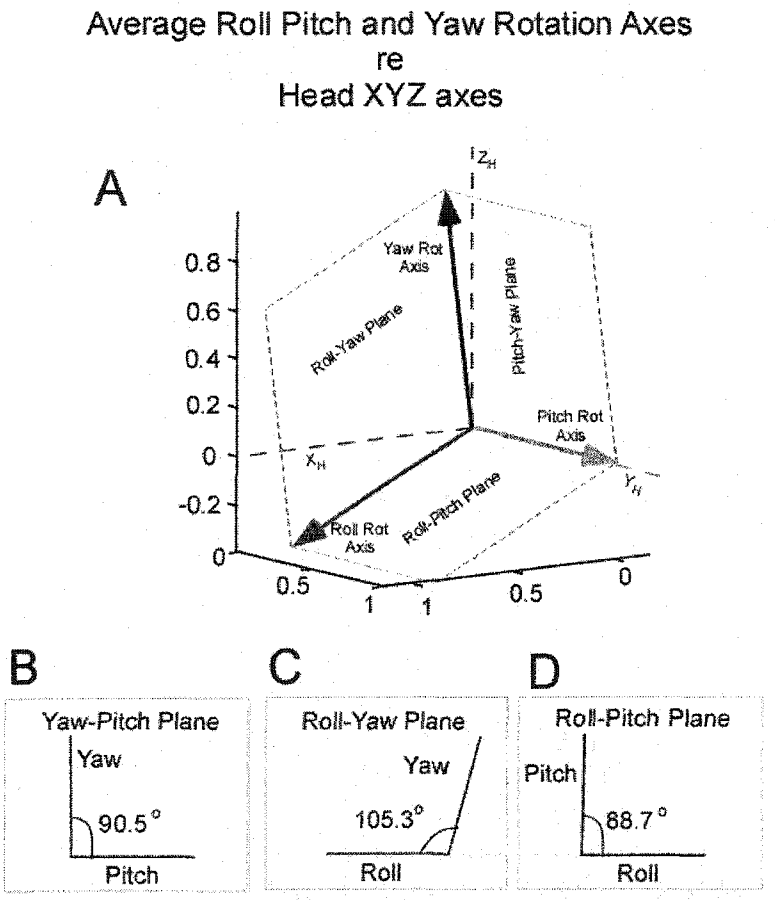

Fig 7.1 **A.** Average Roll, Pitch, and Yaw Rotation Axes in Head Coordinate Frame, **B.** The angle between Pitch and Yaw Rotation Axes, **C.** The angle between Roll and Yaw Rotation Axes, **D.** The angle between Roll and Pitch Rotation Axes.

The yaw rotation axis (Yaw Rot Axis) is tipped from Z_H about 7.5° (Fig 7.1A). The pitch axis is maintained along Y_H, while the roll rotation axis has components along all three head axes (Fig 7.1). The relative orientation of the rotation axes are such that pitch and yaw are approximately orthogonal (Fig 7.1B) while roll is approximately orthogonal to pitch (Fig 7.1D) it is not orthogonal to yaw (Fig 7.1C).

We next considered where the pitch and the yaw average rotation axes intersect the pitch and the yaw planes of the head when the head is oscillated about the primary position with a small angle, so that within this range the variation in axes as a function of head position was negligible (X_H-Y_H, X_H-Z_H) (Fig 7.2B, Fig 7.3B). The Y_H-Z_H plane was not considered, since roll was not an orthogonal axis.

The pivot points were obtained by fitting the head trajectory with incremental displacements (Eq. 6.45), but constraining the displacement to the two-dimensional plane orthogonal to the rotation axis. For the yaw rotation axis the sequence of head rigid body configurations was transformed into coordinate system whose Z-axis was aligned with the average angular velocity. In this coordinate system the yaw component of rotation and the X and Y components of translation were used to determine the "pivot point" of the incremental displacement in the X_H-Y_H plane (using increment of 11 data points). Each point in the figure represents an instantaneous pivot and the conglomeration of points represents all the instantaneous pivots throughout the trial. A velocity threshold was applied in finding the pivot points. Since the velocity was maximum when the head rotated through primary position, velocity thresholding eliminated data that were far from the primary position. These pivot points were subsequently transformed into the rotating

head coordinate frame and their mean was computed (Fig 7.2B, Dots in the X_H-Y_H plane).

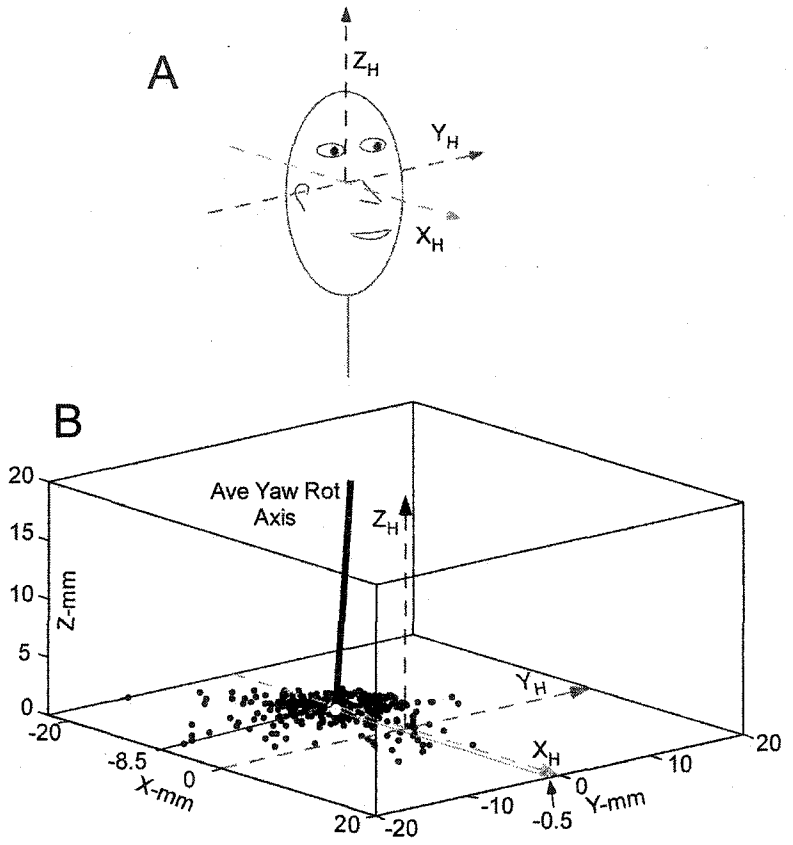

Fig 7.2 Axis-line of Yaw Rotation in Head Coordinates: **A.** Head Coordinate Frame, **B.** Instantaneous Pivot Points in the Yaw Plane obtained during a 10-second interval of head shaking (black dots) and the Average Axis-line of Yaw Rotation (see label).

For yaw rotation, the pivot point in the X_H-Y_H plane was at 8.5 mm behind the X_H-Z_H plane average

Since the pitch rotation axis was orthogonal to the X_H-Z_H plane, the same incremental algorithm was applied to the X and Z components of translation and the negative pitch component of rotation.

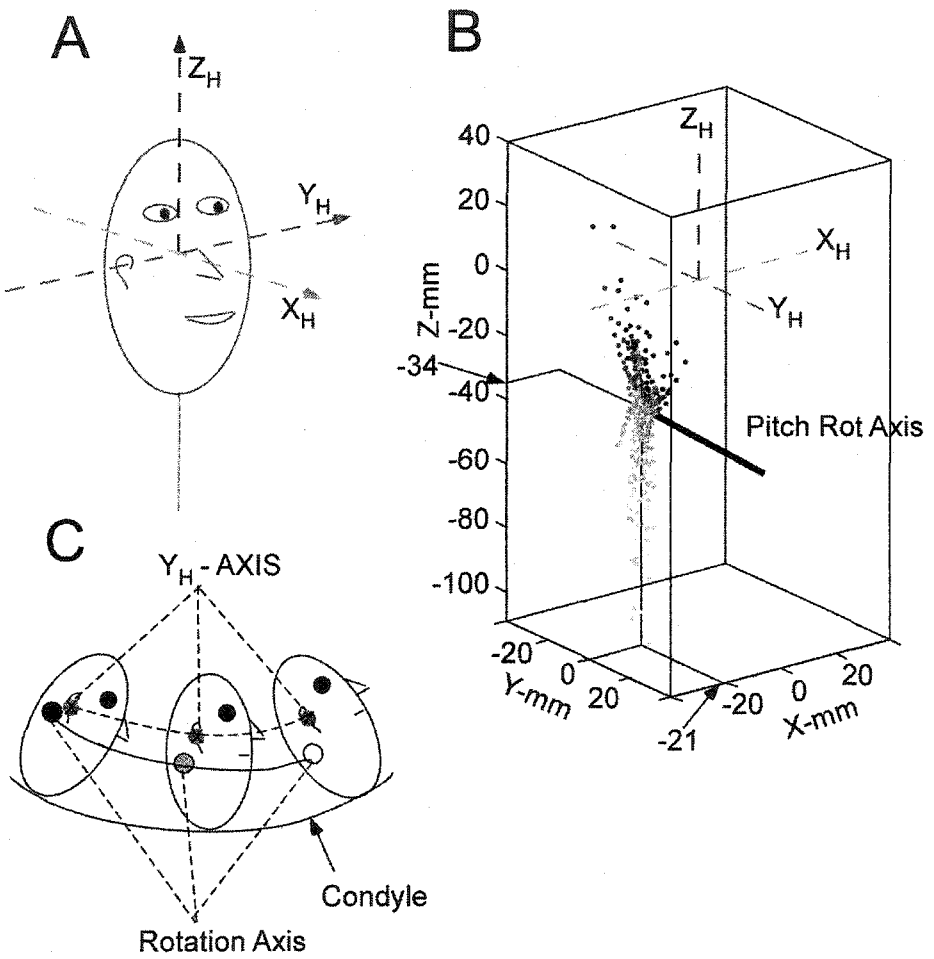

Fig 7.3 Axis-line of Pitch Rotation in Head Coordinates: **A.** Head Coordinate Frame, **B.** Instantaneous Pivot Points in the Pitch Plane obtained during a 10-second interval of head shaking (colored from black for max positive pitch to light gray for min negative pitch) and the Average Axis-line of Pitch Rotation (see label), **C.** Diagram of the Instantaneous Pitch Head Rotation Axis-line with for Different Head Positions on the Condyles.

It should be noted that the axes associated with the head shaking about orthogonal axes were close to being orthogonal for the pitch and yaw axes (Fig 7.1). The roll axis was not orthogonal to the others. The pitch axis was also closely aligned with Y_H axis. Since the pitch and yaw vectors are closest to being orthogonal, the Gram-Schmidt orthonormalization procedure was used to generate an orthonormal basis starting with the pitch vector, then adjusting the yaw vector and then finally finding the roll vector. The coordinate vectors could then be related by a single rotation matrix to the head coordinate frame. We call such coordinate obtained from voluntary head rotations "natural". The axis-angles of the natural coordinate frames relative to the landmark coordinate tables are shown in (Table 7-6).

Table 7-6 Orientation of the natural coordinate frames relative to the landmark coordinate frames

Subject	n_x	n_y	n_z	φ
mjd	0.0701	0.9966	0.0441	14.6
mm	-0.4952	-0.7337	0.4652	1.9
pj	0.2130	0.9184	0.3333	13.7
xlz	-0.6761	0.6951	-0.2443	6.0

7.2 Pitch and Yaw Axes Of Head Rotation As A Function Of Head Orientation

This chapter shows how we extended the determination of the axes in primary position, to determine the axes of pitch and yaw rotations when the head was placed in a variety of orientations (Fig 7.4). Roll was not considered in these tertiary head positions,

since it was virtually impossible to make a pure roll head movement in these positions. The angle of the yaw axis from rotations about yaw was compared with comparable results from MRI radiographs of the dens of C2 (Courtesy of Dr. Bradley Delman, Dept. of Radiology, Mount Sinai School of medicine). This tested the hypothesis that the head rotates in yaw about an axis that is coincident with the axis of the dens. Our hypothesis on pitch head movements is that pitch arises from movement of the head on the condyles, which rotate with yaw rotation in a gimbaled fashion.

7.2.1 Experimental Protocol for Determining Rotation Axes:

The subjects were instructed to position their heads 0° (primary position), 10°, 20°, and 30° in extension (looking up, negative pitch), and then back to the primary position, and then 10°, 20°, and 30° flexions (looking down, positive pitch) (Fig 7.4). At each of these positions, subjects were instructed to voluntarily oscillate their head about their yaw axis while keeping the average position approximately at their initial orientation. In addition, five positions were tested for pitching: 0° (primary position), left, right, up, and down. All angular positions of the head were measured relative to the primary position when the Z_H-Axis of the head is aligned with the Z-Axis of the trunk and gravity and the Y_H axis is aligned with trunk Y_K axis. Unlike yaw oscillation experiments, the angles of the head orientations about which the subject oscillated their head were not monitored: the subjects simply chose an angle that they considered appropriate. We used average values of the yaw and pitch angles to describe the positions of the head for each of the experiments. The average axis of the head rotation and the angle between its projection onto the head yaw plane and the Y-Axis of the head were determined. We observed that the rotation axis during pitching stays approximately

invariant relative to the head: for zero yaw positions (up, down, straight) the angle was within 3°, while when pitching at 48.7° to the left, the angle was only 8.7°. Our conclusion is that the axis of the pitch rotation is determined by the condyles, whose position is fixed relative to the head. As the head rotates in yaw, the condyles rotate in yaw by the same amount, and so does the axis of pitch rotation. The average results of the pitch-oscillation experiments are summarized in Table 7-7 and support our hypothesis.

Table 7-7 Summary of the pitch-shaking experiments. All angles are in degrees.

	Up	Down	Left	Right	Straight
Average Yaw	-1.9	-2.1	48.7	-52.1	2.6
Average Pitch	-22.6	25.7	5.8	4.1	0.1
Average Angle	0.8	-2.7	8.7	-6.4	-1.1

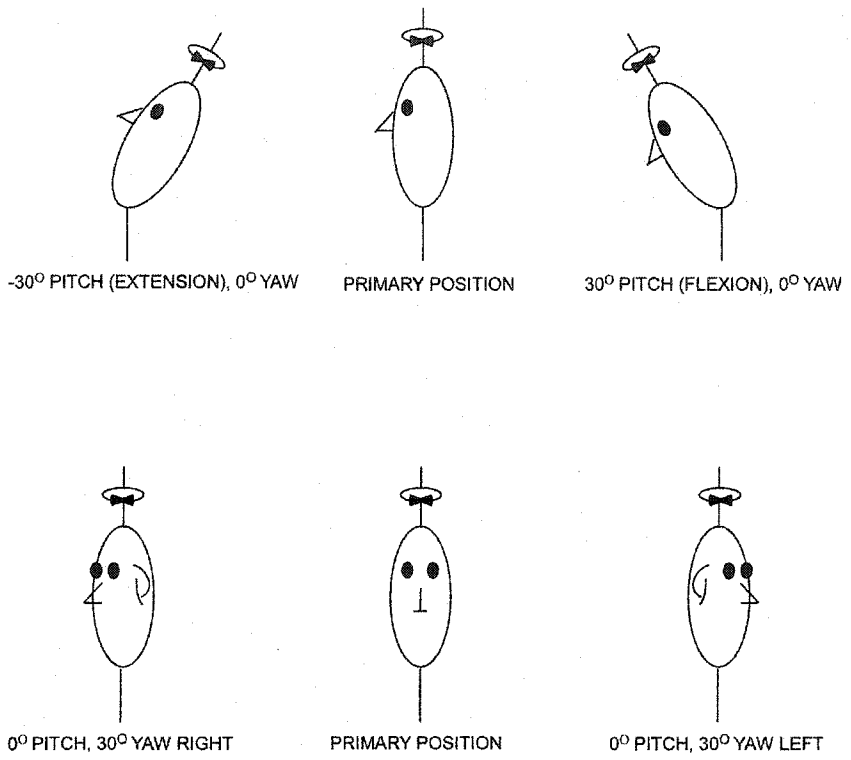

Fig 7.4 Oscillation orientations

7.2.2 Results on Direction of the average axis of the head yaw rotation

The angle between the Z-Axis of the head and projection of the averaged yaw axis of rotation onto the pitch plane of the head was plotted as a function of head pitch (Fig 7.5, Fig 7.6 and Fig 7.7). For different yaw positions the plots showed similar patterns (Fig 7.5, Fig 7.6 and Fig 7.7). When the average yaw position was 0° (Fig 7.5), the angle between the yaw rotation axis and Z_H in head coordinates increased with increased extension (Larger negative angles of pitch). Thus, the rotation axis tended to stay invariant in space as the head was tipped back (Fig 7.5, Extension). In contrast, as the head was pitched forward (Larger positive angles of pitch), the rotation axis tended to be invariant relative to Z_H, indicating that the rotation axis was aligned with the head for

flexion (Fig 7.5, Flexion). Similar results were obtained when the head was turned to the right and left (Fig 7.6 and Fig 7.7, respectively).

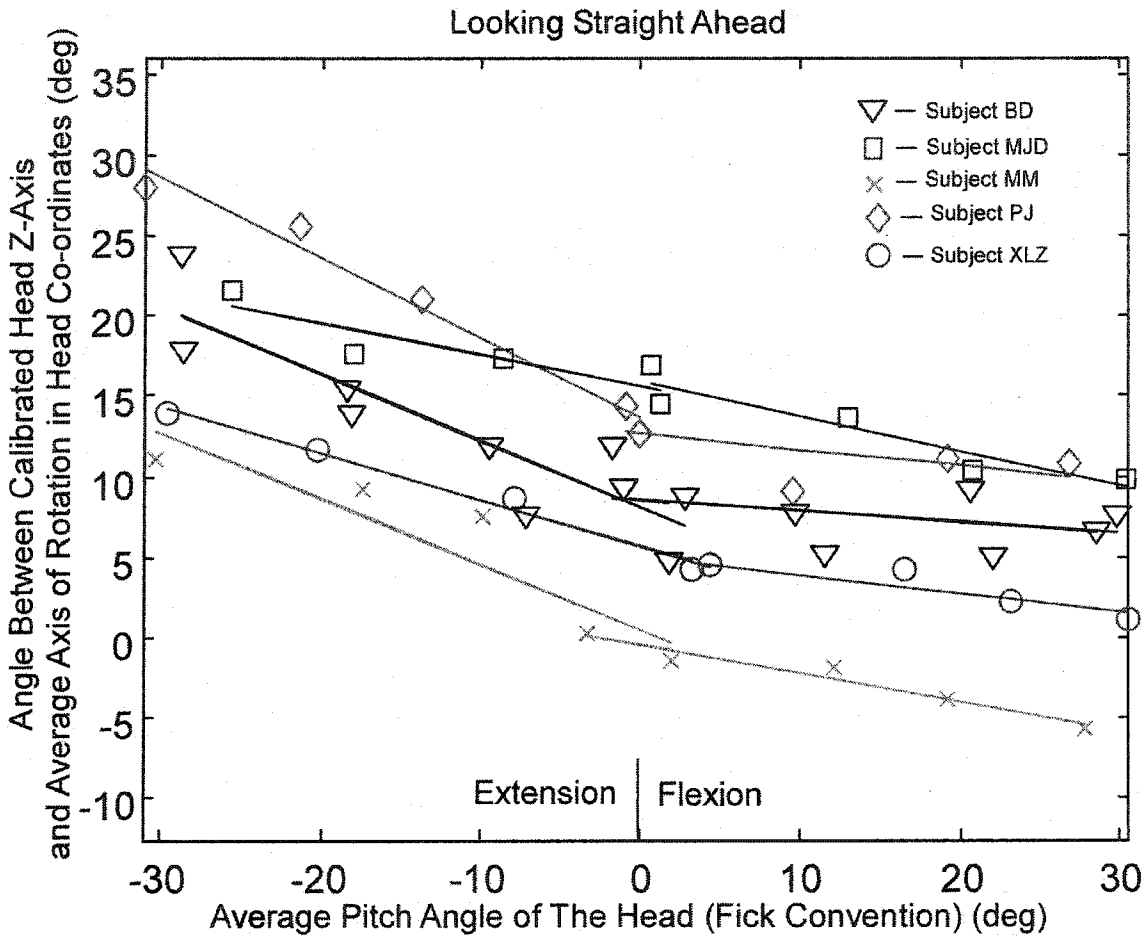

Fig 7.5 Angle between the Z-axis of the head and the axis of yaw rotation while oscillating about primary yaw position.

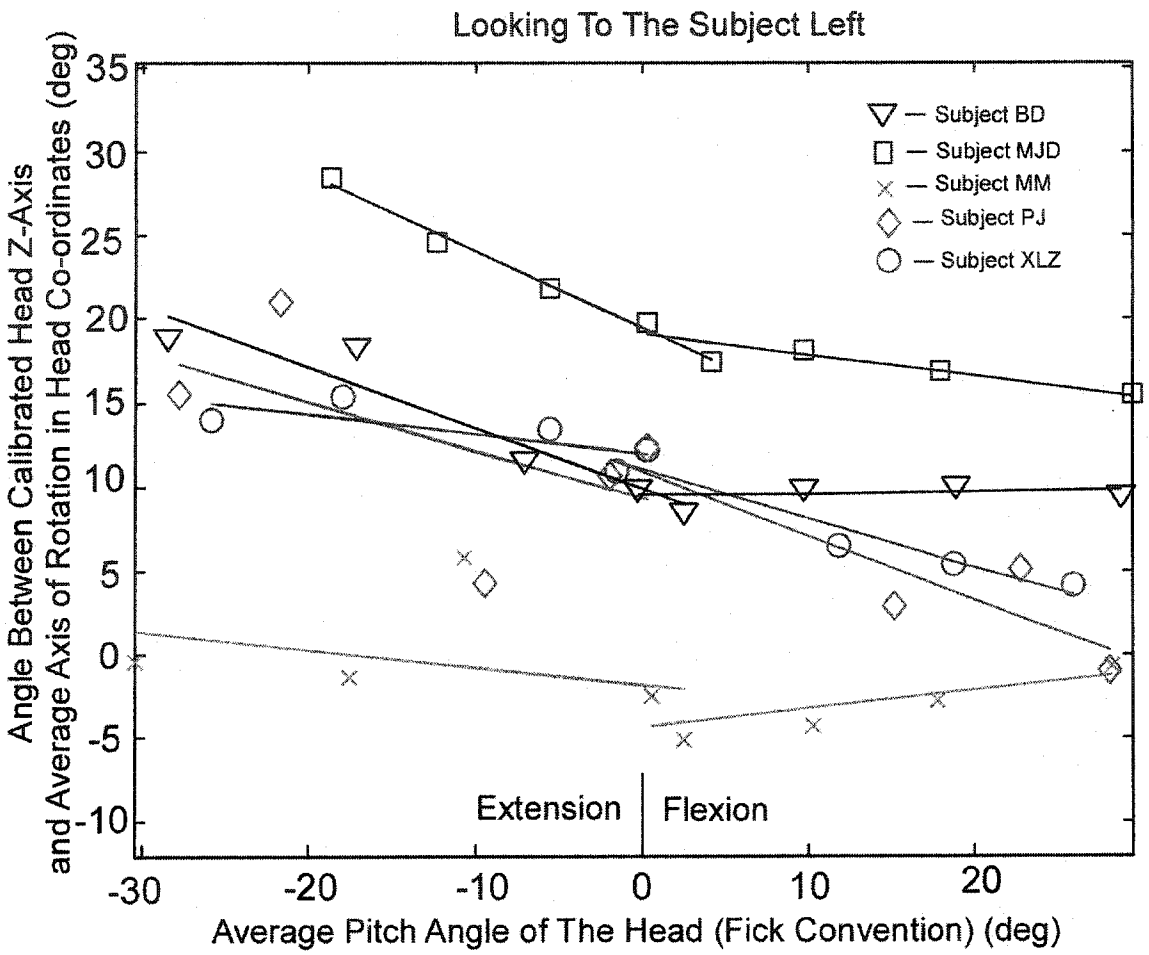

Fig 7.6 Angle between the Z-axis of the head and the axis of yaw rotation while oscillating about yaw position to the left.

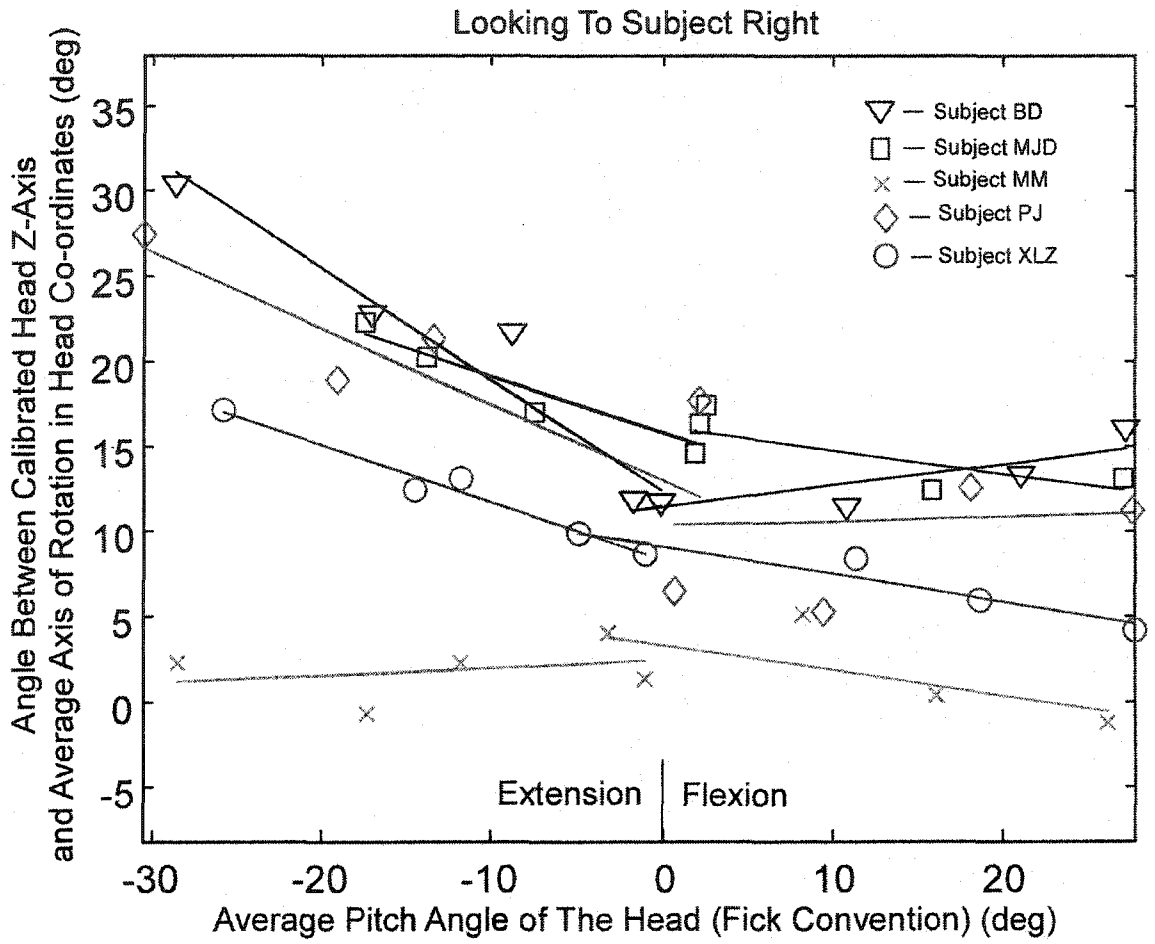

Fig 7.7 Angle between the Z-axis of the head and the axis of yaw rotation while oscillating about yaw position to the right.

The axis of the dens from MRI radiographs was examined for similar flexion and extensions of the head. This was done by first examining sagittal cuts of the MRI at the level of each set of semicircular canals (Fig 7.8). Best fitting planes to each of the lateral canals was computed (Fig 7.8A, B, Line 1) and an optimal average plane was determined (Fig 7.8C, Line 1). The intersection of this averaged plane with the midsagittal plane could then be referenced to the tangent of the dorsal portion of the dens (Fig 7.8D, Axis

of the Dens) and the angle between these planes viewed in the midsagittal plane could be determined. (Fig 7.8D).

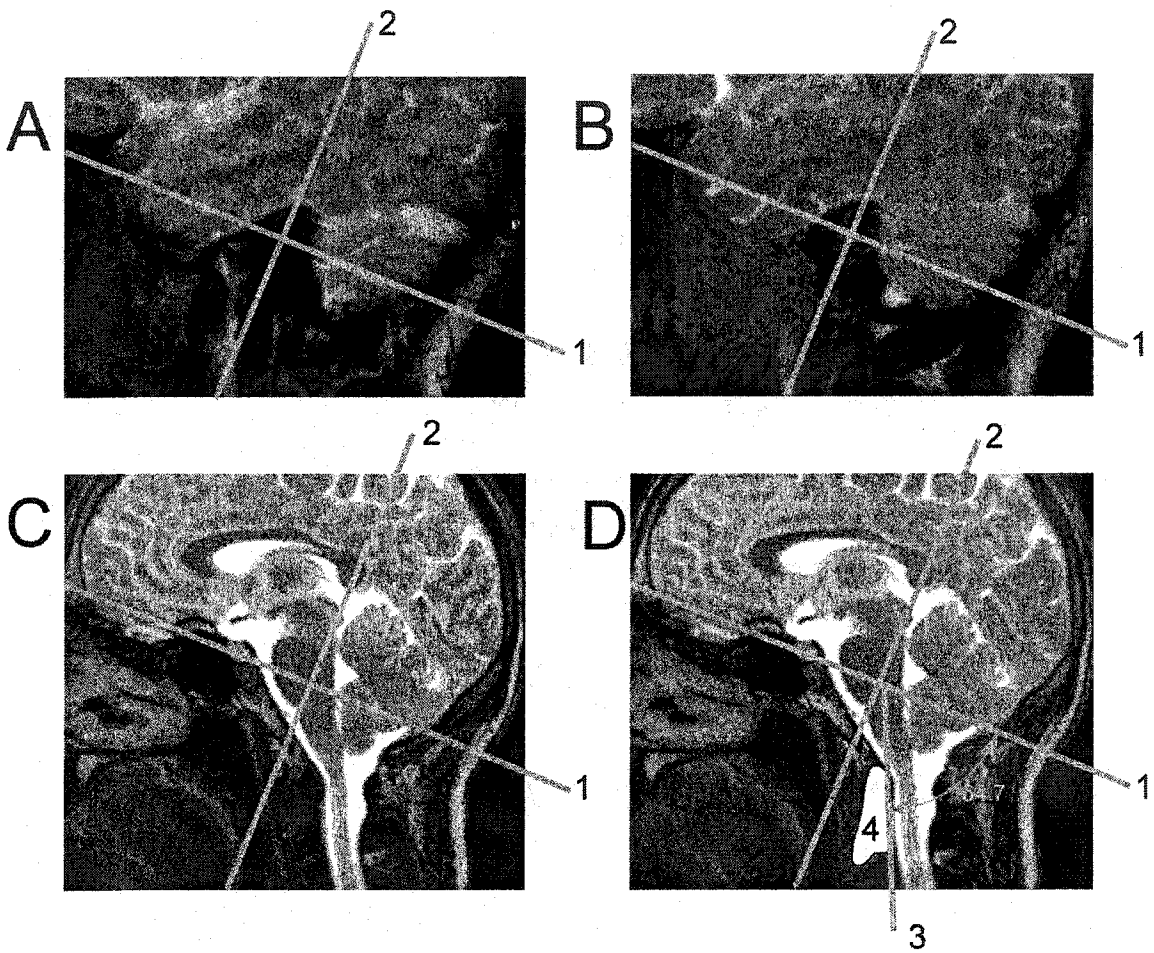

Fig 7.8 MRI of the Semi-Circular Canals: **A.** Left Semi-Circular Canal with its best fitting plane **B.** Right semicircular canal and its best fitting plane **C.** Average Plane of the two Semi-Circular Canals **D.** Angle between the Average Plane and the Dorsal Portion of the Dens

To compare these angles with the results from rotation, the corresponding angle of the dens relative to the head Z-axis was determined (Fig 7.9). The normal to the average plane of the lateral semicircular canals was computed (Fig 7.8A, B, C, D, Line 2). This

line was drawn relative to the head Z-axis and axis of dens (Fig 7.9). Because the axis of the dens relative to the plane of the lateral canal was 64.7° in the primary position of the head, the angle of the normal to the lateral canal relative to the axis of the dens was the complement being equal to 25.3°. The axis of the dens in this position was estimated as 7.5° relative to the head Z-axis, Z_H (Fig 7.9). Thus, the normal to the lateral canals was computed to be 17.8° relative to Z_H, consistent with earlier estimates of the lateral canal relative to the head Z-axis (Simpson and Graf 1985).

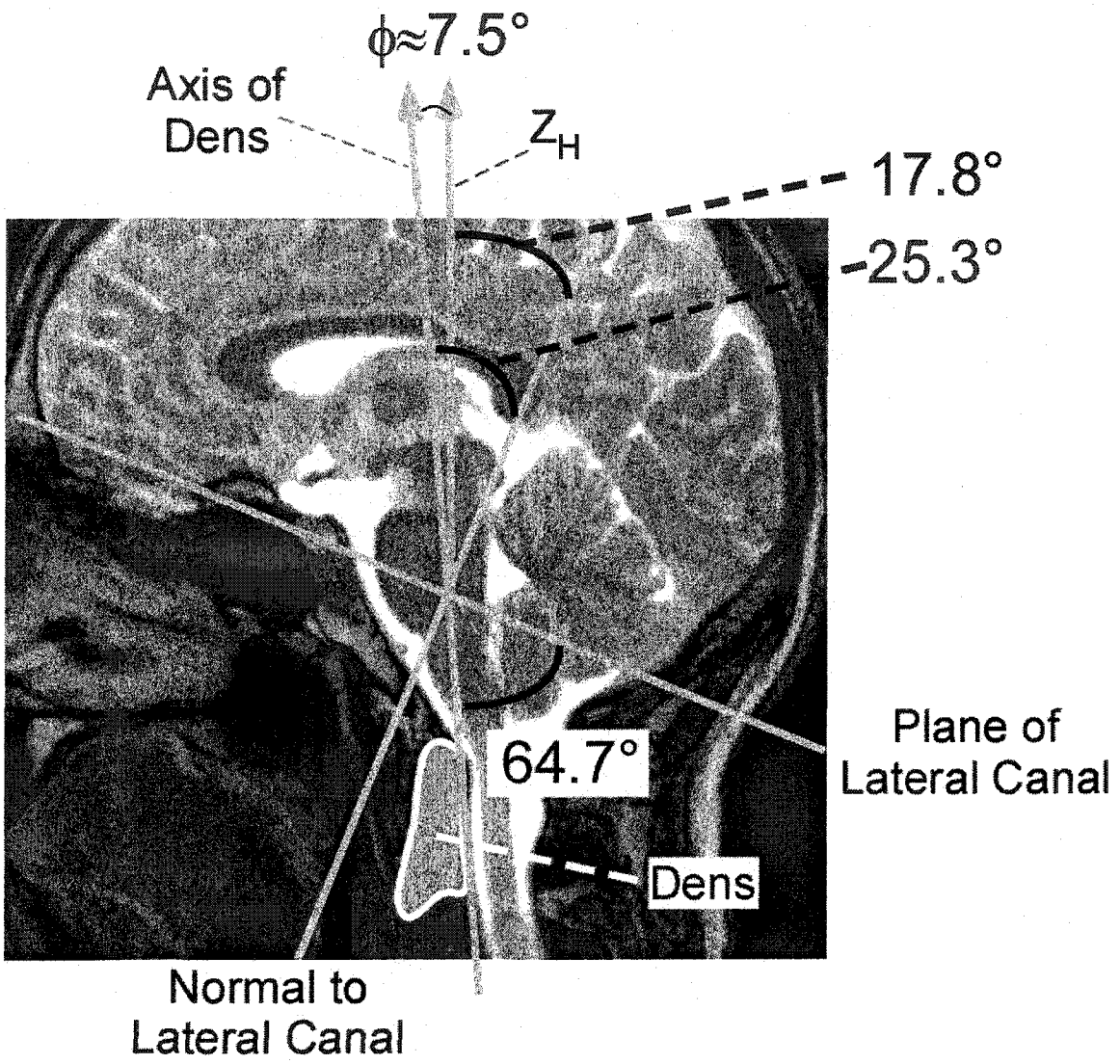

Fig 7.9 Angles between the Axis of the Dens, Normal to the Lateral Canals, and the Calibrated Z Axis of the Head.

The angles of the plane of the lateral semicircular canals relative to the axis of the dens was also computed for two positions of extension and two positions at four different angles of yaw (Table 7-8).

Table 7-8 MRI data

		Pitch			
		-2 Extension	-1 Extension	+1 Flexion	+2 Flexion
Yaw	-2	50.9	64.9	69.9	68.6
	-1	42.3	62.9	72.2	66.0
	+1	51.4	64.4	64.8	69.1
	+2	59.2	68.8	73.0	78.7
	Mean	51.0	65.3	70.0	70.6
	S.D.	6.9	2.5	3.7	5.6

The average results from the rotation data for each subject and the average results at each pitch position from the MRI data were overlaid to determine how the angle of the dens relative to the Z-axis compared to the rotation axis relative to the Z-axis (Fig 7.10).

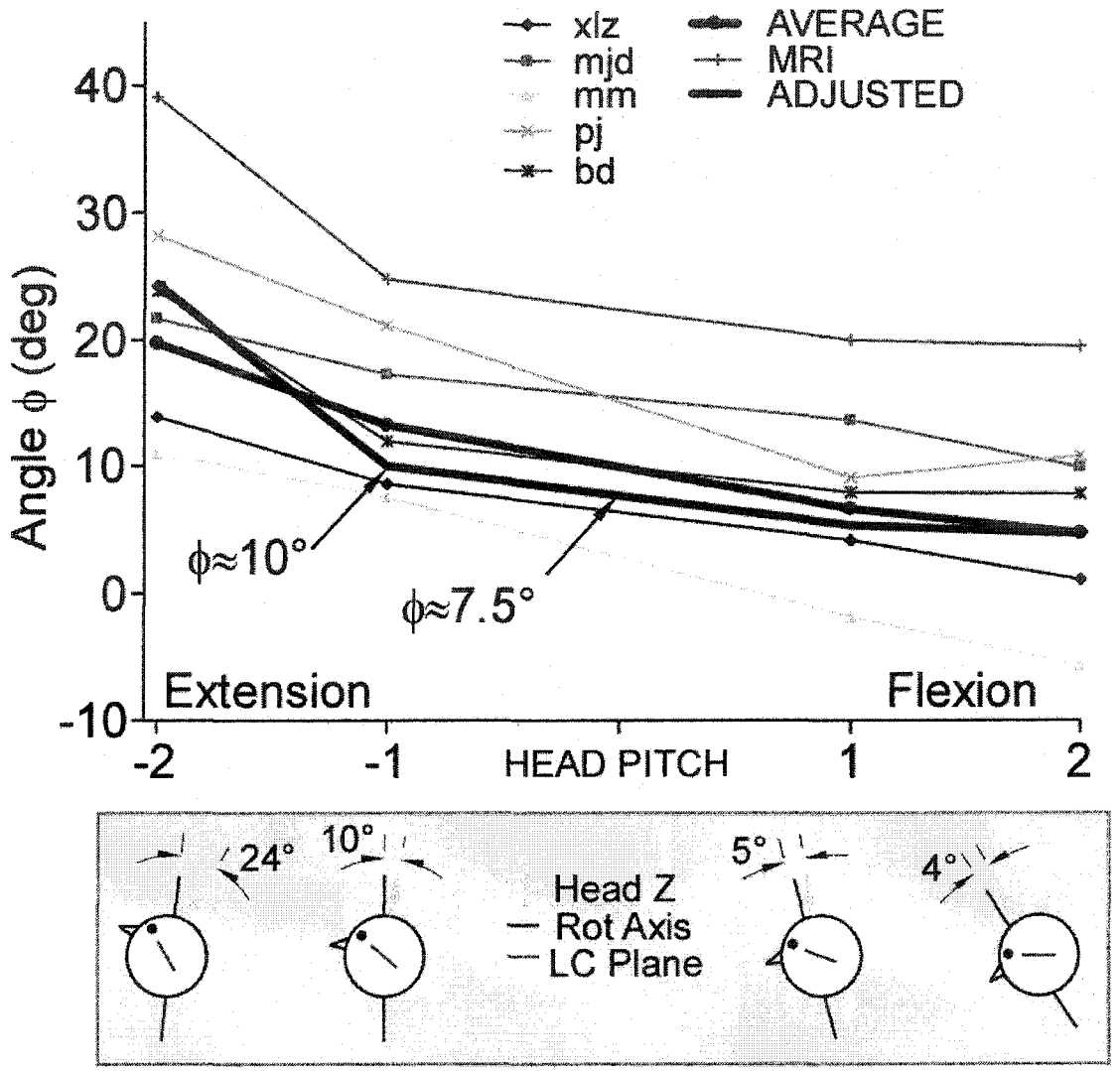

Fig 7.10 Angle between the Z Axis and the Average Axis of Yaw Rotation. Average results from the rotation data for each subject are overlaid by the average result at each pitch position from the MRI data

The results indicate that the extension-flexion data for MRI closely match the data from 6 subjects. The original MRI data (Fig 7.10, 'MRI') shows a trend similar to the average of all subjects (Fig 7.10, 'AVERAGE'), up to an offset, depending on the subject. This angle was determined by computing the angle between the calibrated Z-axis of the head and the normal of the canal plane. This angle was estimated by finding the offset that

would minimize the sum of squared errors for each of the pitch position in data presented in (Fig 7.10). The offset was obtained by first computing the average over all pitch positions of the angles between the normal to the lateral canal and the axis of the dens obtained from the MRI. The average of the angles between the head Z-axis and the axis of yaw rotation over all subjects in all pitch positions was then computed. The offset was the difference between these two averages. The 'ADJUSTED' trace in the figure shows the MRI data from which the angle was subtracted.

CHAPTER 8 ANALYSIS OF HEAD AND TRUNK DISPLACEMENTS IN THREE DIMENSIONS DURING LOCOMOTION

In this chapter, we consider the data obtained from treadmill locomotion described in CHAPTER 5 and applied the displacement matrix approach to determine the characteristics of the head displacement during straight locomotion. While in CHAPTER 5 we showed that there was a head fixation point, which could be closely linked to the gain and phase of the IVCR, the question that we address in this chapter is whether there is a consistent head fixation in three dimensions (pitch and yaw). Our hypothesis is that just as in two dimensions, there is a head fixation point in three dimensions, but this method will give us averages close to that obtained in CHAPTER 5, but the variations using displacement matrices will be higher due to the noise in the head trajectory during locomotion. We therefore considered an extension to three dimensions of the approach used in CHAPTER 5 by finding the closest point of naso-occipital axes in three dimensions. Previous results (Moore, Hirasaki et al. 2001) examined the head fixation points in the pitch and yaw planes separately and found them to be disparate. Our results indicate that there is only a single head fixation point in three dimensions. The results of analyzing the head fixation point in two separate planes may be due to how lines in three dimensions project onto planes in three dimensions and not to the process itself. The findings here add a certain consistency to the operation of the system in three dimensions and support the idea that head fixation point is a useful measure of compensation due to the IVCR in three dimensions. This methodology also allowed us to compute the rotation axes of the whole body during treadmill locomotion to determine what additional

compensatory components such as the angular vestibulo-collic reflex (aVCR) contribute to the maintenance of the approximate invariance of the HFP.

8.1 Three-dimensional analysis of head rotation in space during treadmill locomotion

We used the methods of CHAPTER 6 to determine the head fixation point using the following procedure: The instantaneous axis lines, which are determined by a vector in the direction of the line and a point in three dimensions through which the line passes was computed. This point is referred to as the *instantaneous pivot point* of the head rotation in space. The axis lines were then referenced to the head coordinate frame to account for the fact that the subject randomly drifted on the treadmill during data taking. The nearest point to the resulting set of axis lines (C) was computed, and was used as a measure of the head fixation point (HFP) in three dimensions. The point on each axis line closest to the HFP was computed.

The head fixation point in three dimensions and their projections onto the pitch and yaw spatial planes were determined during treadmill locomotion for a variety of walking conditions (Fig 8.1 - Fig 8.12). During walking in light while fixating a target at 1 m (Fig 8.1), the X coordinate of the pivot was 32.1, 49, and 67.5 cm, for slow, medium and fast walking respectively (Fig 8.1). This was consistent with the findings obtained from the methods described in CHAPTER 5 and previous results (Hirasaki, Moore et al. 1999). However, this methodology produced a large variation in the distribution of the pivot points. The variations in three dimensions were obtained by applying the Karhunen-Loeve transformation (6.6) to the pivot points in three dimensions (Fig 8.2). The

eigenvalue for each principal component is a measure of the variance along that direction and the ratio, e, given by:

$$e = \frac{\lambda_3}{\sqrt{\lambda_1 \lambda_2}} \tag{8.1}$$

is a measure of the eccentricity of the distribution of the pivot points.

For all walking conditions, i.e., walking in light while fixating at 1 m (Fig 8.2), walking with a collar while fixating at 1m (Fig 8.5), walking in darkness (Fig 8.11), and walking while fixating at 20 cm (Fig 8.8), the distribution was approximately spheroidal at low walking velocities and became flattened in the Z direction as walking velocity increased (Fig 8.2, Fig 8.5, Fig 8.11, and Fig 8.8). The eigenvalues, representing variances along the principal components were generally large, being in the range of 50-100 cm.

These findings were compared with HFP's found using the minimum variance of the naso-occipital axes in three dimensions (Fig 8.3, Fig 8.6, Fig 8.9, and Fig 8.12). Head fixation points determined by these two methods were close to each other. This indicates that the HFP in three dimensions is a fairly good indicator of compensatory behavior of the lVCR, although it is not a good estimate of instantaneous head compensation. It suggests that the goal of the head compensation is to maintain global invariance of the head trajectory at the expense of instantaneous invariance.

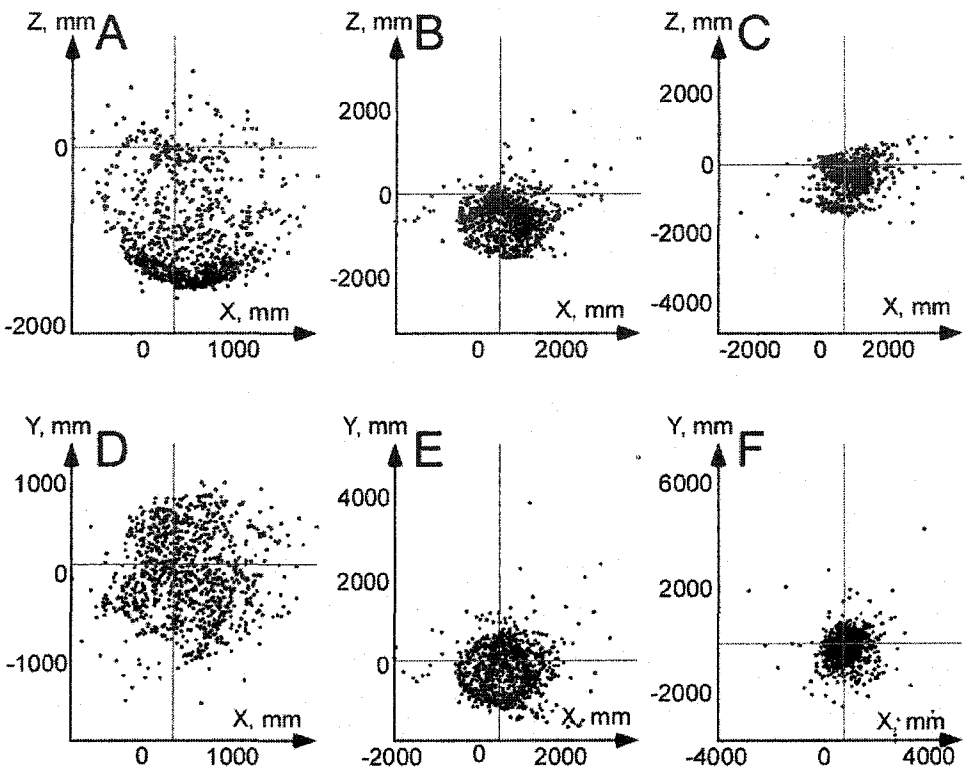

Fig 8.1 Projections of the instantaneous pivot points onto the pitch (A, B, C) and yaw (D, E, F) planes for slow (A, D), medium (B, E), and fast (D, F) locomotion on treadmill while fixating a point at 1m. The intersection of thin lines denotes the projection of the virtual intersection point of the axis lines onto the corresponding plane. Since the directions of the lines are not aligned with the coordinate planes, the projection of the virtual intersection point is not at the average of the pivot point projections.

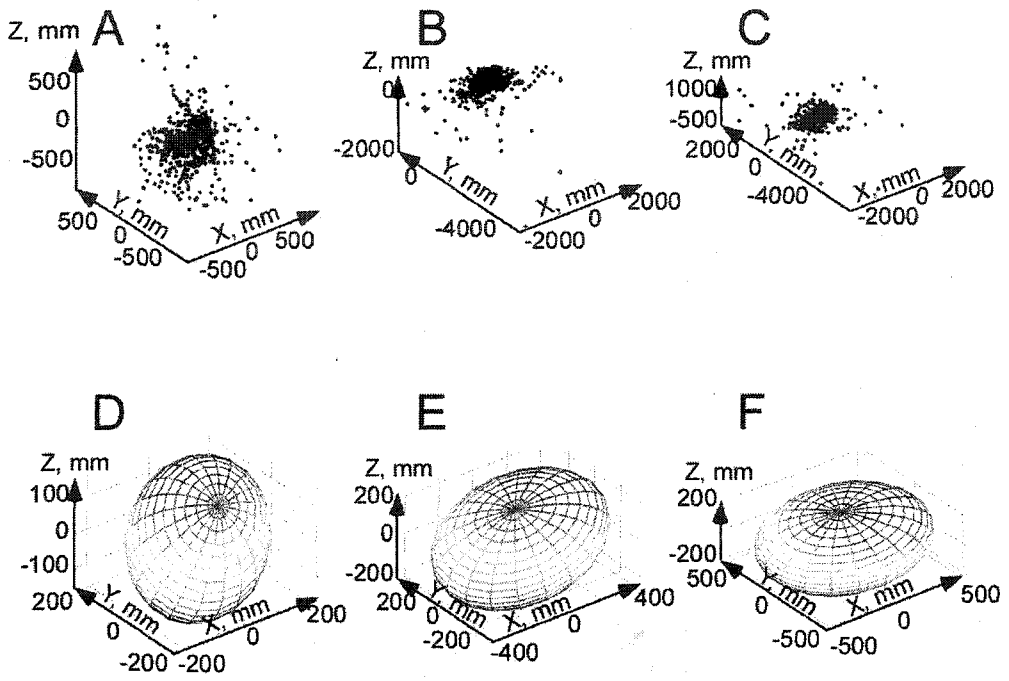

Fig 8.2 Pivot distribution (A, B, C) and the ellipsoids defined by the principal components of the distributions (D, E, F) for slow (A, D), medium (B, E), and fast (C, F) locomotion while fixating a point 1 m.

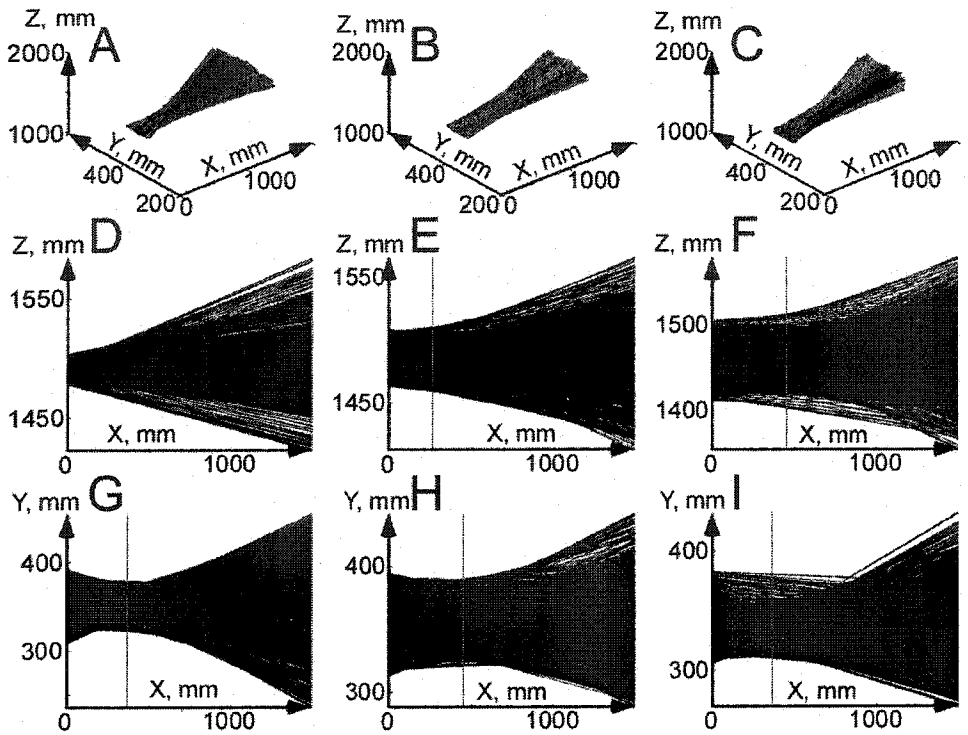

Fig 8.3 Pitch-yaw (A, B, C), vertically (D, E, F), and horizontally (G, H, I) projected HFD computed by minimum variance for slow (A, D, G), medium (B, E, H), and fast (C, F, I) locomotion while fixating a point at 1m.

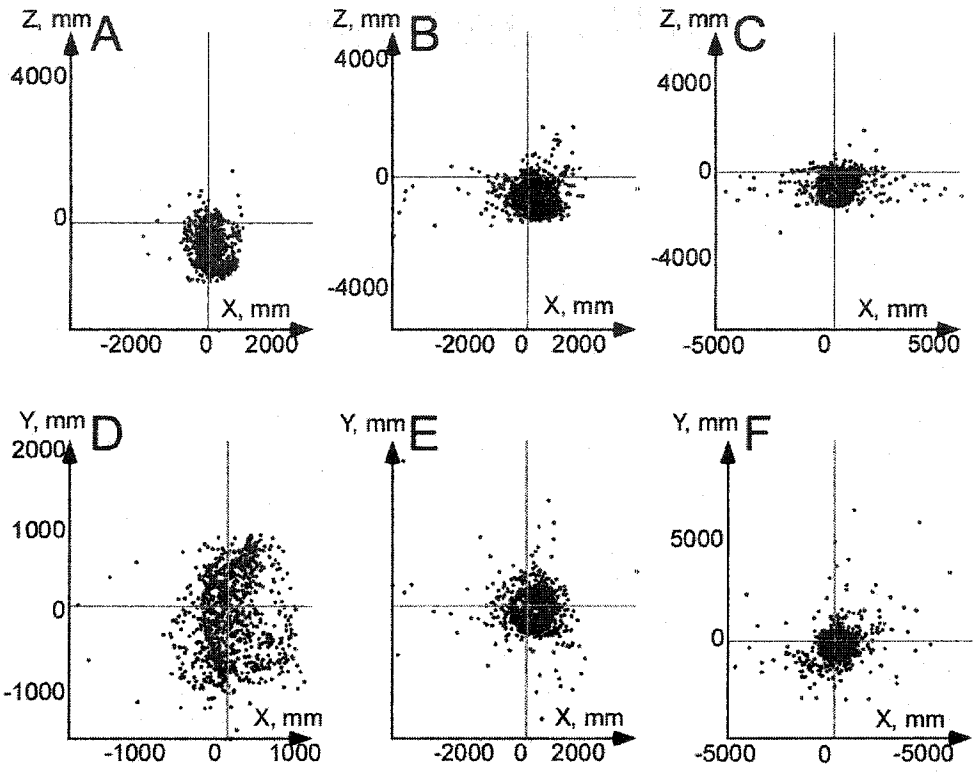

Fig 8.4 Projections of the instantaneous pivot points onto the pitch (A, B, C) and yaw (D, E, F) planes for slow (A, D), medium (B, E), and fast (D, F) locomotion on treadmill while wearing collar

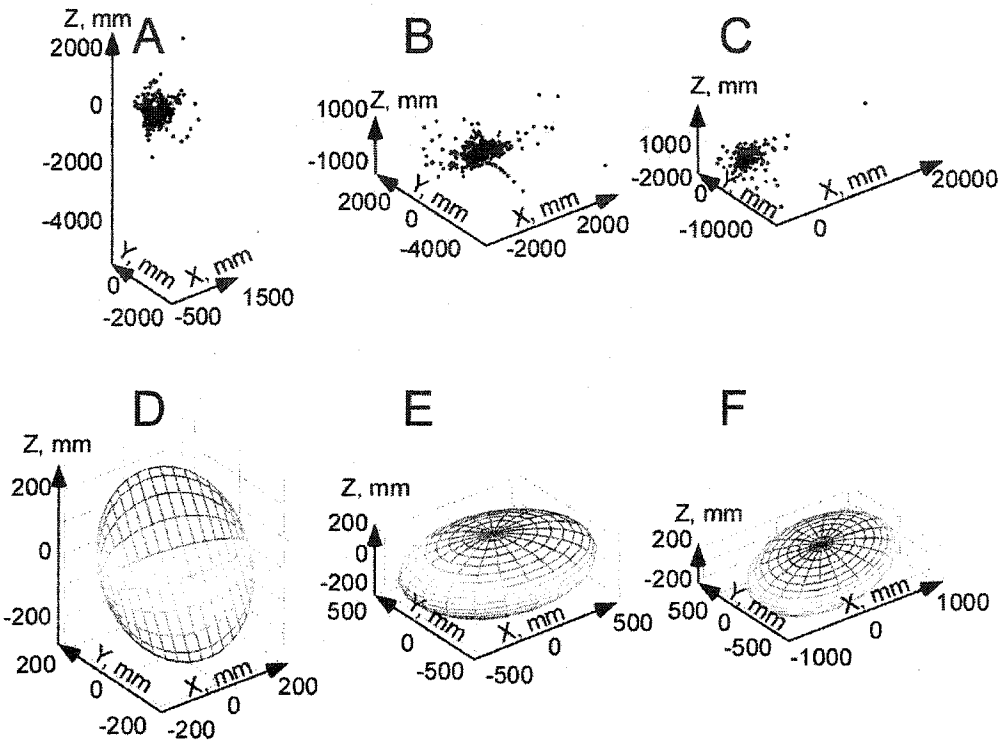

Fig 8.5 Pivot distribution (A, B, C) and the ellipsoids defined by the principal components of the distributions (D, E, F) for slow (A, D), medium (B, E), and fast (C, F) locomotion while wearing collar

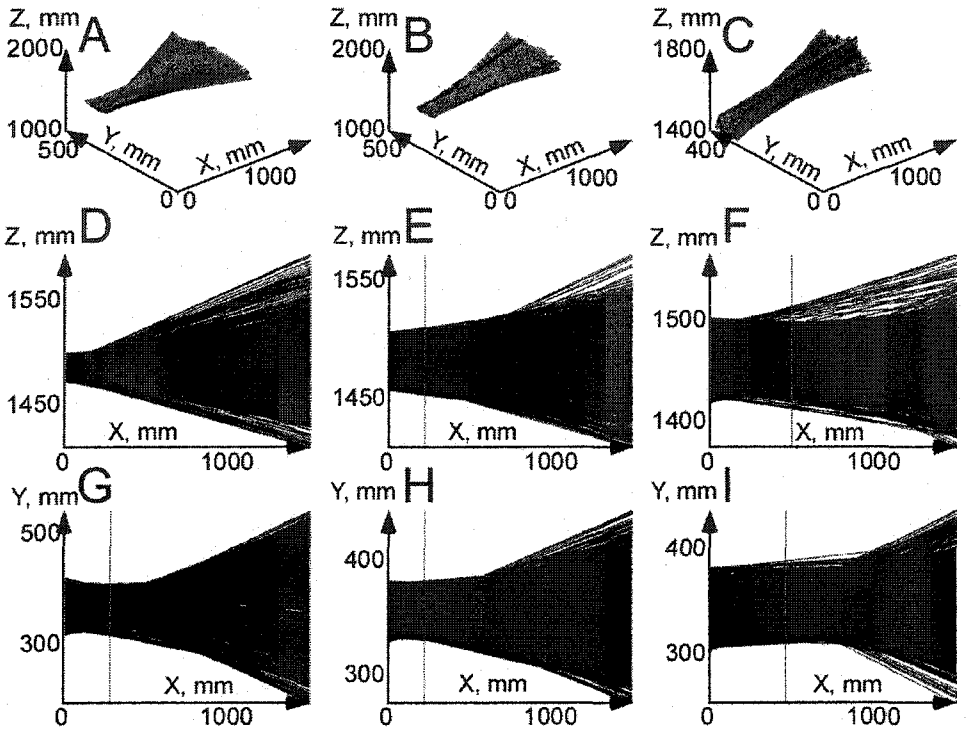

Fig 8.6 Pitch-yaw (A, B, C), vertically (D, E, F), and horizontally (G, H, I) projected HFD computed by minimum variance for slow (A, D, G), medium (B, E, H), and fast (C, F, I) locomotion while wearing collar

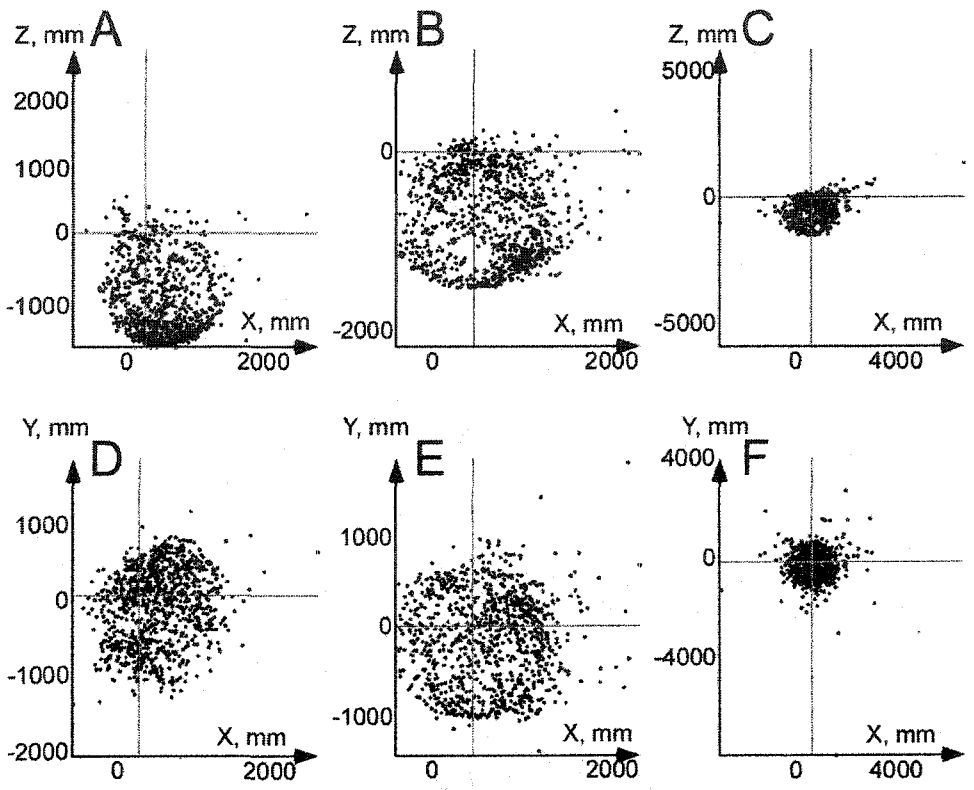

Fig 8.7 Projections of the instantaneous pivot points onto the pitch (A, B, C) and yaw (D, E, F) planes for slow (A, D), medium (B, E), and fast (D, F) locomotion on treadmill while fixating a point at 20 cm

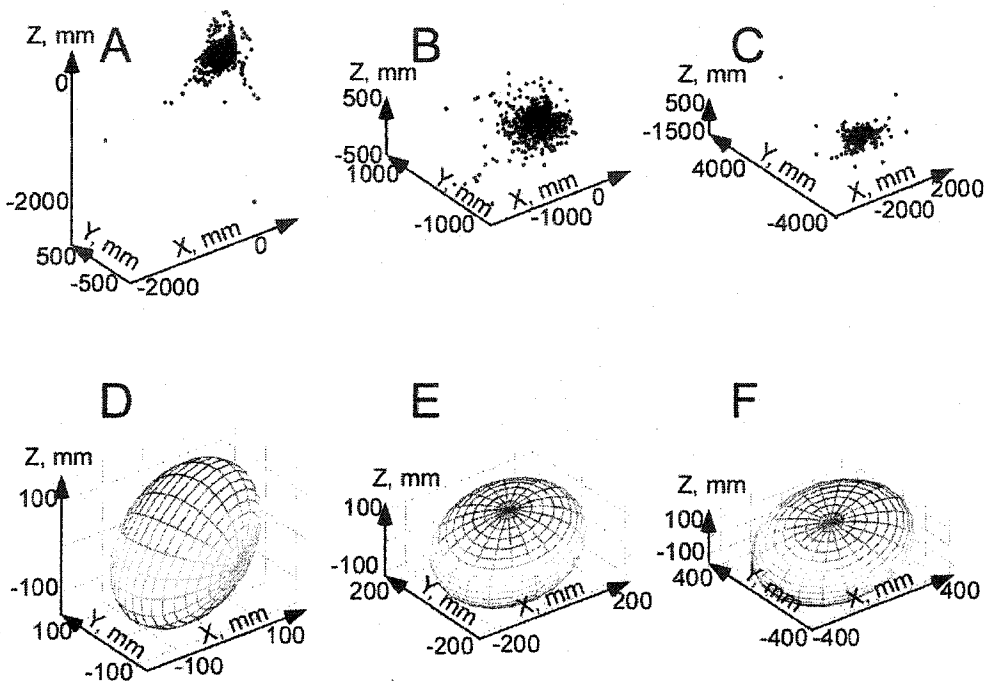

Fig 8.8 Pivot distribution (A, B, C) and the ellipsoids defined by the principal components of the distributions (D, E, F) for slow (A, D), medium (B, E), and fast (C, F) locomotion while fixating a point at 20cm

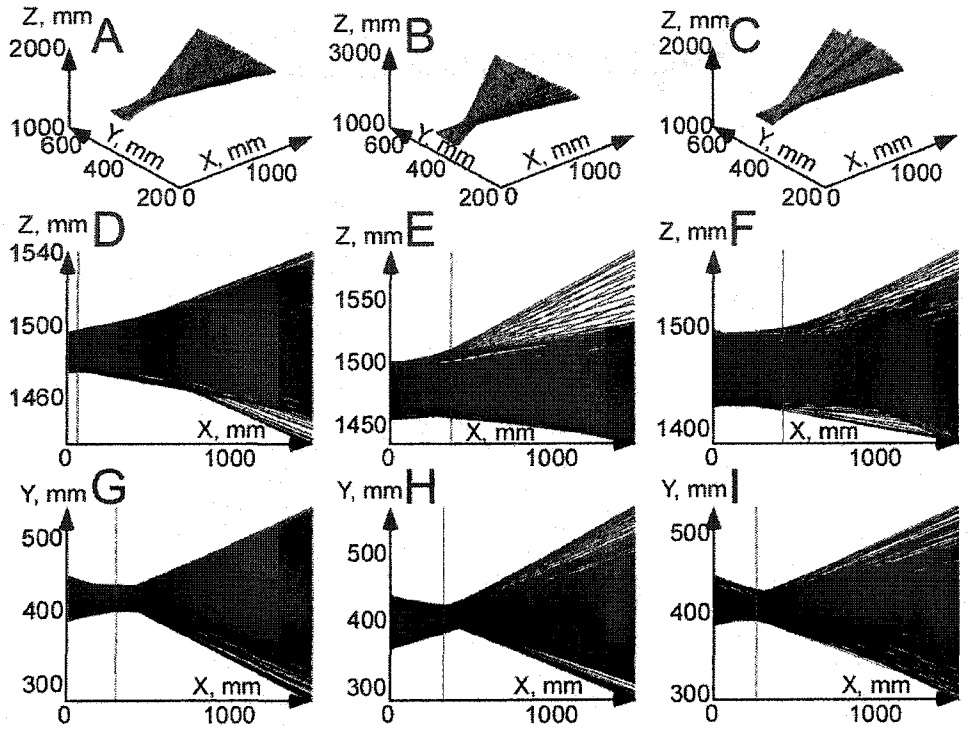

Fig 8.9 Pitch-yaw (A, B, C), vertically (D, E, F), and horizontally (G, H, I) projected HFD computed by minimum variance for slow (A, D, G), medium (B, E, H), and fast (C, F, I) locomotion while fixating a point at 20 cm

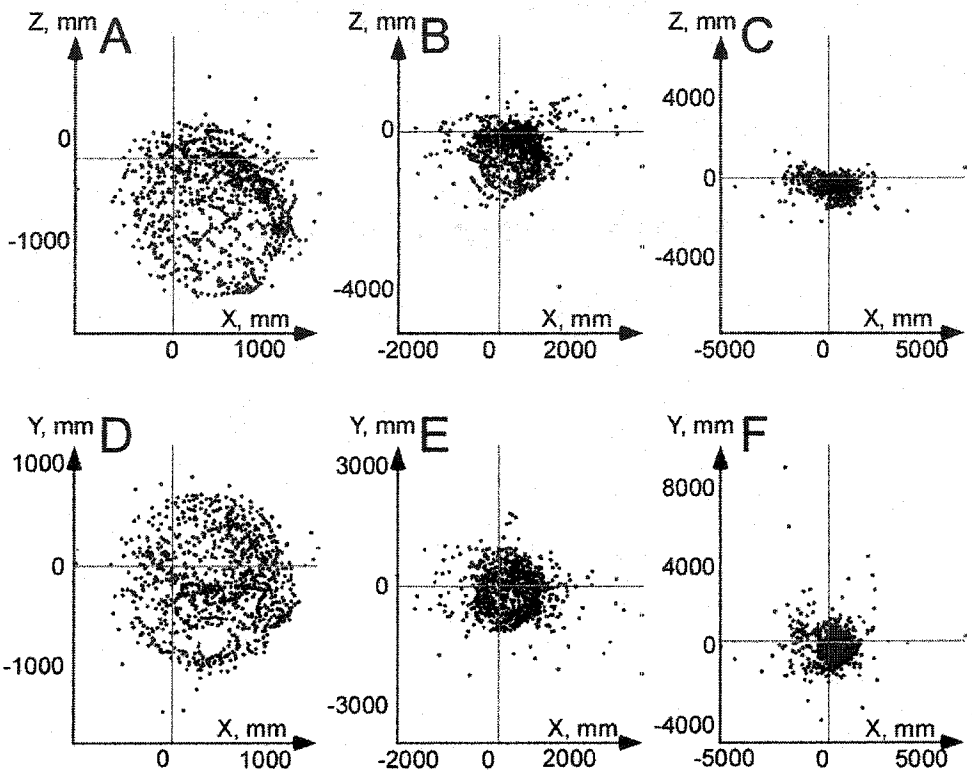

Fig 8.10 Projections of the instantaneous pivot points onto the pitch (A, B, C) and yaw (D, E, F) planes for slow (A, D), medium (B, E), and fast (D, F) locomotion on treadmill while walking in darkness

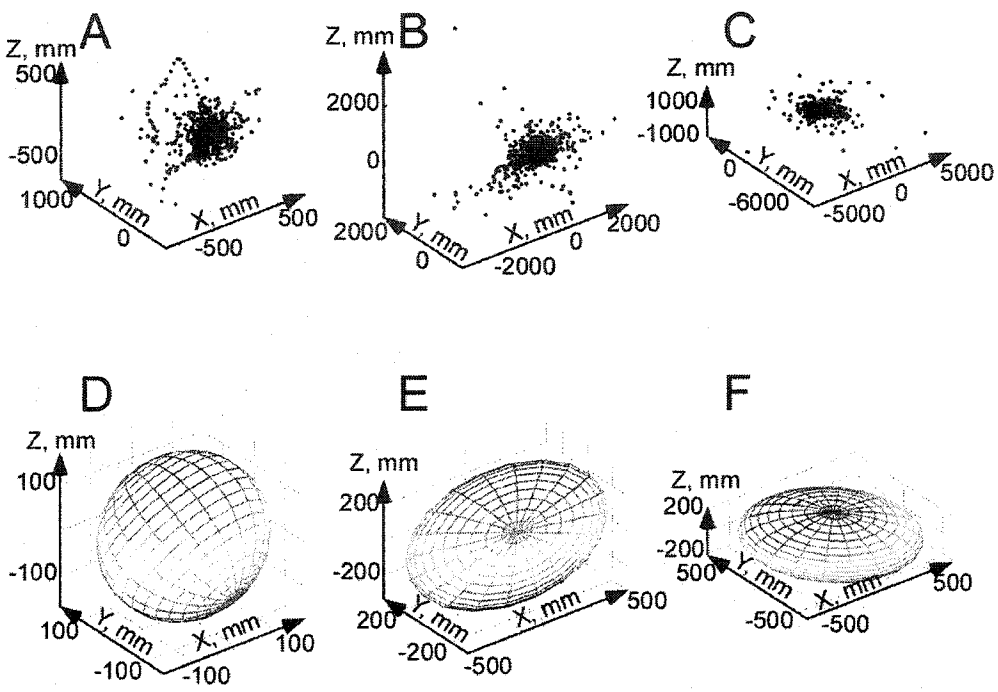

Fig 8.11 Pivot distribution (A, B, C) and the ellipsoids defined by the principal components of the distributions (D, E, F) for slow (A, D), medium (B, E), and fast (C, F) locomotion while walking in darkness

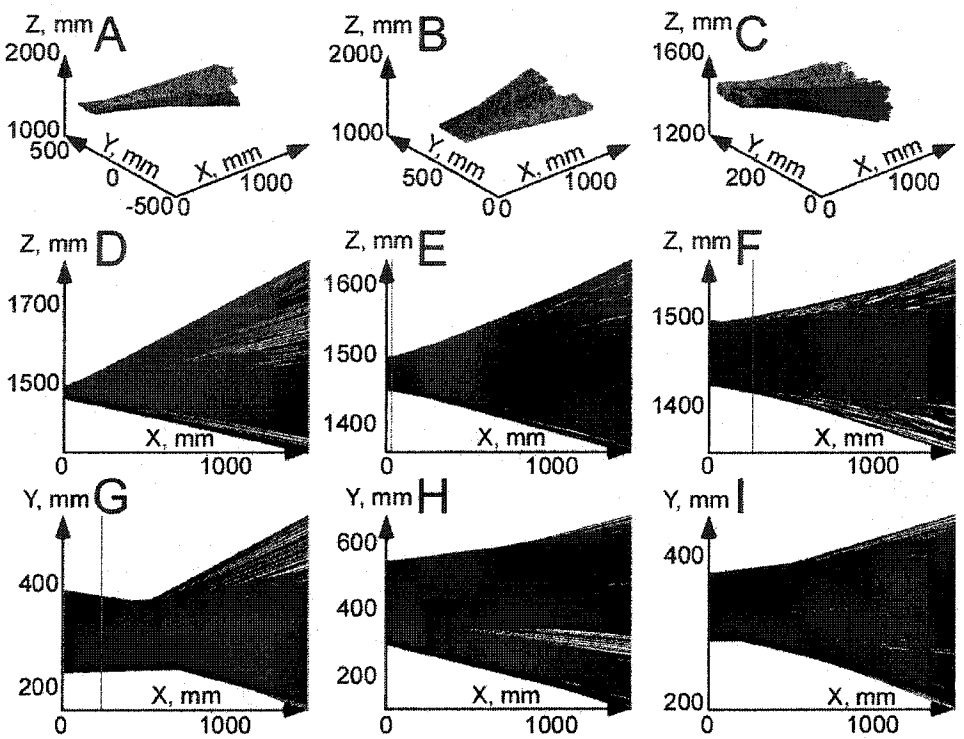

Fig 8.12 Pitch-yaw (A, B, C), vertically (D, E, F), and horizontally (G, H, I) projected HFD computed by minimum variance for slow (A, D, G), medium (B, E, H), and fast (C, F, I) locomotion while walking in darkness

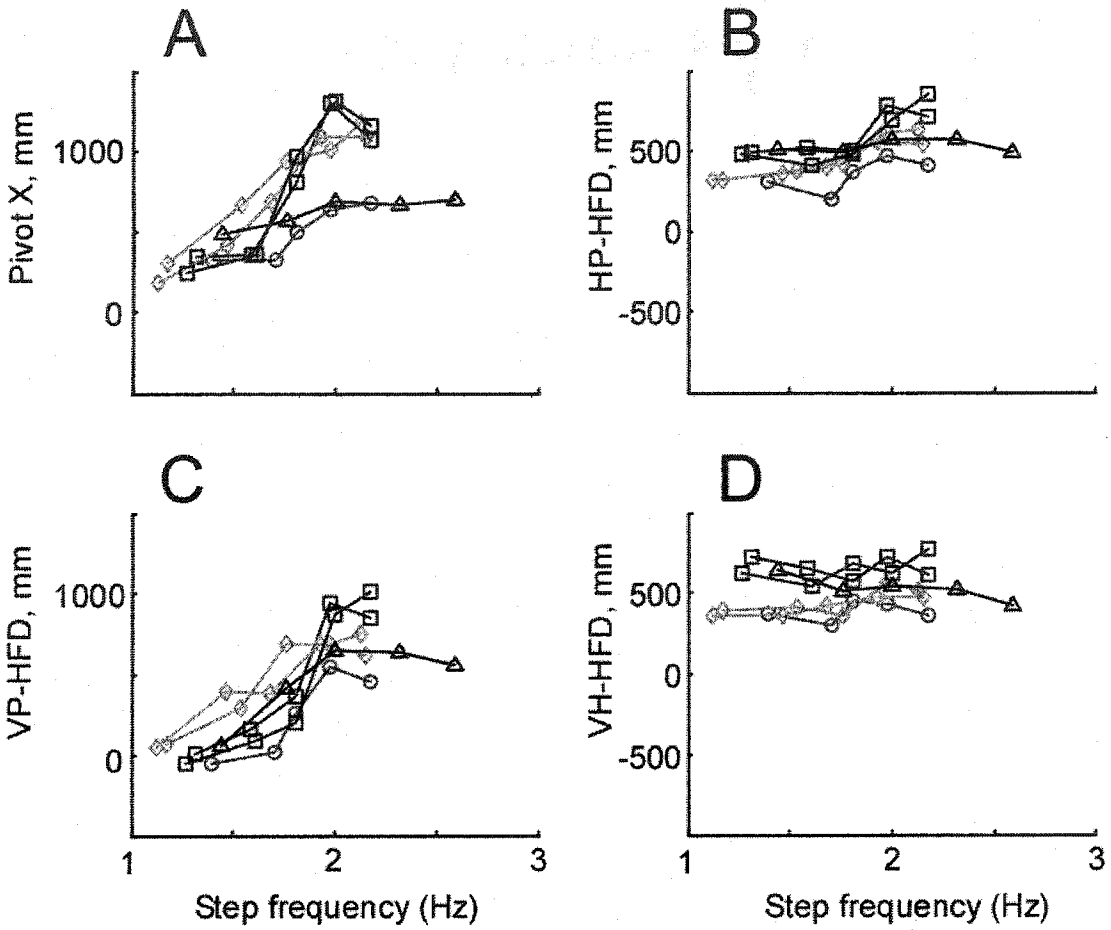

Fig 8.13 The X-coordinate of the virtual pivot point (A), horizontally-projected HFD (B), vertically-projected HFD (C), and the HFD computed from both vertical (Pitch, Z) and Horizontal (Yaw, Y) components (D) during locomotion on treadmill while fixating a point at 1m.

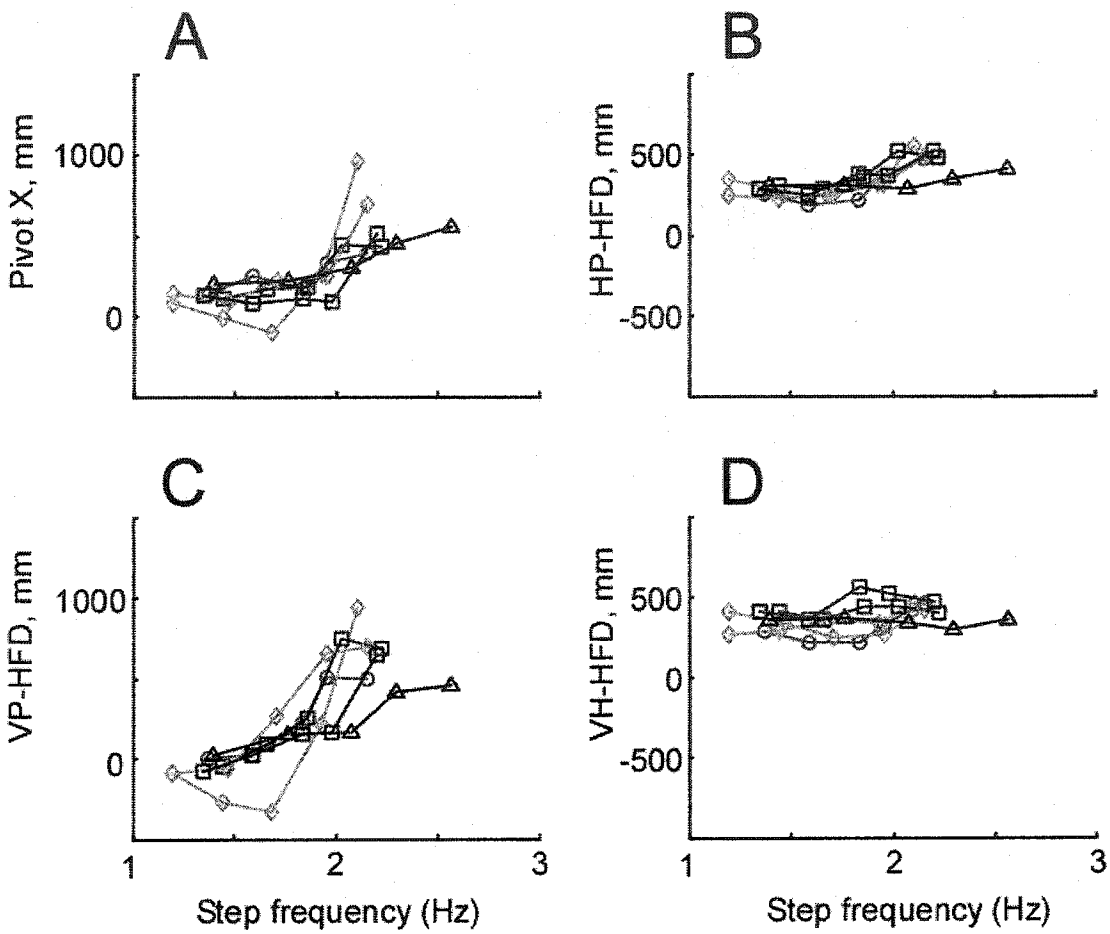

Fig 8.14 The X-coordinate of the virtual pivot point (A), horizontally-projected HFD (B), vertically-projected HFD (C), and the HFD computed from both vertical (Pitch, Z) and Horizontal (Yaw, Y) components (D) during locomotion on treadmill while wearing a neck constraint

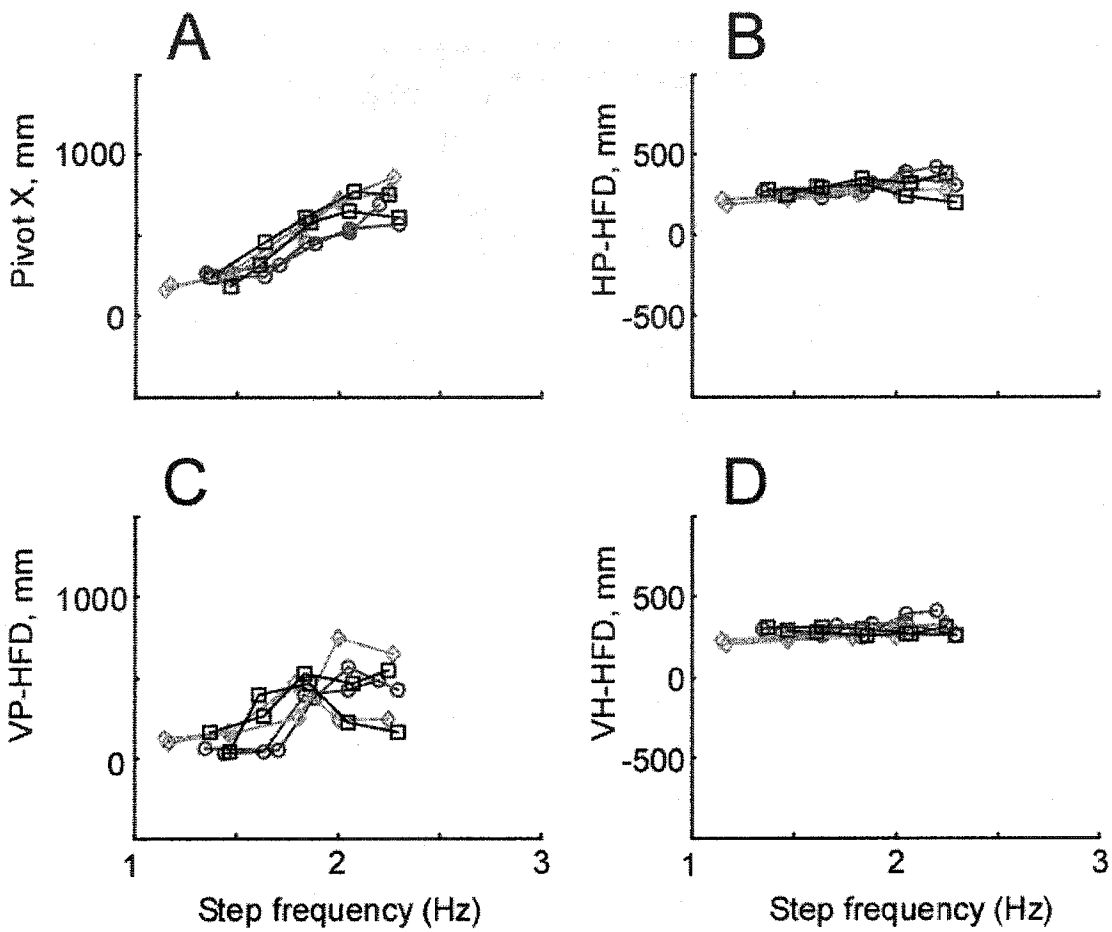

Fig 8.15 The X-coordinate of the virtual pivot point (A), horizontally-projected HFD (B), vertically-projected HFD (C), and the HFD computed from both vertical (Pitch, Z) and Horizontal (Yaw, Y) components (D) during locomotion on treadmill while fixating a target at 20 cm

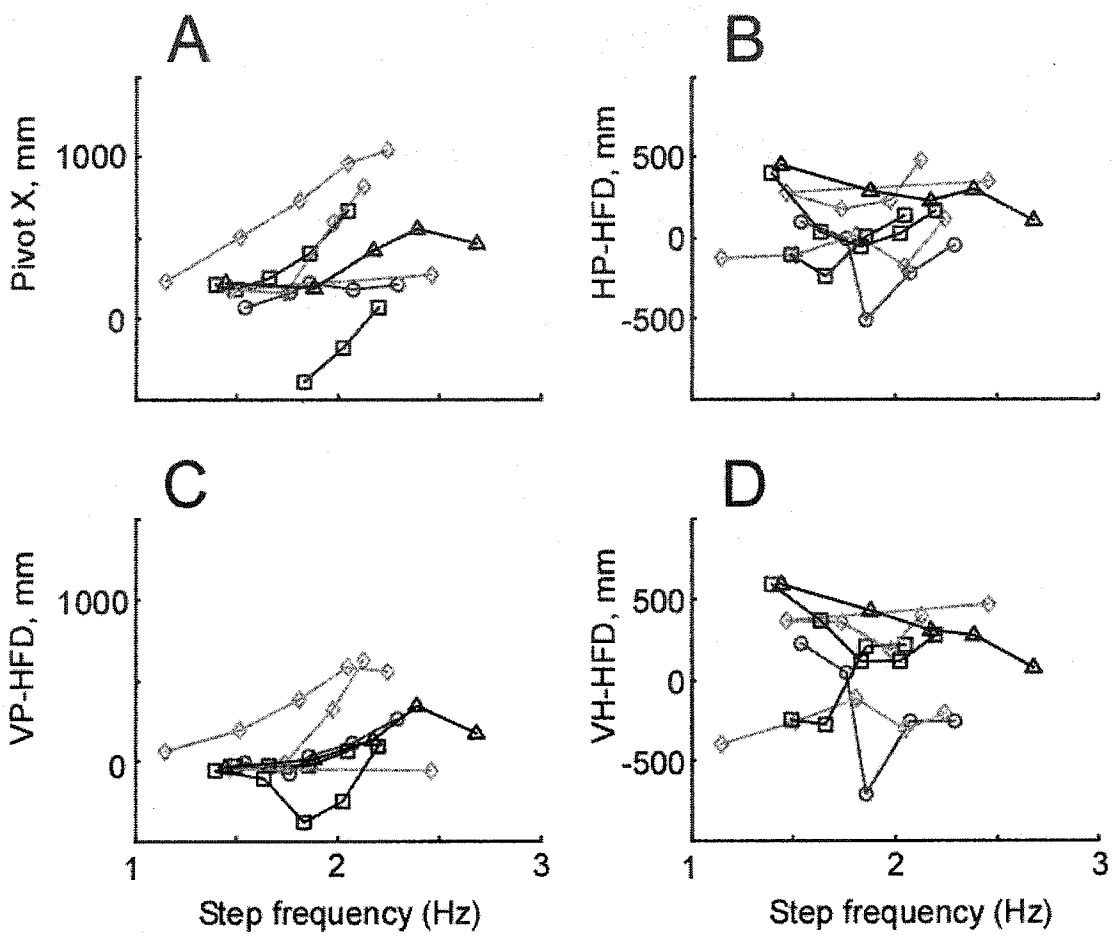

Fig 8.16 The X-coordinate of the virtual pivot point (A), horizontally-projected HFD (B), vertically-projected HFD (C), and the HFD computed from both vertical (Pitch, Z) and Horizontal (Yaw, Y) components (D) during locomotion on treadmill while walking in darkness (eyes closed)

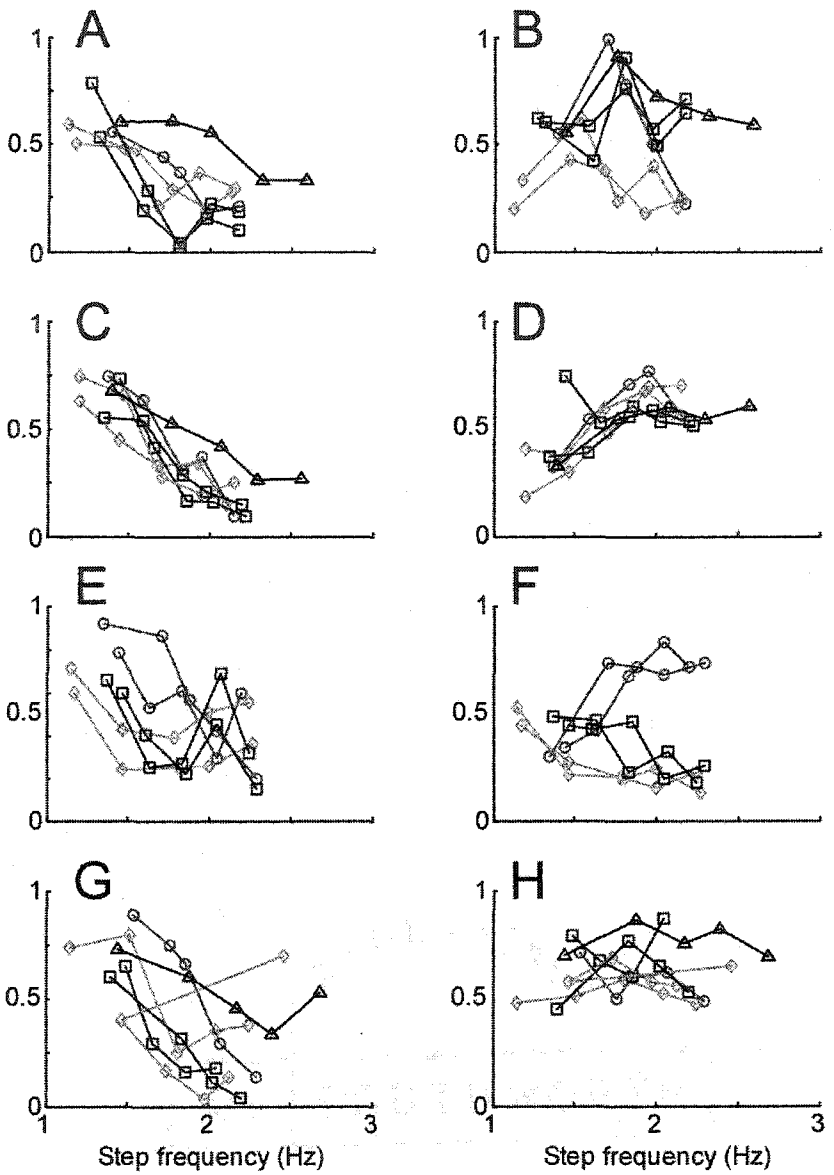

Fig 8.17 Eccentricities of principal components ellipsoids of the pivot points (A, C, E, G), and the angular velocities (B, D, F, H) while fixating a point at 1m (A, B), wearing a collar (C, D), fixating a point at 20 cm (E, F), and walking in darkness (G, H).

8.2 Rotation axis of the Trunk:

Example of pivot point distribution of the trunk motion during locomotion on treadmill is presented in the following figures.

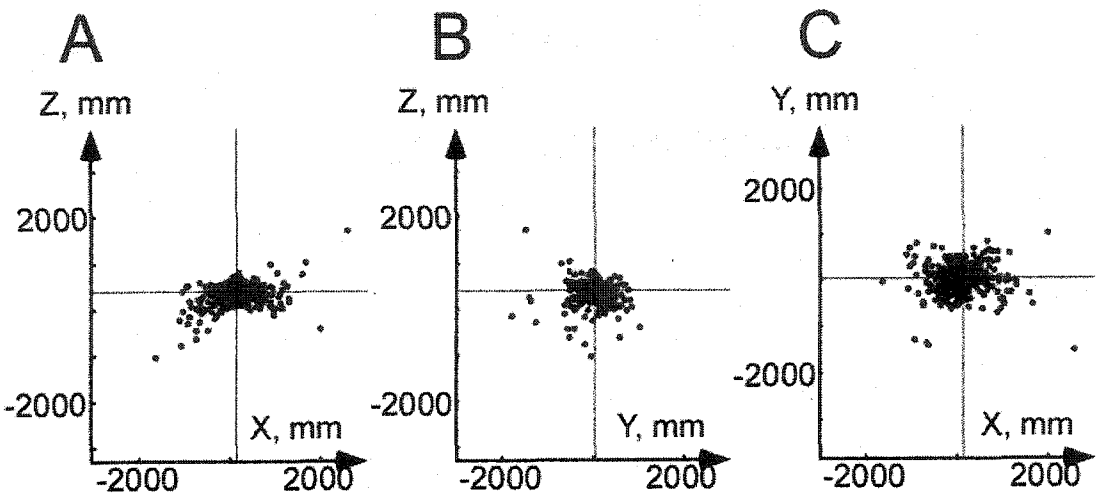

Fig 8.18 Projections of the instantaneous pivot points onto the **A.** pitch, **B.** roll, pitch, and **C.** yaw planes.

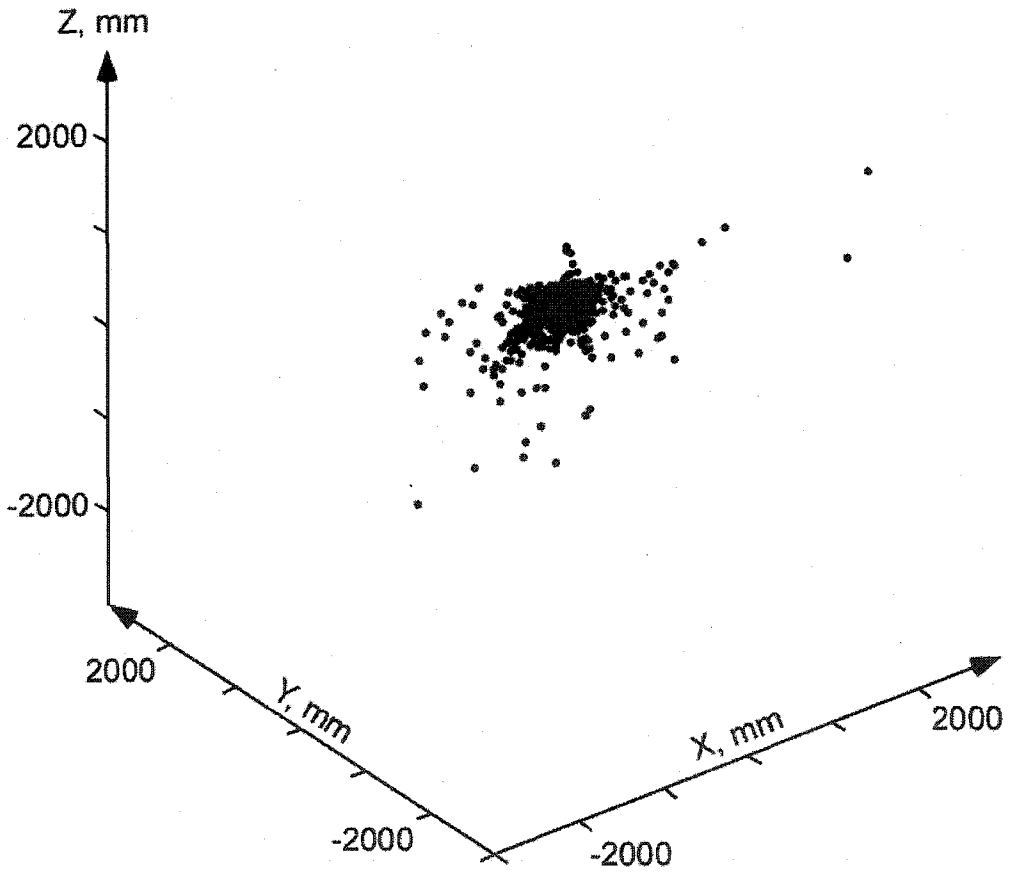

Fig 8.19 Distribution of the pivot points in three dimensions.

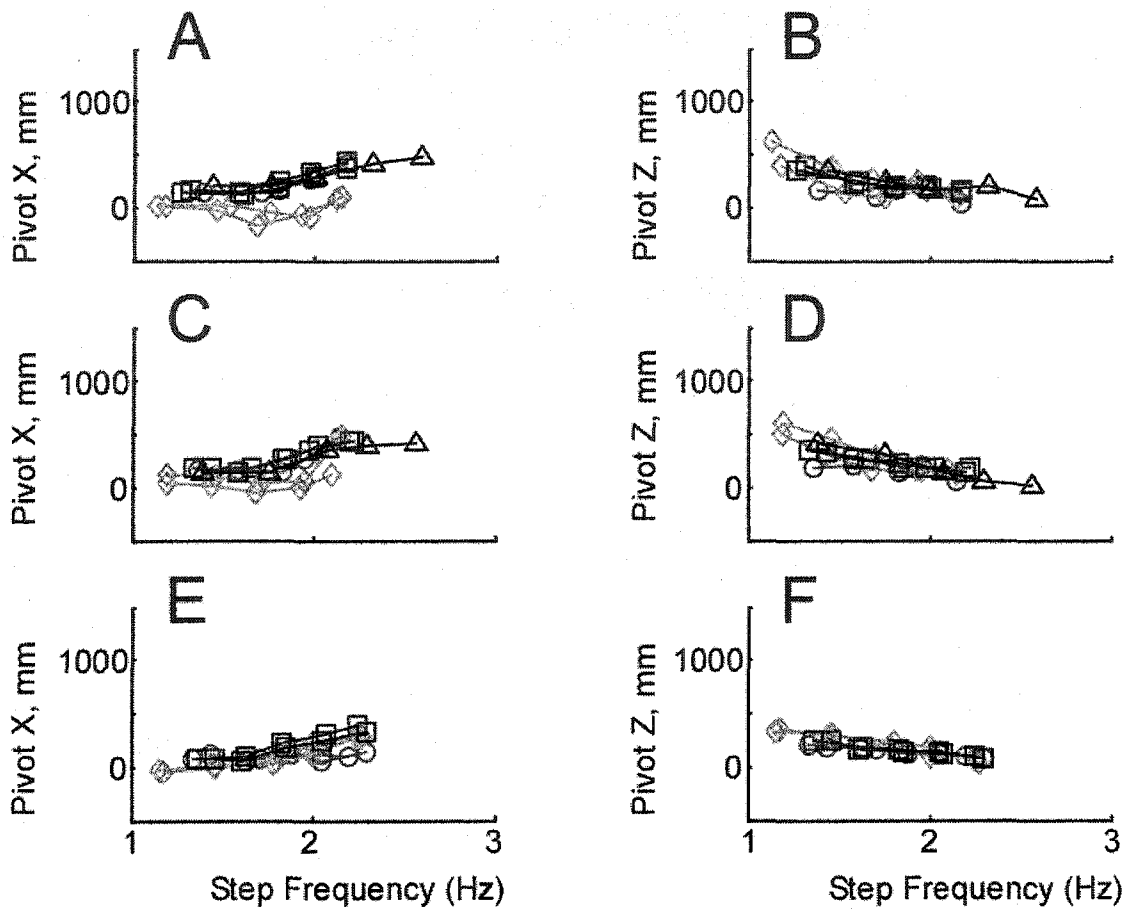

Fig 8.20 The X (A, C, E), and Z (B, D, F) coordinates of the trunk virtual pivot point determined relative to the instantaneous position of the trunk during locomotion on treadmill while fixating a point at 1m (A, B), wearing a neck-restraining collar (C, D), and fixating a point at 20 cm (E, F).

These data indicate that during locomotion the axis of rotation of the body moves away from the body for increases in walking speed (Fig. 8.20 (A, C, E). It also moves lower along the vertical direction (Fig. 8.20 B, D, F) and its dependence on neck constraints or visual fixation appears to be negligible. These results indicate that increased walking velocity increases body pitch around a further and lower point relative to the body and may impact the role of the aVCR in head control. This is a subject for further study.

CHAPTER 9 SUMMARY AND CONCLUSION

9.1 Summary and Conclusions

In this thesis, a computational approach to studying the compensatory responses of the head during natural treadmill and overground locomotion over a wide range of walking conditions has been developed. A key postulate of this work was that during walking, the vestibulocollic reflex played an important role in determining head movements to generate approximate invariant points in space presumably as a reference for generating eye movements to optimize gaze in space. A number of technical achievements have been made that for the first time allowed the study of head movements during locomotion using coordinate frames that were precisely related to landmarks of the head and trunk (CHAPTER 3). Precise calibration procedure for establishing head and trunk coordinate frames with respect to anatomical landmarks was developed. This enabled recording of kinematical data in reliable and repeatable way, eliminating the differences due to OPTOTRAK rigid bodies placement on the subject in different experiments and different subjects. To make it possible to do the experiments in a reasonably efficient manner, a scripting environment was developed to control NDI software and the OPTOTRAK during data acquisition and conversion phases. This significantly decreased the time necessary to perform an experiment, increasing efficiency of the experimental process.

Using the theory of homogeneous matrices (Fu, Gonzales et al. 1987; Murray, Li et al. 1994), we have devised a filtering procedure for what we have defined as displacement matrices that could determine rotation axes and their pivot points in three

dimensions. This allowed us to determine axes of head movements about roll, pitch, and yaw of the head that predicted the axis of the dens obtained from MRI recordings (CHAPTER 7). In CHAPTER 5, we have also developed new approaches for analyzing pitch head movements during locomotion on a treadmill and compared them with overground locomotion. Comparisons were also done during constraints of the head movement by a soft collar. A key finding from these studies was that there is considerable phase difference between the head pitch velocity and the vertical acceleration that generates it. As such, HFP has considerable variability and is better described by a trajectory in phase space than by a single point. However, over many cycles of locomotion, the HFP is a fairly good estimate of the compensatory capability of the lVCR.

The data and analysis techniques developed in this study gave insight into the differences in head compensation during overground and treadmill locomotion (CHAPTER 5). It was surprising that naso-occipital acceleration was not significantly different between the two paradigms. We had anticipated that there would be greater naso-occipital acceleration during overground locomotion because the treadmill was rolling under the foot following heel strike. Upon closer examination, however, it became clear that in both cases velocity is maintained relative to the ground and accelerations are relative to this platform, consistent with Galileo's law of relative motion (Galileo 1638), and our results.

Another interesting outcome of this project is the finding that phase between the head pitch velocity and vertical linear acceleration was different from 90° (CHAPTER 5). This phase difference causes deviations of the HFP over time and contributes to the

destabilization of the HFP. By developing a technique to determine phase difference over a small time interval, it could be shown that by adjusting the phase, the HFP was maintained. Interestingly, despite the fact that the there were large phase variations over the locomotion cycle, the HFP approached a stable value over many cycles. The present study further showed that the HFP was connected to the gain of the lVCR. When the relationship of head pitch to head acceleration was multiplied by the dominant radian frequency of walking and HFP, a gain was established, which rose as a function of walking velocity. The gain and phase could be approximated by a second order model of the lVCR with feedback from the aVCR (Keshner and Peterson 1988; Keshner, Cromwell et al. 1995; Keshner, Hain et al. 1999; Peng, Hain et al. 1999) supporting the idea that the LVCR is responsible for the head pitch as the head is vertically accelerated during locmotion (Pozzo, Berthoz et al. 1989; Pozzo, Berthoz et al. 1990; Pozzo, Berthoz et al. 1991; Bloomberg, Peters et al. 1997; Hirasaki, Moore et al. 1999; Bloomberg and Mulavara 2003).

The present work also showed that there was a close association of the yaw axis of the head rotation with the dens of C2 (CHAPTER 7). A number of studies of head movements in three dimensions have generally been described by rotation vectors (Glenn and Vilis 1992; Winters, Peles et al. 1993; Tweed, Glenn et al. 1995) and the exact pivot point or lines in space about which the head rotates had not been explored. Knowledge of the rotation axes is important for understanding how the angular vestibulo-ocular reflex (aVOR) should compensate for rotation about eccentric axes (Virre, Tweed et al. 1986; Crane, Virre et al. 1997). It was critical for the investigations determining HFP. Medendorp et al (Medendorp, Melis et al. 1998) utilized helical axis parameters (Spoor

and Veldpaus 1980; Woltring, Huiskes et al. 1985) to determine the axis of voluntary head rotation. The movements utilized were large, being greater than 25°. More importantly, the methodology could not be applied for movements of less than 6°, which limited the ability to accurately compute velocity (Medendorp, Melis et al. 1998). The head movements that were considered in this thesis were all less than 6°, especially during locomotion. The method developed in this thesis could be applied for angles as small as 1-2°. Moreover, the precise calibration allowed the prediction of the data relative to precise landmarks, which could be associated with the cervical entities that presumably govern the axes of head rotation. The overlaying of the data from behavioral head rotations with MRI results of the axis of the dens (C2) was quite remarkable.

The most striking aspects of the findings in this thesis is the three dimensional aspects of head movement during locomotion. Head fixation point had been considered as an important parameter of locomotion for pitch head motion in relation to vertical acceleration (Pozzo, Berthoz et al. 1989; Pozzo, Berthoz et al. 1990; Pozzo, Berthoz et al. 1991; Hirasaki, Moore et al. 1999; Hirasaki, Moore et al. 1999; Moore, Hirasaki et al. 1999). This had been extended to yaw head movements by considering separate head fixation points for yaw and pitch (Moore, Hirasaki et al. 2001). The conclusion was that there were different mechanisms producing the pitch and yaw compensatory head movements. The present study shows that HFP can be computed as a single point in three-dimensional space (CHAPTER 8). The differences between pitch and yaw arises because of how lines that do not intersect in three dimensions are projected onto the pitch and yaw planes. The present findings add a rigor to the understanding of how HFP characterizes head compensation arising in the lVCR in three dimensions. This study

shows that despite the large variability in the dynamics of HFP, our hypothesis that HFP is importantly related to the compensatory characteristics of head rotation in response to head translation is generally supported.

9.2 Future Research

This thesis laid the groundwork for a number of future studies.

1) The unique calibration procedure developed in this thesis allows us to explore a number of theoretical issues regarding how the axes of head rotation are related to landmarks of the spinal column. In this thesis, we showed a remarkable association between the axis of head yaw rotation with the dens of C2. In future work, we hope to model the pitch axis axes of head rotation and how they might be related to the condyles.
2) Design better controlled experiments for treadmill and over ground locomotion in order to obtain more stationary data (eliminate transient, possibly voluntary, movements).
3) The wide ranging eigenvalues in the three-dimensional analysis of head movements suggests that these compensatory movements may be non-linear and non-stationary. Thus, a wavelet analysis of these data may give better insight into the instantaneous compensation rather than the global compensation.
4) Apply these methods during circular walking. Circular locomotion brings into play the orientation components of head movement. An analysis of head orientation using the calibrated methods developed in this thesis would give better insight into how the vestibulo-collic reflex orients head movements to align with the GIA.

5) In this study, we have found that perturbations had little effect on straight walking. Further studies to examine the effects of perturbations on circular locomotion would be important in understanding how mechanisms related to orientation respond to transient perturbations and under what conditions these can be recovered from.

6) Develop extension to include the eye movements and gaze fixation during walking. Applying the methods developed in this thesis would be important in better understanding gaze in three dimensions during walking.

7) Finally, it would be important to develop a model that simulates the compensatory and orientation behavior described in this thesis. We have begun to identify the important parameters of head movement in one dimension. An extension of these ideas, based on three dimensional compensation and orientation could lead to a better understanding of the system.

APPENDIX A

One-dimensional differentiation based on a least-squares fit

An elementary technique used for numerical differentiation involves fitting a least-squares polynomial to the data and then using the derivative of that polynomial as the approximation. In the simplest case a polynomial of degree one can be used.

Consider a sequence of data points $\{(x_i,y_i)\}$ such that y_i approximates a value of some function $y_i=f(x_i)$, and the derivative of f with respect to x is to be estimated. To estimate the derivative $f'(x_i)$, one could use the fact that

$$f(x_{i+k}) - f(x_{i-k}) \approx f'(x_i)(x_{i+k} - x_{i-k}) \tag{A.1}$$

for a reasonably small k. Denoting the desirable estimate to $f'(x_i)$ as m, y_{i+k}-y_{i-k} as Δ_{ky}, and x_{i+k}-x_{i-k} as Δ_{kx}, the squared error of such approximation is given by $S_k=(\Delta_{ky}-m\Delta_{kx})^2$. Taking n points from the vicinity of x_i yields:

$$S = \tfrac{1}{2}\sum_{k=1}^{n}(\Delta_{ky} - m\Delta_{kx})^2 \tag{A.2}$$

the value of m that minimizes S can be found as a solution of the system of linear equations:

$$\frac{\partial S}{\partial m} = \sum_{k=1}^{m} (\Delta_{ky} - m\Delta_{kx})\Delta_{kx} = 0 \tag{A.3}$$

Simplifying

$$\sum_{k=1}^{n} \Delta_{ky}\Delta_{kx} = m\sum_{k=1}^{n} \Delta_{kx}^2 \tag{A.4}$$

Assuming

$$\begin{aligned} x_k &= t_o + k\Delta t \\ \Delta_{xk} &= 2k\Delta t \end{aligned} \tag{A.5}$$

Further simplification is possible

$$2\Delta t\sum_{k=1}^{n} k\Delta_{ky} = m(2\Delta t)^2\sum_{k=1}^{n} k^2 = 2m\Delta t\frac{n(n+1)(2n+1)}{3} \tag{A.6}$$

Therefore

$$m = \frac{3\sum_{k=1}^{n} k\Delta_{ky}}{\Delta t\, n(n+1)(2n+1)} \tag{A.7}$$

Note that this derivation remains valid when Δ_{ky} are vector valued as long they are linear with respect to Δ_{kx}.

APPENDIX B

This appendix illustrates in a didactical fashion the elements of Chasles theorem. Michel Chasles was a French mathematician who lived from 1793 – 1880. Although he did work most of his work in geometry, he is attributed with having discovered the fundamental relationship between movement of a rigid body to rotation and translation relative to some coordinate frame. The theorem is:

Chasles Theorem:

Any displacement of a rigid body that is not a pure translation can be realized as a rotation about an axis followed by a translation along that axis.

Intuitively, it is clear that given a rigid body configuration at two different instances in the plane, one can be obtained from another by a rotation and translation. The rotation of the rigid body is about its local coordinate system origin so that its orientation is the same as in the target position, and then translate it into the target position (Fig B.1).

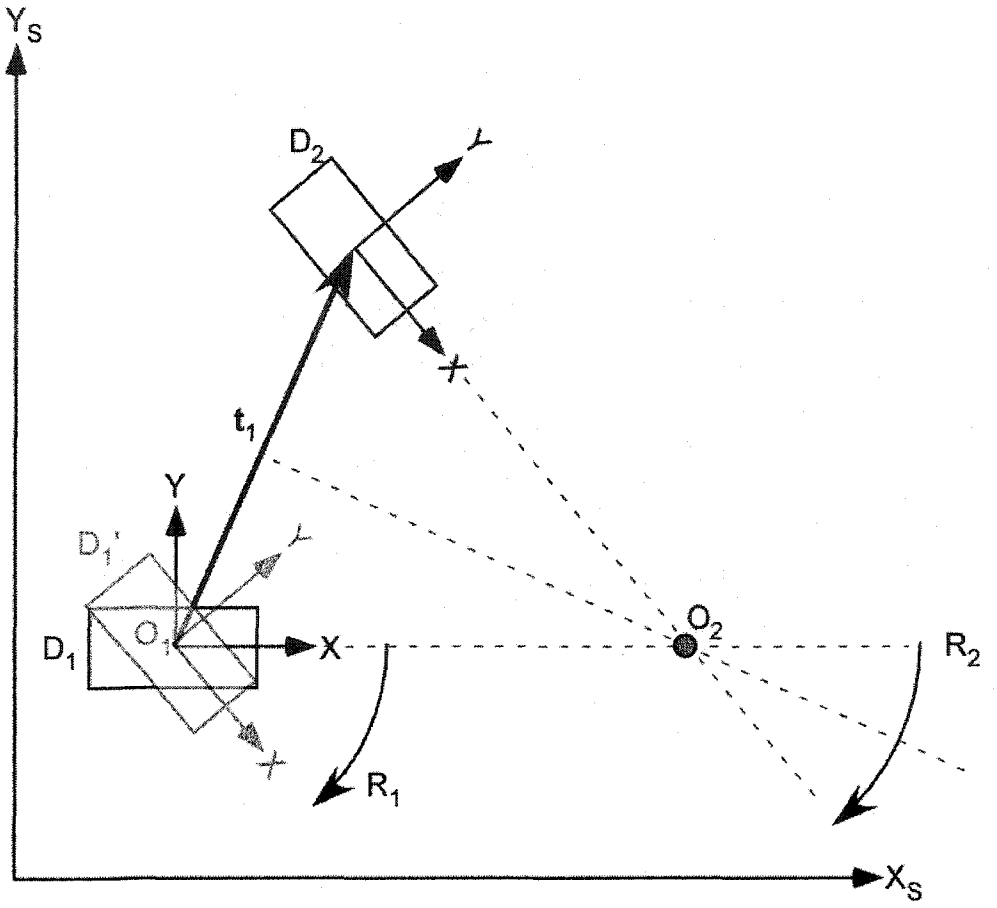

If the initial and final orientations are not the same, one can find a point in the plane such that a single rotation about that point transforms the rigid body into the target position: a configuration of a rigid body (only SE(2)) is determined by coordinates of two points attached to the rigid body, and the intersection of the bisectors of the segments formed by connecting the spatial image of each point in source and target configurations gives the center of rotation (in non-degenerate cases, where the lines connecting the images of points within each configuration intersect in the center). Note that the angle of the rotation is the same whether the rotation is followed by a translation or not.

In three dimensions, the rigid body may also translate along a direction that is not contained in the plane, and according to Chasles theorem there is always a plane such that the "additional" out of plane translation is perpendicular to the plane of rotation.

REFERENCES:

Assaiante, C. and B. Amblard (1992). Head-trunk coordination and locomotor equilibrium in 3- to 8-year-old children and adults. The head-neck sensory motor system. A. Berthoz and W. Graf. Oxford, Oxford University Press: 121-125.

Assaiante, C. and B. Amblard (1993). "Ontogenesis of head stabilization in space during locomotion in children: influence of visual cues." Exp Brain Res **93**(3): 499-515.

Berthoz, A. and T. Pozzo (1988). Intermittent head stabilization during postural and locomotory tasks in humans. Posture and Gait: Development, Adaptation and Modulation. B. Amblard, A. Berthoz and F. Clarac. Amsterdam, Elsevier: 189-198.

Bloomberg, J. J. and A. P. Mulavara (2003). "Changes in walking strategies after spaceflight." IEEE Eng Med Biol Mag **22**(2): 58-62.

Bloomberg, J. J., B. T. Peters, et al. (1997). "Locomotor head-trunk coordination strategies following space flight." J Vestib Res **7**(2-3): 161-77.

Bloomberg, J. J., M. F. Reschke, et al. (1992). "The effects of target distance on eye and head movement during locomotion." Ann N Y Acad Sci **656**: 699-707.

Blum, E. K. (1972). Numerical analysis. Reading, Addison-Wesley.

Crane, B., E. S. Virre, et al. (1997). "The human horizontal vestibulo-ocular reflex during combined linear and angular acceleration." Exp. Brain Res. **114**: 304-320.

Crane, B. T. and J. L. Demer (1997). "Human gaze stabilization during natural activities: translation, rotation, magnification, and target distance effects." J Neurophysiol **78**(4): 2129-44.

Crawford, J. D., J. C. Martinez-Trujillo, et al. (2003). "Neural control of three-dimensional eye and head movements." Curr Opin Neurobiol **13**(6): 655-62.

Demer, J. L. and E. S. Virre (1996). "Visual-vestibular interaction during standing, walking and running." J Vest. Res. **6**: 295-313.

Denavit, J. and R. S. Hartenberg (1955). "A kinematic notation for lower-pair mechanisms based on matrices." Journal of Applied Mechanics(June): 215-221.

Dodge, R. and T. S. Cline (1901). "The angular velocity of eye movements." Psychol. Rev. **8**: 145-157.

Fu, K. S., R. C. Gonzales, et al. (1987). Control, sensing, Vision, and Intelligence. New York, McGraw Hill.

Galileo, G. (1638). The discourses and mathematical demonstrations relating to two new sciences. The Netherlands, Elzevir.

This is a discourse between Salviato, Sagredo, and Simplicio

Glenn, B. and T. Vilis (1992). "Violations of Listing's law after large eye and head gaze shifts." J. Neurophysiol **68**: 309-318.

Goldstein, H. (1980). Classical Mechanics. Reading, MA., Addison-Wesley.

Grasso, R., P. Prevost, et al. (1998). "Eye-head coordination for the steering of locomotion in humans: an anticipatory synergy." Neuroscience Letters **253**: 115-118.

Grossman, G. E., R. J. Leigh, et al. (1988). "Frequency and velocity of rotational head perturbations during locomotion." Exp. Brain Res. **70**: 470-476.

Hirasaki, E., T. Kubo, et al. (1993). "Analysis of head and body movements of elderly people during locomotion." Acta Otolaryngol Suppl **501**: 25-30.

Hirasaki, E., S. T. Moore, et al. (1999). Effect of walking velocity on horizontal head and body movements during locomotion. 5th International Symposium on the Head/Neck System, Tokyo, JAPAN.

Hirasaki, E., S. T. Moore, et al. (1999). "Effects of walking velocity on vertical head and body movements during locomotion." Exp Brain Res **127**(2): 117-130.

Imai, T., S. T. Moore, et al. (2001). "Interaction of the body, head and eyes during walking and turning." Exp. Brain Res. **136**: 1-18.

Inman, V. T., H. J. Ralston, et al. (1981). Human walking. Baltimore, Williams and Wilkins.

Keshner, E. A., R. W. Cromwell, et al. (1995). "Mechanisms controlling human head stabilization. II. Head-neck characteristics during random rotations in the vertical plane." J. Neurophysiol. **73**(6): 2302-2312.

Keshner, E. A., T. C. Hain, et al. (1999). "Predicting control mechanisms for human head stabilization by altering the passive mechanics." J. Vest. Res. **9**: 423-434.

Keshner, E. A. and B. W. Peterson (1988). "Motor control strategies underlying head stabilization and voluntary head movements in humans and cats." Prog. Brain Res. **76**: 329-339.

Klier, E. M., H. Wang, et al. (2002). "Midbrain control of three-dimensional head orientation." Science **295**(5558): 1314-6.

Kunin, M., B. Delman, et al. (2004). Head yaw rotation axes and their relationship to the orientation of the dens. Soc. for Neurosc Abstracts, San Diego, Calif.

Kunin, M., C. Wall, et al. (2003). "Head fixation point during normal and perturbed locomotion: a countermeasure assessment criteria." Soc. Neurosci. Abstracts **33**: 268.16.

Ledebt, A., B. Bril, et al. (1995). "Trunk and head stabilization during the first months of independent walking." Neuroreport **6**(13): 1737-40.

Ledebt, A. and S. Wiener-Vacher (1996). "Head coordination in the sagittal plane in toddlers during walking: preliminary results." Brain Res Bull **40**(5-6): 371-3.

Medendorp, W. P., B. J. M. Melis, et al. (1998). "Off-centric rotation axes in natural head movements: implications for vestibular reafference and kinematic redundancy." J. Neurophysiol. **79**(4): 2025-2039.

Mergner, T. and T. Rosemeier (1998). "Interaction of vestibular, somatosensory and visual signals for postural control and motion perception under terrestrial and microgravity conditions--a conceptual model." Brain Res Brain Res Rev **28**(1-2): 118-35.

Moore, S. T., E. Hirasaki, et al. (1999). "Effect of viewing distance on the generation of vertical eye movements during locomotion." Exp. Brain Res. **129**: 347-361.

Moore, S. T., E. Hirasaki, et al. (2001). "The human vestibulo-ocular reflex during linear locomotion." Ann NY Acad Sci **942**: 139-147.

Murray, R. M., Z. Li, et al. (1994). A mathematical introduction to robotic manipulation. Boca Raton, CRC Press, Inc.

Peng, G. C. Y., T. C. Hain, et al. (1999). "Predicting vestibular, proprioceptive, and biomechanical control strategies in normal and pathological head movements." IEEE Trans Biomed Eng. **46**: 1269-1280.

Pozzo, T., A. Berthoz, et al. (1989). "Head kinematics during various motor tasks in humans." Progress in Brain Research **80**: 377-383.

Pozzo, T., A. Berthoz, et al. (1990). "Head stabilization during various locomotor tasks in humans. I. Normal subjects." Exp Brain Res **82**: 97-106.

Pozzo, T., A. Berthoz, et al. (1991). "Head stabilization during various locomotor tasks in humans. II. Patients with bilateral peripheral vestibular deficits." Exp Brain Res **85**: 208-217.

Press, W. H., S. A. Teukolsky, et al. (1992). Numerical recipes in C: The art of scientific computing. New York, Cambrige University Press.

Proakis, J. G. and D. G. Manolakis (1992). Digital signal processing: principles, algorithms, and applications. New York, New York, Macmillan Publishing Company.

Raphan, T. (1997). Modeling control of eye orientation in three dimensions. Three-Dimensional Kinematics of Eye, Head, and Limb Movements. M. Fetter, T. Haslwanter, H. Misslisch and D. Tweed. Amsterdam, Harwood Academic Publishers: 359-374.

Raphan, T. (1998). "Modeling control of eye orientation in three dimensions. I. Role of muscle pulleys in determining saccadic trajectory." J. Neurophysiol. **79**: 2653-2667.

Raphan, T., M. Kunin, et al. (2004). Head Rotation Axes in Three Dimensions and Their Relationship to Orientation of the Dens in Different Head Positions. Barany Society XXIII International Congress, Journal of Vestibular Research Abstracts No. O083, Paris, France.

Reschke, M. F., J. J. Bloomberg, et al. (1994). "Space flight and neurovestibular adaptation." J Clin Pharmacol **34**(6): 609-17.

Robinson, D. A. (1964). "The mechanics of human saccadic eye movement." J. Physiol (London) **174**: 245-264.

Robinson, D. A. (1965). "The mechanics of smooth pursuit eye movement." J. Physiol. (London) **180**: 569-591.

Rodriguez, O. (1840). "Des lois geometriques qui regissent les desplacements d'un systeme solide dans l'espace et de la variation des coordonnees provenant de deplacements consideres independamment des causes qui peuvent les produire." J. de Mathematiques Pures et Appliquees **5**: 380-440.

Schnabolk, C. and T. Raphan (1994). "Modeling three dimensional velocity-to-position transformation in oculomotor control." J. Neurophysiol. **71**: 623-638.

Schwartz, M. and L. Shaw (1975). Signal processing discrete spectral analysis, detection, and estimation. New York, McGraw-Hill.

Simpson, J. I. and W. Graf (1985). The selection of reference frames by nature and its investigators. Adaptive Mechanisms in Gaze Control; Reviews of Oculomotor Research. A. Berthoz and G. M. Jones. Amsterdam, Elsevier. **1:** 3-16.

Spoor, C. W. and F. E. Veldpaus (1980). "Rigid body motion calculated from spatial co-ordinates of markers." J. Biomech **13**: 391-393.

Tou, J. T. and R. C. Gonzalez (1974). Pattern Recognition Principles, Addison Wesley.

Tweed, D., B. Glenn, et al. (1995). "Eye-head coordination during large gaze shifts." J Neurophysiol **73**: 766-779.

Veldpaus, F. E., H. J. Woltring, et al. (1988). "A least-squares algorithm for the equiform transformation from spatial marker co-ordinates." J Biomech **21**(1): 45-54.

Virre, E., D. Tweed, et al. (1986). "A reexamination of the gain of the vestibuloocular reflex." J. Neurophysiol **56**: 439-450.

Weber, E. and W. Weber (1836). "Mechanik der Mensclichen Gehwerkzeuge. Eine anatomisch physiologische Untersuchung."

Winter, D. A. and P. Eng (1995). "Kinetics: our window into the goals and strategies of the central nervous system." Behav Brain Res **67**(2): 111-20.

Winter, D. A., C. D. MacKinnon, et al. (1993). "An integrated EMG/biomechanical model of upper body balance and posture during human gait." Prog Brain Res **97**: 359-67.

Winters, J. M., J. D. Peles, et al. (1993). "Three-dimensional head axis of rotation during tracking movements." Spine **18**: 1178-1185.

Woltring, H. J., R. Huiskes, et al. (1985). "Finite centroid and helical axis estimation from noisy landmark measurements in the study of human joint kinematics." J. Biomech **18**: 379-389.

Zatsiorky, V. M., S. L. Werner, et al. (1994). "Basic kinematics of walking. Step length and step frequency. A review." J Sports Med Phys Fitness **34**(2): 109-34.